IntechOpen

Flexible Electronics

Edited by Simas Rackauskas

FLEXIBLE ELECTRONICS

Edited by **Simas Rackauskas**

Flexible Electronics
http://dx.doi.org/10.5772/intechopen.72522
Edited by Simas Rackauskas

Contributors

Phuong Viet Pham, Almudena Rivadeneyra, Aniello Falco, Florin Loghin, Sílvia Cruz, Luís Rocha, Julio Viana, Yunnan Fang, Manos Tentzeris, Peiyun Yi, Yuwen Zhu, Yujun Deng

Notice

Statements and opinions expressed in the chapters are these of the individual contributors and not necessarily those of the editors or publisher. No responsibility is accepted for the accuracy of information contained in the published chapters. The publisher assumes no responsibility for any damage or injury to persons or property arising out of the use of any materials, instructions, methods or ideas contained in the book.

First published in London, United Kingdom, 2018 by IntechOpen
eBook (PDF) Published by IntechOpen, 2019
IntechOpen is the global imprint of INTECHOPEN LIMITED, registered in England and Wales, registration number: 11086078, The Shard, 25th floor, 32 London Bridge Street
London, SE19SG – United Kingdom
Printed in Croatia

British Library Cataloguing-in-Publication Data
A catalogue record for this book is available from the British Library

Additional hard and PDF copies can be obtained from orders@intechopen.com

Flexible Electronics
Edited by Simas Rackauskas

p. cm.

Print ISBN 978-1-78923-456-5

Online ISBN 978-1-78923-457-2

eBook (PDF) ISBN 978-1-83881-697-1

Meet the editor

Simas Rackauskas defended his PhD degree in Physics from the Aalto University, Finland, in 2011. He held postdoctoral positions at the Aalto University and State University of Campinas, Brazil. He had fellowships at the Swiss Federal Institute of Technology in Lausanne (EPFL), Switzerland; Technical University of Denmark (DTU); and University of Nagoya, Japan. From 2016, he is a Marie Curie Fellow at the University of Turin, Italy. His research interests mainly focus on flexible electronics, carbon nanomaterials, and noncatalytic growth of metal oxide nanowires.

Contents

Preface

The interest in flexible electronics is on the rise as it brings an added functionality and esthetic value in the unconventional interfaces, such as biomonitoring systems, wearables, flexible textiles, paper-based technologies, and many other curves of soft schemes, for which traditional electronics are not suitable. The demand in new flexible platforms turns to a pursuit for functional materials and technologies commonly compatible with a low temperature, high-throughput processing, and novel methods for device integration. New device design leads to an immense field from fundamental research to the new technologies and engineering methods bringing advanced functionality. A wide range of functional materials involving nanoparticles, composites, semiconductor and metallic nanowires, carbon nanomaterials, polymers, conductive inks, and different hybrid structures are particularly interesting. Printing technologies have been demonstrated to be highly efficient and compatible with many flexible substrates; furthermore, surface preparation methods play an important role for the fabrication of electronic devices. This book brings a comprehensive overview on the most important technology development in the field of flexible electronics.

Simas Rackauskas
University of Turin
Turin, Italy

Chapter 1

Surface Modification of Polyimide Films for Inkjet-Printing of Flexible Electronic Devices

Yunnan Fang and Manos M. Tentzeris

Additional information is available at the end of the chapter

http://dx.doi.org/10.5772/intechopen.76450

Abstract

Kapton polyimide films are one of the most commonly used flexible and robust substrates for flexible electronic devices due to their excellent thermal, chemical, mechanical, and electrical properties. However, such films feature an inert and highly hydrophobic surface that inhibits the deposition of functional materials with water-based fluids (solutions, suspensions, inkjet inks, *etc*.), which raise the need for their surface modification to reduce their inherent surface inertness and/or hydrophobicity in order to allow for the fabrication of electronic devices on the substrates. Traditional Kapton surface modification approaches use harsh conditions that not only cause environmental and safety problems but also compromise the structural integrity and the properties of the substrates. This chapter focuses on two recently-developed mild and environmentally friendly wet chemical approaches for surface modification of Kapton HN films. Unlike the traditional methods that target the polyimide matrix of Kapton films, these two methods target the slip additive embedded in the polyimide matrix. The surface modified Kapton films resulted from these two methods allowed for not only great printability of both water- and organic solvent-based inks (thus facilitating the full-inkjet-printing of entire flexible electronic devices) but also strong adhesion between the inkjet-printed traces and the substrate films.

Keywords: surface modification, Kapton, polyimide, flexible electronic devices, sensors, inkjet-printing

1. Introduction

Kapton HN films, which are well known to be made of polyimide polymer, are one of the most commonly used substrates for flexible electronics due to their excellent physical and

electrical properties as well as exceptional thermal and chemical stability. However, such films feature an inert and highly hydrophobic surface. Hydrophilic (e.g. water-based) fluids (solutions, suspensions, inks, *etc*.) will ball up on such surfaces (due to "lotus effect") [1, 2]. However, for fabrication of an entire electronic device, both organic solvent- and water-based fluids are usually needed to deposit functional materials on the same substrate surface. As a result, surface modifying polyimide substrates to reduce their inherent surface hydrophobicity and/or inertness is usually needed to allow for the continuous and uniform deposition with both organic solvent- and water-based fluids.

Traditionally, polyimide substrates are surface modified with a number of methods including plasma [3, 4] and ion-beam [5, 6] etching, UV/ozone exposure [3, 7], acid [3, 8] and/or base [9, 10] treatments, and laser ablation [11, 12]. These methods, however, usually compromise the structural integrity and the properties (such as the cohesive strength, and the thermal and chemical stability) of the polyimide substrate, since they utilize relatively harsh conditions to oxidize and/or tear out part of the surface polyimide. Additionally, the wastes and by-products (such as acrolein which is extremely irritating, strong bases and acids which are corrosive, and benzene which is carcinogenic) generated from these harsh treatments can raise serious environmental and safety issues (especially when the treatments are performed indoors and/or in large scales). For example, incubation with a sodium hydroxide solution has been one of the most common traditional methods to tune the surface properties of Kapton polyimide substrates [9, 10, 13], but such a treatment not only generates highly corrosive strong base waste but also tears out some surface polyimide resulting in pits in the Kapton surface [14]. The defects on structurally damaged Kapton films would result in not only poor deposition quality of the device components but also weakened mechanic strength of the resulting devices. The increasingly growing of flexible electronic devices (such as flexible displays [15], electronic paper [16, 17], photovoltaic cells [18, 19], sensors [1, 2, 20–23], LEDs [24], electronic textiles [25], RF tags [26], and electrochemical devices [27], *etc*.) is calling for mild and environmentally friendly surface modification approaches which can minimize the compromise to the structural integrity and the properties of Kapton polyimide substrates while efficiently tuning the surface properties of the substrates. To take full advantage of the properties of Kapton HN films, any surface modification to such films should avoid as much as possible compromising their structural integrity and properties. For extremely thin Kapton HN films, such as Kapton 30HN (thickness 7.5 μm), 50HN (thickness 12.7 μm), and 75HN (thickness 19.1 μm), it is critical to make sure that their surface modification is non- or minimally destructive.

Kapton HN films have a slip additive incorporated in the polyimide matrix to enhance their mechanical properties [13]. The nature of the additive, however, has been very scarcely reported in the literature. Williams *et al.* has mentioned, but without providing supporting data, that the additive in Kapton HN films was calcium phosphate dibasic ($CaHPO_4$) [14]. This chapter first describes the characterization of Kapton 500HN films particularly of their slip additive, then introduces two recently-developed mild and environmentally friendly wet chemical approaches for surface modification of Kapton HN films to allow for not only great printability of both water- and organic solvent-based inks but also strong adhesion between the inkjet-printed traces and the surface modified substrates. Unlike the aforementioned traditional Kapton surface modification methods which target, and oxidize and/or tear out part of, the surface polyimide matrix, the approaches described in this chapter target the electric charges on the slip additive particles.

2. Characterization of Kapton HN films

In this section, a number of characterizations were performed on as-received Kapton 500HN films (a gift from Dupont, Wilmington, DE, USA) particularly on their slip additive. The optical microscopy analysis of the films showed particles of varying sizes which were imbedded in Kapton HN polyimide matrix (**Figure 1a**). These particles have been shown to be the slip additive to the polyimide matrix of Kapton HN [14, 28]. As shown in **Figure 1a**, the majority of the slip additive particles exuded to the substrate surface, which is consistent with a previous observation [29]. The large hump (with 2θ ranging from ˜10° to ˜35°) and the sharp narrow peaks in the X-ray diffraction (XRD) pattern of the Kapton HN films (**Figure 1b**) indicated the presence of amorphous and crystalline components, respectively. Apparently the amorphous moiety was the polyimide polymer and crystalline moiety the slip additive. While calcium phosphate dibasic ($CaHPO_4$) might be present in the additive as previously reported [14], the crystalline peaks in the XRD pattern of the Kapton HN films matched very well with those of calcium carbonate ($CaCO_3$) (ICDD reference code 04–001-7249) (**Figure 1b**) but did not match any of the $CaHPO_4$ peaks. Significant carbon and oxygen peaks and a small calcium peak showed up in the energy dispersive X-ray spectroscopy (EDX) pattern of the Kapton substrate (**Figure 1c**).

To better characterize the slip additive in Kapton HN films, efforts were made to minimize the interference from the polyimide polymer matrix. Kapton HN films were fired at 800°C for 2 hours in air (this firing treatment has been shown to be efficient to pyrolyze the entire polyimide polymer moiety in Kapton HN [30]) to remove the polyimide polymer. The remaining inorganic components were characterized with scanning electron microscopy (SEM), EDX, and XRD analyses.

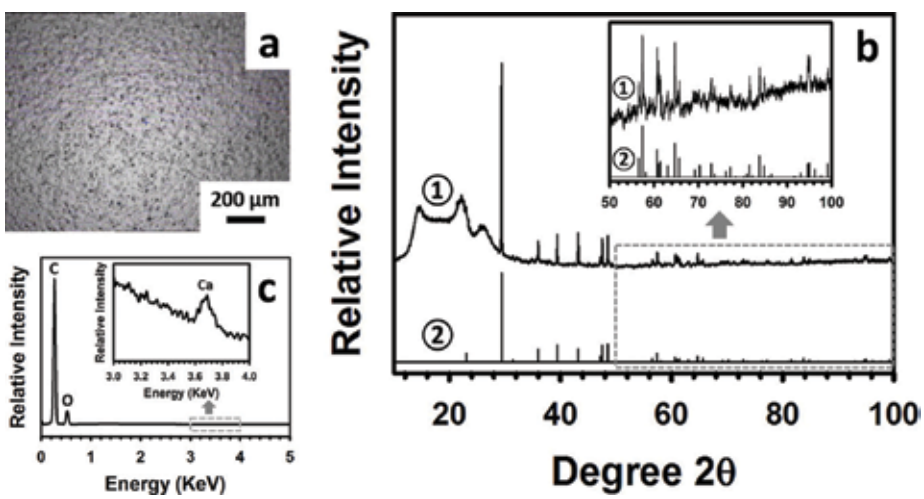

Figure 1. Kapton HN film characterization. (a) Optical microscopy analysis of a blank Kapton HN film. (b) XRD analysis of the specimen shown in (a) (pattern ①) and reference $CaCO_3$ (pattern ②, ICDD reference code 04–001-7249) (inset: Locally enlarged XRD pattern to show the area with a 2θ of from 50° to 100°). (c) EDX analysis of the specimen shown in (a) (inset: Locally enlarged EDX pattern to show the calcium peak) [2] (licensed under creative commons attribution 4.0 international license).

As shown in **Figure 2a** and **b**, the size of the ash particles varied significantly, from less than 100 nm to several microns, with the large particles probably resulting from the sintering and agglomeration of the fine ones [14]. The EDX analysis of the ash showed the presence of the elements of oxygen, calcium, and phosphorus (**Figure 2c**). The XRD analysis of the ash showed the presence of only calcium pyrophosphate $Ca_2P_2O_7$ (ICDD Reference code 04–009-6231) (**Figure 2d**). Compared with the XRD pattern of the as-received Kapton HN films (**Figure 1b**), the XRD pattern of the pyrolyzed films (**Figure 2d**) indicated the disappearance of $CaCO_3$ and the presence of $Ca_2P_2O_7$. The composition change was due to the multiple chemical reactions (such as the decomposition of $CaCO_3$ into CaO and CO_2 [31]) taken place during the pyrolyzing process. Combining **Figure 1** (characterization of Kapton HN) and **Figure 2** (characterization of the Kapton HN ash resulted from pyrolysis), we can conclude that the additive in Kapton HN was composed of $CaCO_3$ (crystalline) and one or more phosphorus-containing compounds (crystalline or amorphous). Any calcium phosphate compounds, if present as previously reported [14] in the additive, must be either crystalline but in a small amount (i.e. beyond the detection limit of the diffractometer used for the XRD analyses) or amorphous, or both. While the exact nature of the additive in Kapton HN is probably proprietary

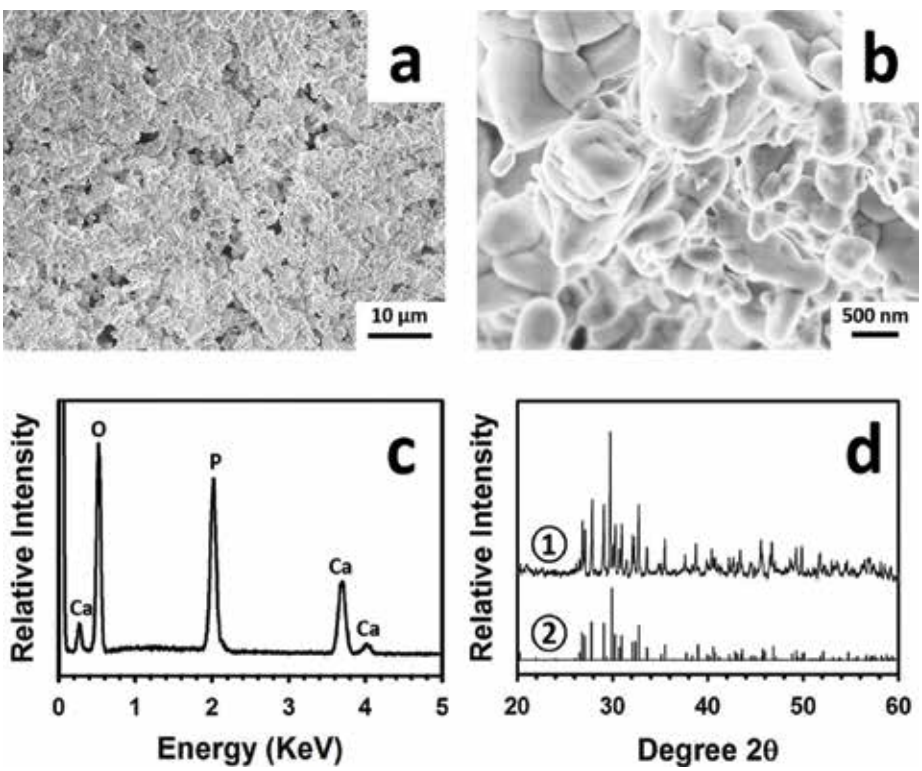

Figure 2. Characterization of the Kapton HN ash resulted from the pyrolysis of Kapton HN films at 800°C for 2 hours in air. (a) and (b) SEM images of the ash with low (a) and high (b) magnifications. (c) EDX pattern of the ash. (d) XRD patterns of both the ash (pattern ①) and reference calcium pyrophosphate $Ca_2P_2O_7$ (pattern ②. ICDD reference code 04–009-6231) [2] (licensed under creative commons attribution 4.0 international license).

and unknown to the public, XRD analyses showed that crystalline $CaCO_3$ was present in the additive in a significant amount (**Figure 1b**). With an isoelectric point of 8.2 [32], crystalline $CaCO_3$ bears positive charges at a neutral or acidic pH. The two recently developed mild and environmentally friendly wet chemical approaches described below both target the surface electric charges borne by the additive particles imbedded in the polyimide matrix of Kapton HN films.

3. A bio-enabled maximally mild layer-by-layer Kapton surface modification approach

Protamine has been clinically used to reverse the anticoagulant effects of heparin by binding to it [33, 34]. The development of the present bio-enabled surface modification approach was inspired by the *in vivo* antagonizing interaction of these two clinically used biological molecules. In this surface modification process, negatively charged heparin and positively charged protamine were used to uniformly deposit a thin film of protamine-heparin complex on Kapton HN substrates in a layer-by-layer fashion. The surface modification process was conducted under maximally mild conditions (in aqueous solutions of clinical biomolecules, and at a neutral pH, room temperature and atmospheric pressure). During the process the positively charged additive particles (e.g. $CaCO_3$ particles) on the Kapton HN surface enabled binding of the initial heparin (negatively charged) layer via electrostatic interaction. After the initial binding of heparin, the layer-by-layer uniform deposition of the protamine-heparin complex on Kapton HN was realized by the electrostatic interaction between the oppositely charged protamine and heparin molecules.

As far as we know, the present bio-inspired method was the first to use environmentally friendly clinical biomolecules for substrate surface modification. It is also the first surface modification approach performed under maximally mild and minimally destructive conditions.

3.1. Surface modification of Kapton HN films

A small Kapton piece with appropriate dimensions (e.g., 50 mm × 50 mm) was cut from a Kapton 500HN sheet. After a brief rinse with a phosphate buffer (0.2 M, pH 7.0), the Kapton piece was incubated for 10 min with a heparin sodium solution (10 mg/ml, pH 7.0) in the phosphate buffer followed by rinsing three times with the phosphate buffer. The Kapton piece was then incubated for 10 min with a protamine sulfate solution (10 mg/ml, pH 7.0) in the phosphate buffer followed by rinsing three times with the phosphate buffer. This process (heparin/rinse/protamine/rinse) was performed for a total of 5 times. Finally, the Kapton piece was rinsed with DI water and dried in air at 60°C for 2 hours.

A control surface modification process was conducted to validate the hypothesis that the surface modification process was facilitated by the positive electric charges on the Kapton HN surface. The control process was similar to the standard process described earlier, except that the heparin solution used in each deposition cycle was supplemented with 1 M sodium chloride.

3.2. Printability assessment

Figure 3a and **b** show the optical images with low and high magnifications, respectively, of some proof-of-concept silver interdigitated electrode (IDE) patterns inkjet-printed on a surface-modified Kapton substrate with an ethanediol-based silver nanoparticle ink (Sun Chemical Corporation, Parsippany, NJ, USA), while **Figure 3c** shows the optical image of some proof-of-concept graphene patches inkjet-printed on a surface modified Kapton substrate with a cyclohexanone/terpineol-based graphene ink which had been formulated based on the procedures described by Secor *et al.* [35]. Both the silver (**Figure 3a** and **b**) and the graphene (**Figure 3c**) patterns printed with organic solvent-based inks were very similar to the designs and exhibited accurately controlled shapes with sharp edges.

A number of shapes (rectangle, circle with a 100 μm-wide gap in the center, and diamond) were then printed on both surface unmodified and surface modified Kapton HN films with a home-made water-based graphene oxide (GO) ink. As shown in **Figure 4a–c**, accurately controlled shapes were able to be inkjet-printed as designed on a surface modified Kapton HN film. On the other hand, the GO ink drops balled up and formed isolated small "islands" on a surface unmodified Kapton HN film (**Figure 4d–f**). As shown in **Figure 4g–i**, the GO ink that was printed on the Kapton film which had been treated with the control process (which was similar to the standard process except that the heparin solution used in each deposition cycle was supplemented with 1 M sodium chloride) balled up and exhibited isolated small "islands," similar to the patterns with surface unmodified Kapton HN shown in **Figure 4d–f**. This validated the hypothesis that the present surface modification method was made possible by the electric charges on the Kapton HN surface. Indeed, with such a high concentration of NaCl present in the heparin solution, the Cl^- ions will screen the positive electric charges on the Kapton HN film surface. As a result, the initial heparin binding to the blank substrate film, and the subsequent protamine and heparin binding to the substrate, will all be drastically

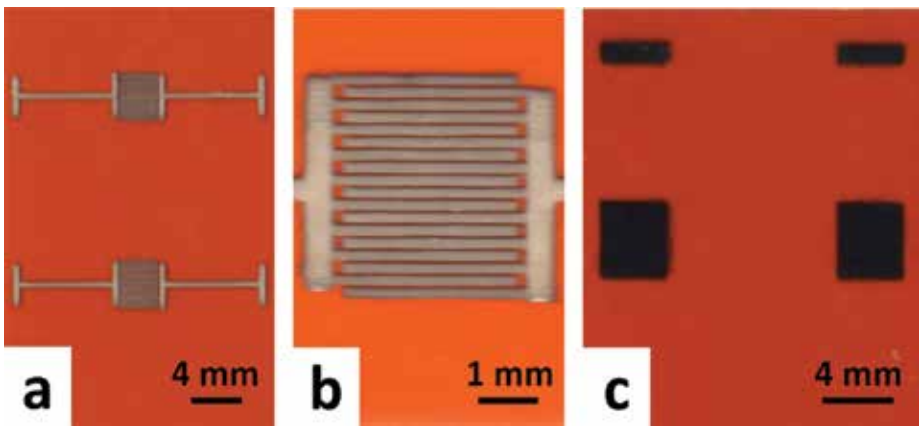

Figure 3. Optical images of proof-of-concept silver IDEs and graphene patches printed on surface modified Kapton HN films with an ethanediol-based silver nanoparticle ink and a cyclohexanone/terpineol-based graphene ink, respectively. (a) and (b) Low (a) and high (b) magnification optical images of the silver IDEs fabricated by printing (for five passes) the silver nanoparticle ink on a surface modified Kapton film followed by annealing at 120°C for 3 hours. (c) Optical image of the graphene patches fabricated by printing (for five passes) the graphene ink on a surface modified Kapton film followed by drying at 100°C for 1 hour [2] (licensed under creative commons attribution 4.0 international license).

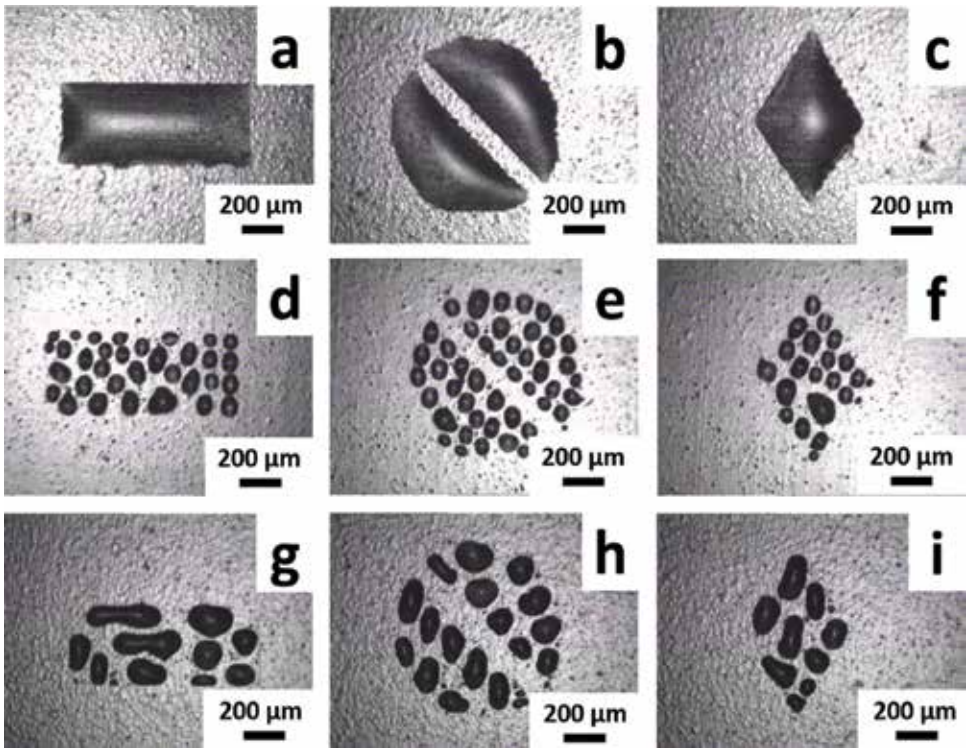

Figure 4. Printability assessment of a water-based GO ink on regularly surface modified (a, b, c), surface unmodified (d, e, f) Kapton HN, and Kapton HN which had been surface modified with a control process which was similar to the regular surface modification process except that 1 M NaCl was supplemented to the heparin solution (g, h, i) [2] (licensed under creative commons attribution 4.0 international license).

reduced. Consequently, the Kapton HN film will not be properly surface modified and its surface properties were hardly tuned.

For ink particles which are electrically charged under particular experimental conditions, the present surface modification method can enhance the uniformity of the thin films deposited on the resulting substrate. This is realized via reduction of "coffee ring effect" during the drying process. In the case of inkjet-printing, "coffee ring effect" results in an appreciable amount of more solid ink material deposited at the substrate perimeter than the other areas upon ink drying. The present surface modification method can choose to terminate the substrate surface with either negatively charged heparin or positively charged protamine. Terminating the substrate surface with opposite electric charges of the ink particles will enable local electrostatic interaction between the substrate surface and the ink particles. Consequently, the migration of the ink particles to the substrate perimeter during drying will be drastically reduced and the uniformity of the inkjet-printed thin films significantly enhanced after drying.

3.3. Fabrication and sensing tests of all-inkjet-printed flexible gas sensors

A flexible multilayered gas sensor was inkjet-printed adhering to the following steps: A Kapton HN film was treated with the process described in the present work, and a water-based

GO ink was then used to inkjet-print a GO patch on the resulting Kapton substrate. The electrically non-conductive GO patch was converted into its conductive reduced graphene oxide (rGO) counterpart by firing at 300°C for 1 hour in nitrogen. A selector layer was inkjet-printed on the resulting rGO patch with a dimethylformamide- (DMF-) based ink containing 10 mg/ml of 2-(2-hydroxy-1, 1, 1, 3, 3, 3-hexafluoropropyl)-1-naphthol. An ethanediol-based silver nanoparticle ink was then used to print two silver electrodes. To achieve an optimum contact between the rGO patch and the silver electrodes, both electrodes overlapped the rGO patch by 1.5 mm. Finally the resulting multi-layered sensor prototype was fired at 120°C for 3 hours to remove the organic molecules coated on the silver nanoparticles and to anneal the silver nanoparticles for desired conductivity. **Figure 5a** shows an optical image of a typical multi-layered gas sensor prototype fabricated with the procedures described above. A flexible single-layered sensor was similarly fabricated except that the selector layer was not printed. Both the multi- and the single-layered sensors were flexible, ultra-lightweight (˜25 mg), and miniature sized (~1.5 cm x 1.0 cm).

Gas sensing was then performed with both multi- and single-layered sensors. A dimethyl methylphosphonate (DMMP) vapor of 2.5 ppm was generated from a DMMP permeation tube (KIN-TEK Laboratories, Inc., La Marque, TX, USA) installed in a FlexStream™ Gas Standards Generator (KIN-TEK Laboratories, Inc.) and carried by nitrogen with a flow rate of 500 sccm. The relative sensitivity of a multi-layered (black solid line) and a single-layered (red-dashed line) sensor upon exposure to 2.5 ppm DMMP is shown in **Figure 5b**. The relative sensitivity (S) is defined by the following formula:

$$S = \frac{R - R_0}{R_0}$$

where R_0 is the resistance between the two silver electrodes of a sensor before the exposure to the DMMP vapor and R that at a particular time after the exposure.

SEM analyses were performed to examine the micro-/nano-morphology of the inkjet-printed GO patterns. A GO patch inkjet-printed (ten passes) on a surface modified Kapton HN film was dried at 95°C under vacuum overnight (to remove the glycerol and the water in the GO ink) and then subjected to SEM analyses. Under a scanning electron microscope, the dried GO

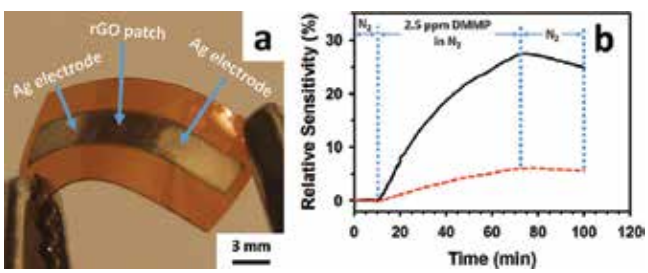

Figure 5. (a) Optical image of a flexible, rGO-based, multi-layered gas sensor inkjet-printed on a surface modified Kapton HN film (the GO ink was printed for 10 passes, the selector ink for one pass, and the silver ink for 5 passes). (b) Relative sensitivity of the multi-layered (black solid line) and the single-layered (red dashed line) gas sensors upon exposure to 2.5 ppm dimethyl methylphosphonate [2] (licensed under creative commons attribution 4.0 international license).

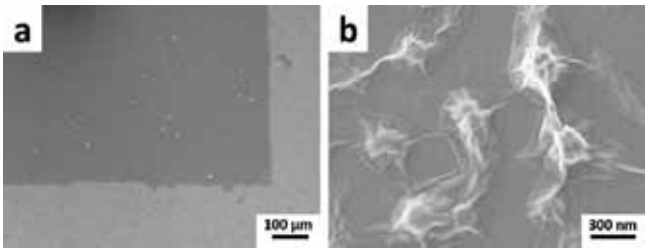

Figure 6. SEM images with low (a) and high (b) magnifications of an inkjet-printed (10 passes) and dried GO film on a surface modified Kapton HN film [2] (licensed under creative commons attribution 4.0 international license).

square had sharp edges as designed and the GO flakes were well interconnected with no observable cracks (**Figure 6a** and **b**).

3.4. Bend cycling tests on an all-inkjet-printed flexible gas sensor

A four-point bend tester (TestResources, Inc., Shakopee, MN, USA) controlled by R Controller software (TestResources, Inc.) was used to conduct the bend cycling tests. A fully inkjet-printed single-layered gas sensor was mounted on the bend tester with a home-made mounting system. The sensor was bent, with an amplitude of 20 mm and a bend rate of 1 mm/second, to a radius of curvature of 1 cm 1000 times in tension and then another 1000 times in compression to the same radius of curvature. After the 2000 bending cycles, the resistance of the sensor was measured with a multimeter and its morphology examined with an optical microscope. It was found that the resistance of the sensor after the bend test was virtually the same as that before the test (i.e. ~14 kΩ) and no morphological changes were observed during the optical analyses. Keeping the amplitude and the bend rate the same, the radius of curvature was reduced to 0.5 cm and the sensor was bent 1000 times in tension and another 1000 times in compression, followed by conductivity and morphology examination. Again, apparent conductivity or morphological changes were not observed.

3.5. Peel testes on an all-inkjet-printed flexible gas sensor

Peel tests were performed via a qualitative Scotch-tape peel test to evaluate the adhesion of an inkjet-printed single-layered gas sensor to the surface modified Kapton film. The adhesive side of a piece of Scotch® magic tape (3 M Company, St. Paul, MN, USA) was firmly pressed against the sensor and then peeled off [36, 37]. By visual inspection and optical microscopic analyses, all three components of the sensor (two silver electrodes and one rGO patch) remained attached to the substrate and retained their intactness after the tape had been peeled off.

4. A computer-controlled polyelectrolyte multilayer-based layer-by-layer Kapton surface modification approach

This is a computer-controlled, facile, environmentally friendly, low-cost, readily scalable, and layer-by-layer deposition process. This process used two weak polyelectrolytes, poly

(acrylic acid) (PAA) and polyethylenimine (PEI), to apply polyelectrolyte multilayers (PEMs) on flexible Kapton HN films in an alternating, layer-by-layer fashion under controlled pH and ionic strength. Compared to strong polyelectrolytes, weak electrolytes have the advantage of controlling the PEM properties more systematically and simply [38]. To our knowledge, this work is the first to use only weak polyelectrolytes to surface modify Kapton substrates.

4.1. Computer-controlled polyelectrolyte multilayer-based surface modification of Kapton HN films

Small pieces of Kapton 500HN with appropriate dimensions (e.g. 95 mm x 95 mm) were cut from a Kapton 500HN sheet and cleaned by sonication, first with a 10 g/L suspension of Powdered Precision Cleaner (Alconox, Inc., White Plains, NY, USA) in DI water for 10 min and then with acetone for 10 min, in an ultrasonic cleaner (Model 2510. Branson Ultrasonics, Danbury, CT, USA). The cleaned Kapton films were rinsed three times with DI water, placed in the sample chamber of a custom-built, computer-controlled, automated deposition system, and then subjected to a layer-by-layer PEM deposition process. The PEM deposition process involved alternating exposure to two solutions of oppositely charged, relatively small polyelectrolyte molecules, polyethylenimine (PEI. Branched, M.W. 1800 Dalton; Alfa Aesar, Ward Hill, MA, USA) and poly (acrylic acid) (PAA. Average M.W. ~1800 Dalton; Sigma-Aldrich, St. Louis, MO, USA). In a typical deposition cycle, the cleaned Kapton pieces were incubated for 10 min in a PAA aqueous solution (10 mg/ml. pH adjusted to 5.1 with NaOH) containing 0.5 M NaCl followed by rinsing three times with a 0.5 M NaCl aqueous solution. The Kapton pieces were then incubated for 10 min in a PEI aqueous solution (10 mg/ml. pH adjusted to 2.5 with HCl) containing 0.5 M NaCl followed by rinsing three times with a 0.5 M NaCl aqueous solution. Such a cycle was repeated to deposit the desired number of PEM layers on the Kapton pieces. To automate the deposition process, a peristaltic pump was used to deliver each of the polyelectrolyte solutions and the 0.5 M NaCl rinse solution to the sample chamber of the system. A two-way drain valve was used to remove the polyelectrolyte or the rinse solution to a waste chamber after a given incubation or rinsing step had been completed. A properly programmed microprocessor was used to operate the peristaltic pumps and the drain valve. After the desired number of deposition cycles has been finished, the resulting Kapton films were rinsed with DI water and dried in air at 60°C for 2 hours.

4.2. Contact angle measurements

Contact angle measurements were conducted (on a Rame-Hart goniometer equipped with a CCD camera (Rame-Hart Instrument Co., Succasunna, NJ, USA)) to evaluate the wetting of water, organic solvents, and inkjet inks on surface unmodified and PEM-modified Kapton HN films. **Table 1** shows that water and the water-based GO ink (which contained 60 wt% of glycerol for viscosity adjustment) exhibited an average contact angle of 76.6° and 72.4°, respectively, on a surface unmodified Kapton HN film. Organic solvents (ethanol and DMF), on the other hand, had quite small contact angles (<13°) on the same film. The commercial ethanol-based silver ink, with the presence of additional components such as a binder and a stabilizer, exhibited an average contact angle of 25.2° which was slightly higher than those of the two organic solvents. After PEM deposition on the Kapton HN film, the contact angles of both water and the water-based GO ink were significantly and reproducibly reduced. The

	Unmodified Kapton	Kapton with 1 PEM layer	Kapton with 3 PEM layers	Kapton with 4 PEM layers
Water	76.6 ± 3.9	41.0 ± 2.4	39.8 ± 1.9	37.4 ± 1.2
Ethanol	10.4 ± 2.5	12.1 ± 1.4	10.4 ± 1.9	12.2 ± 4.8
DMF	11.5 ± 1.3	12.5 ± 1.5	12.9 ± 0.1	13.3 ± 2.6
Water-based GO ink	72.4 ± 3.5	55.5 ± 2.6	53.7 ± 1.9	51.5 ± 1.2
ethanediol-based silver ink	25.2 ± 1.8	23.6 ± 0.3	24.1 ± 1.1	26.4 ± 1.6

Table 1. Contact angles of different solvents/inks on surface unmodified and PEM-modified Kapton HN films [1] (with permission from the Royal Society of Chemistry).

average contact angles of water and the water-based GO ink were reduced to 41.0° and 55.5°, respectively, after the deposition of only one layer of PEM, whereas the contact angles of the organic solvents (DMF and ethanol) and the ethanediol-based silver ink were essentially not changed (**Table 1**). It has been shown that the wetting of fluids onto sequentially adsorbed PEM layers was affected primarily by the outermost layer [39, 40]. In agreement with this previous observation, when additional PEM layers were deposited on the Kapton film, all the inks and the solvents examined in this work (water-based GO ink, ethanediol-based silver ink, DMF, ethanol, and water) exhibited little further changes in their contact angles (**Table 1**).

4.3. Printability assessment

Two organic solvent-based inks (a commercial ethanediol-based silver nanoparticle ink (Sun Chemical Corporation, Parsippany, NJ, USA) and a cyclohexanone/terpineol-based graphene ink (home-formulated based on the procedures described by Secor *et al.* [35])) and a water-based GO ink were examined for their inkjet printability on Kapton HN films before and after the PEM-based surface modification.

Figures 7 and **8** show high-resolution scanned images of silver IDE patterns and graphene patches, respectively, that were inkjet-printed on surface unmodified Kapton HN and Kapton HN which had been deposited with 1, 3 and 4 layers of PEMs. All of the silver IDEs and graphene patches exhibited uniform morphologies and precisely controlled shapes with sharp edges, as designed, irrespective of whether they had been printed on surface unmodified or PEM-modified Kapton HN films.

Figure 9a shows a square that was printed (five passes) with the GO ink on a surface unmodified Kapton KN film. The ink drops balled up to form isolated small "islands." On the other hand, after 1, 3, or 4 PEM layers had been deposited on a Kapton HN film, precisely controlled ink squares with sharp edges were able to be printed as designed. A typical GO ink square printed on a Kapton HN film that had been deposited with 4 PEM layers is shown in **Figure 9b**.

For electrically charged ink particles, similar to the bio-enabled method described above, this PEM-based surface modification method can also enhance the uniformity of the inkjet-printed thin films (by reducing the "coffee ring effect" during drying) compared with traditional Kapton surface modification methods.

4.4. Adhesion sustainability tests after chemical functionalization

For sensing applications, GO films normally need to be surface functionalized for the purpose of sensitivity and/or selectivity enhancement. Such surface functionalization includes reduction/oxidation and introduction and/or amplification of particular surface chemical groups

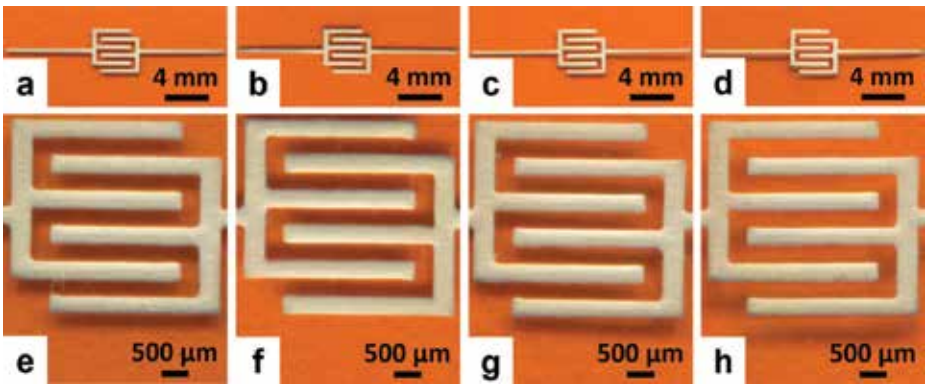

Figure 7. Scanned high-resolution images of silver IDE patterns printed on surface unmodified and PEM-modified Kapton HN films with a commercial ethanediol-based silver nanoparticle ink. (a), (b), (c) and (d) are low magnification images of silver IDEs inkjet-printed on surface unmodified, 1-PEM-layer-modified, 3-PEM-layer-modified and 4-PEM-layer-modified Kapton HN films, respectively. (e), (f), (g) and (h) are the high magnification counterparts of (a), (b), (c) and (d), respectively. All these silver IDE patterns were fabricated by inkjet-printing for 5 passes the silver ink on the appropriate Kapton films followed by drying at 120°C for 3 hours [1] (with permission from the Royal Society of Chemistry).

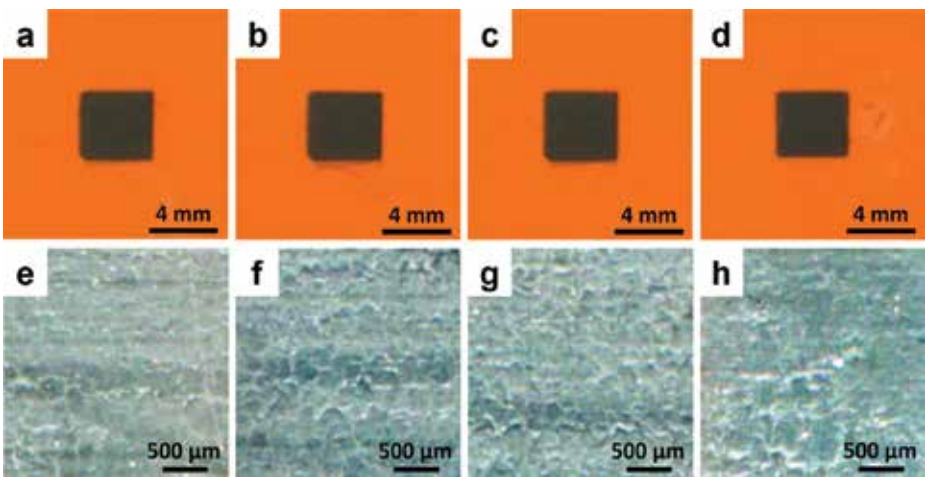

Figure 8. Scanned high-resolution images of graphene patches printed on surface unmodified and PEM-modified Kapton HN films with a cyclohexanone/terpineol-based graphene ink. (a), (b), (c) and (d) are low magnification images of graphene patches inkjet-printed on surface unmodified, 1-PEM-layer-modified, 3-PEM-layer-modified and 4-PEM-layer-modified Kapton HN films, respectively. (e), (f), (g), and (h) are the high magnification counterparts of (a), (b), (c), and (d), respectively. All these graphene patches were fabricated by inkjet-printing for 5 passes the graphene ink on the appropriate Kapton films followed by drying at 100°C for 1 hour [1] (with permission from the Royal Society of Chemistry).

and so on. The adhesion between the inkjet-printed GO films and the substrates has to be strong enough to survive such chemical functionalization.

To assess the adhesion of inkjet-printed rGO-based flexible sensors on Kapton HN substrates after such chemical functionalization, Kapton HN films were first surface modified via three approaches: UV/ozone treatment (traditional method), plasma treatment (traditional method), and the standard PEM-based deposition process described in this work. The UV/ozone treatment was conducted on a 95 mm x 95 mm Kapton HN film with a UVO Cleaner (Jelight Company Inc., Irvine, CA, USA) for 5 min. The plasma treatment was performed on a 95 mm x 95 mm Kapton HN film with a plasma cleaner (model PDC-001. Harrick Scientific Corp., Ossining, NY, USA) in air for 20 min with the RF power set to the "high" level. GO patches were then inkjet-printed on the resulting surface modified Kapton films with the water-based GO ink. The inkjet-printed GO traces were then fired in nitrogen for one hour to be reduced to their rGO counterparts, followed by chemical treatments to introduce various surface chemical functional groups (hexafluoroisopropyl, amine, acrylate, and hydroxyl groups) to the resulting rGO patches.

After the reduction or a GO film functionalization process, the adhesion between the rGO patches and the surface-modified Kapton substrates was evaluated by visual inspection while slowly bending (to a radius of curvature of ˜1 cm) the rGO-on-Kapton structure. The structures were first bent 150 times in tension and then another 150 times in compression. **Table 2** summarizes the results of such adhesion sustainability bend tests. The GO films inkjet-printed on all the surface-modified Kapton HN substrates remained attached to the substrates after the thermal reduction and such bending. After the thermal reduction followed by each of the film functionalization treatments, the GO films printed on the 3-PEM-layer-modified or 4-PEM-layer-modified Kapton HN film remained attached upon bending (**Table 2**). On the other hand, the adhesion of the inkjet-printed GO films on the UV/ozone-, plasma-treated, or 1-PEM-layer-modified Kapton HN substrates was not as universally robust after the thermal reduction followed by the various film functionalization treatments. As shown in **Table 2**, the adhesion sustainability of the inkjet-printed GO films increased with increasing number of PEM layers on the Kapton substrates, which is probably due to the following reasons: each time after a polyelectrolyte (PAA or PEI) had bound to a Kapton HN substrate surface or to the oppositely charged polyelectrolyte which had previously bound to the substrate, there still existed nonoccupied binding

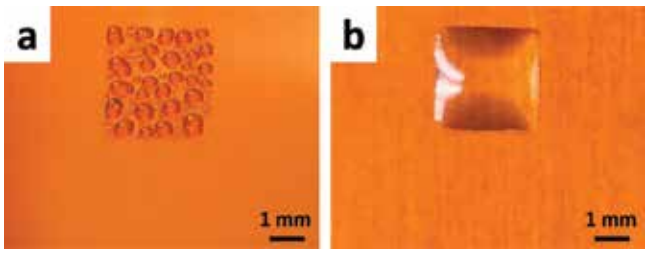

Figure 9. Optical images of GO squares printed (5 passes) with a water-based GO ink on surface unmodified (a) and 4-PEM-layer-modified (b) Kapton substrates [1] (with permission from the Royal Society of Chemistry).

sites (point charges) on the substrate surface [39]. One PEM layer deposited on the substrate would probably be able to cover most (but not all) of the blank Kapton HN surface, which allowed for reasonably good printability for the GO ink. As more PEM layers were deposited, the uncovered substrate surface gradually decreased and the surface positive charge density gradually increased. As a result, when the GO ink particles (negatively charged) were inkjet-printed on, and bound to, such surface modified substrate, the adhesion between the inkjet-printed GO film and the substrate gradually increased.

Modification to GO	**Modification to Kapton**				
	UV/ozone	**Plasma**	**1 PEM layer**	**3 PEM layers**	**4 PEM layers**
Thermal reduction	+	+	+	+	+
Hexafluoroisopropyl addition	—	—	+	+	+
Amine addition	—	—	+	+	+
Acrylate addition	NA	NA	—	+	+
Hydroxyl addition	NA	NA	NA	+	+

Table 2. Adhesion sustainability of GO films on surface-modified Kapton HN substrates upon thermal reduction followed by a number of surface group-introducing reactions ("+": the adhesion survived the corresponding chemical treatment; "—": the adhesion did not survive the corresponding chemical treatment; "NA": the corresponding chemical treatment was not performed since a prior step had peeled the GO film off from the substrate) [1] (with permission from the Royal Society of Chemistry).

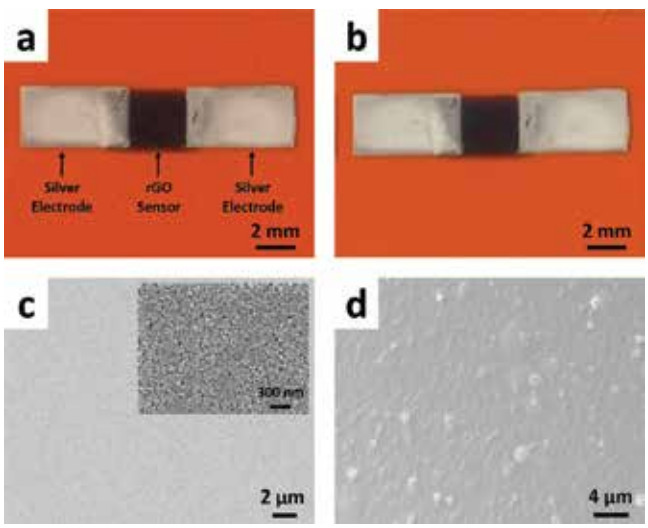

Figure 10. Morphological analyses of a single-layered rGO-based sensor printed on a 4-PEM-layer-modified Kapton HN substrate before and after the bend testing. The water-based GO ink and the ethanediol-based Ag ink were printed for 60 and 5 inkjet passes, respectively. (a) and (b) optical images of the sensor before and after the bend testing, respectively. (c) Low and high (inset) magnification SEM images of a silver IDE of the sensor after the bend testing. (d) SEM image of the rGO patch of the sensor after the bend testing [1] (with permission from the Royal Society of Chemistry).

4.5. Fabrication and bend testing of all-inkjet-printed flexible gas sensors

Single-layered, rGO-based gas sensors were fabricated on a 4-PEM-layer-modified Kapton HN substrate following the procedures described in Section 3.3. A such fabricated sensor, as shown in **Figure 10a**, was subjected to bend testing. The sensor was bent, to a radius of curvature of ~1 cm, 1000 times in tension followed by another 1000 times in compression. During the bending process, conductivity measurements were performed on the sensor after every 50 times of bending. The conductivity of the sensor was found to be virtually the same (i.e. a resistance of ~6 kΩ) throughout the whole bend testing as that before the bending. Optical and SEM microscopic analyses were conducted after such repeated bending to examine the morphology of the sensor. No apparent cracks on either the silver electrodes or the rGO patch were observed and the sensor remained the same morphology as that before the bending (**Figure 10b–d**).

5. Conclusions

The slip additive in Kapton HN films contains a significant amount of crystalline $CaCO_3$. Taking advantage of the electric charges borne by the additive particles at a neutral or acidic pH, two mild and environmentally friendly wet chemical approaches have been recently developed to surface modify Kapton HN films. The resulting surface modified films allowed for not only great printability of both water- and organic solvent-based inks (thus facilitating the full-inkjet-printing of entire flexible electronic devices) but also strong adhesion between the inkjet-printed traces and the substrate films. Different from the traditional Kapton surface modification approaches which target the surface polyimide matrix, these two mild methods targeted the electric charges borne by the additive particles.

The bio-enabled method, which utilized two clinical biomolecules and was conducted in aqueous salt solutions at a neutral pH, room temperature, and atmospheric pressure, was maximally mild and minimally destructive. The flexible rGO-based gas sensors fully inkjet-printed on the resulting surface modified Kapton HN films survived a Scotch-tape peel test and were found insensitive to repeated bending to a small 0.5 cm radius.

The computer-controlled PEM-based method involved the use of only weak polyelectrolytes (to enable systematic and simple control of the PEMs formed via adjustment of the pH of the polyelectrolyte solutions). The adhesion sustainability increased with increasing number of PEM layers. The rGO-based sensors printed on the resulting surface modified (with 4 layers of PEM layers) Kapton HN substrate was insensitive to repeated (1000 times in tension and another 1000 times in compression) bending to a radius of curvature of ~1 cm.

For electrically charged ink particles, both methods can enhance the uniformity of the inkjet-printed films via reduction of the "coffee ring effect" during drying.

The two methods have not only introduced new means to tune the surface properties of Kapton HN films thus allowing for the full-inkjet-printing of flexible and robust electronic devices but also brought forth solutions to significantly reduce of the environmental pollutions associated with inkjet-printing of Kapton-based flexible electronic devices.

Acknowledgements

We thank the financial support from the Defense Threat Reduction Agency (DTRA) (USA) via Award No. HDTRA1-09-14-FRCWMD/TA3.

Conflict of interest

The authors declare no conflict of interests.

Author details

Yunnan Fang[1]* and Manos M. Tentzeris[2]

*Address all correspondence to: yunnan.fang@mse.gatech.edu

1 School of Materials Science and Engineering, Georgia Institute of Technology, Atlanta, Georgia, USA

2 School of Electrical and Computer Engineering, Georgia Institute of Technology, Atlanta, Georgia, USA

References

[1] Fang YN, Hester JGD, deGlee BM, Tuan CC, Brooke PD, Le TR, et al. A novel, facile, layer-by-layer substrate surface modification for the fabrication of all-inkjet-printed flexible electronic devices on Kapton. Journal of Materials Chemistry C. 2016;**4**(29):7052-7060. DOI: 10.1039/c6tc01066k

[2] Fang YN, Hester JGD, Su WJ, Chow JH, Sitaraman SK, Tentzeris MM. A bio-enabled maximally mild layer-by-layer Kapton surface modification approach for the fabrication of all-inkjet-printed flexible electronic devices. Scientific Reports. 2016;**6**:39909. DOI: 10.1038/srep39909

[3] Gouzman I, Girshevitz O, Grossman E, Eliaz N, Sukenik CN. Thin film oxide barrier layers: Protection of Kapton from space environment by liquid phase deposition of titanium oxide. ACS Applied Materials & Interfaces. 2010;**2**(7):1835-1843. DOI: 10.1021/am100113t

[4] Inagaki N, Tasaka S, Hibi K. Surface modification of Kapton film by plasma treatments. Journal of Polymer Science Part A: Polymer Chemistry. 1992;**30**(7):1425-1431. DOI: 10.1002/pola.1992.080300722

[5] Bachman BJ, Vasile MJ. Ion-bombardment of polyimide films. Journal of Vacuum Science & Technology A: Vacuum, Surfaces, and Films. 1989;**7**(4):2709-2716. DOI: 10.1116/1.575779

[6] Shin JW, Jeun JP, Kang PH. Surface modification and characterization of N+ ion implantation on polyimide film. Macromolecular Research. 2010;**18**(3):227-232. DOI: 10.1007/s13233-010-0310-x

[7] Le TR, Lakafosis V, Lin ZY, Wong CP, Tentzeris MM. Inkjet-printed graphene-based wireless gas sensor modules. In: 2012 IEEE 62nd Electronic Components and Technology Conference (ECTC). San Diego, CA, USA: IEEE; 2012

[8] Ghosh I, Konar J, Bhowmick AK. Surface properties of chemically modified polyimide films. Journal of Adhesion Science and Technology. 1997;**11**(6):877-893. DOI: 10.1163/156856197x00967

[9] Huang XD, Bhangale SM, Moran PM, Yakovlev NL, Pan JS. Surface modification studies of Kapton (R) HN polyimide films. Polymer International. 2003;**52**(7):1064-1069. DOI: 10.1002/pi.1143

[10] Thomas RR, Buchwalter SL, Buchwalter LP, Chao TH. Organic-chemistry on a polyimide surface. Macromolecules. 1992;**25**(18):4559-4568. DOI: 10.1021/ma00044a016

[11] Least BT, Willis DA. Modification of polyimide wetting properties by laser ablated conical microstructures. Applied Surface Science. 2013;**273**:1-11. DOI: 10.1016/j.apsusc.2012.12.141

[12] Gallais L, Bergeret E, Wang B, Guerin M, Benevent E. Ultrafast laser ablation of metal films on flexible substrates. Applied Physics A: Materials Science & Processing. 2014;**115**(1):177-188. DOI: 10.1007/s00339-013-7901-2

[13] Ghosh MK, Mittal KL. Polyimides: Fundamentals and Applications. New York, USA: Marcel Dekker; 1996

[14] Williams MK, Smith AE, Huelskamp MA, Armstrong KP, Brandon JL, Lavoie JM. Kapton HN investigations. MOUND. 1990 September;**28**:1990

[15] Zhou LS, Wanga A, Wu SC, Sun J, Park S, Jackson TN. All-organic active matrix flexible display. Applied Physics Letters. 2006;**88**(8). DOI: 10.1063/1.2178213

[16] Ota I, Ohnishi J, Yoshiyam M. Electrophoretic image display (EPID) panel. Proceedings of the IEEE. 1973;**61**(7):832-836. DOI: 10.1109/proc.1973.9173

[17] Gelinck GH, Huitema HEA, Van Veenendaal E, Cantatore E, Schrijnemakers L, Van der Putten J, et al. Flexible active-matrix displays and shift registers based on solution-processed organic transistors. Nature Materials. 2004;**3**(2):106-110. DOI: 10.1038/nmat1061

[18] Granqvist CG. Transparent conductors as solar energy materials: A panoramic review. Solar Energy Materials and Solar Cells. 2007;**91**(17):1529-1598. DOI: 10.1016/j.solmat.2007.04.031

[19] Yoon J, Baca AJ, Park SI, Elvikis P, Geddes JB, Li LF, et al. Ultrathin silicon solar microcells for semitransparent, mechanically flexible and microconcentrator module designs. Nature Materials. 2008;**7**(11):907-915. DOI: 10.1038/nmat2287

[20] Sekitani T, Yokota T, Zschieschang U, Klauk H, Bauer S, Takeuchi K, et al. Organic nonvolatile memory transistors for flexible sensor arrays. Science. 2009;**326**(5959):1516-1519. DOI: 10.1126/science.1179963

[21] Le TR, Lakafosis V, Tentzeris MM, Lin ZY, Fang YN, Sandhage KH, et al. Novel techniques for performance enhancement of inkjet-printed graphene-based thin films for wireless sensing platforms. In: 2013 European Microwave Conference (EuMC); October 6-11 2013; Nuremberg. Germany: IEEE; 2013. pp. 17-20

[22] Shi JD, Li XM, Cheng HY, Liu ZJ, Zhao LY, Yang TT, et al. Graphene reinforced carbon nanotube networks for wearable strain sensors. Advanced Functional Materials. 2016;**26**(13):2078-2084. DOI: 10.1002/adfm.201504804

[23] Fang YN, Akbari M, Sydanheimo L, Ukkonen L, Tentzeris MM. Sensitivity enhancement of flexible gas sensors via conversion of inkjet-printed silver electrodes into porous gold counterparts. Scientific Reports. 2017;**7**. DOI: 10.1038/s41598-017-09174-5

[24] Han TH, Lee Y, Choi MR, Woo SH, Bae SH, Hong BH, et al. Extremely efficient flexible organic light-emitting diodes with modified graphene anode. Nature Photonics. 2012;**6**(2):105-110. DOI: 10.1038/nphoton.2011.318

[25] Schmied B, Gunther J, Klatt C, Kober H, Raemaekers E. STELLA—STretchable ELectronics for large area applications-a new technology for smart textiles. In: Vincenzini P, Paradiso R, editors. Smart Textiles. Advances in Science and Technology. Vol. 60. Stafa-Zurich, Switzerland: Trans Tech Publications Ltd; 2009. pp. 67-73

[26] Myny K, Steudel S, Vicca P, Beenhakkers MJ, van Aerle N, Gelinck GH, et al. Plastic circuits and tags for 13.56 MHz radio-frequency communication. Solid-State Electronics. 2009;**53**(12):1220-1226. DOI: 10.1016/j.sse.2009.10.010

[27] Chen MX. Printed electrochemical devices using conducting polymers as active materials on flexible substrates. Proceedings of the IEEE. 2005;**93**(7):1339-1347. DOI: 10.1109/jproc.2005.851532

[28] Wang PS, Wittberg TN, Wolf JD. A characterization of Kapton polyimide by X-ray photoelectron-spectroscopy and energy dispersive spectroscopy. Journal of Materials Science. 1988;**23**(11):3987-3991. DOI: 10.1007/bf01106825

[29] Hin TY. Materials and processes to enable polymeric waveguide integration on flexible substrates [thesis]. Loughborough: Loughborough University; 2009

[30] McClure DJ. Polyimide film as a vacuum coating substrate. In: Annual Technical Conference Proceedings - Society of Vacuum Coaters; 2010. 53rd ed. pp. 608-12

[31] Halikia I, Zoumpoulakis L, Christodoulou E, Prattis D. Kinetic study of the thermal decomposition of calcium carbonate by isothermal methods of analysis. European Journal of Mineral Processing and Environmental Protection. 2001;**1**(2):89-102

[32] Somasundaran P, Agar GE. The zero point of charge of calcite. Journal of Colloid and Interface Science. 1967;**24**:433-440

[33] Rossmann P, Matousovic K, Horacek V. Protamine-heparin aggregates-their fine-structure, histochemistry, and renal deposition. Virchows Archiv B-Cell Pathology Including Molecular Pathology. 1982;**40**(1):81-98. DOI: 10.1007/bf02932853

[34] Constable S, Winstanley P, Walley T. Medical Pharmacology: A Clinical Core Text for Integrated Curricula with Self Assessment. 3rd ed. Elsevier Limited; 2007

[35] Secor EB, Prabhumirashi PL, Puntambekar K, Geier ML, Hersam MC. Inkjet printing of high conductivity, flexible graphene patterns. Journal of Physical Chemistry Letters. 2013;**4**(8):1347-1351. DOI: 10.1021/jz400644c

[36] Rye RR, Ricco AJ. Patterned adhesion of electrolessly deposited copper on poly(tetrafluoroethylene). Journal of the Electrochemical Society. 1993;**140**(6):1763-1768. DOI: 10.1149/1.2221638

[37] Sener U. Adhesion of Copper to UV Photo-Oxidized Kapton and Upilex-S Polyimide Surfaces [Thesis]. Rochester, NY: Rochester Institute of Technology; 2004

[38] Yoo D, Shiratori SS, Rubner MF. Controlling bilayer composition and surface wettability of sequentially adsorbed multilayers of weak polyelectrolytes. Macromolecules. 1998;**31**(13):4309-4318. DOI: 10.1021/ma9800360

[39] Lowack K, Helm CA. Molecular mechanisms controlling the self-assembly process of polyelectrolyte multilayers. Macromolecules. 1998;**31**(3):823-833. DOI: 10.1021/ma9614454

[40] Amarnath CA, Hong CE, Kim NH, Ku BC, Kuila T, Lee JH. Efficient synthesis of graphene sheets using pyrrole as a reducing agent. Carbon. 2011;**49**(11):3497-3502. DOI: 10.1016/j.carbon.2011.04.048

Chapter 2

Fabrication and Applications of Flexible Transparent Electrodes Based on Silver Nanowires

Peiyun Yi, Yuwen Zhu and Yujun Deng

Additional information is available at the end of the chapter

http://dx.doi.org/10.5772/intechopen.77506

Abstract

There has been an explosion of interests in using flexible transparent electrodes for next-generation flexible electronics, such as touch panels, flexible lighting, flexible solar cells, and wearable sensors. Silver nanowires (AgNWs) are a promising material for flexible transparent electrodes due to high electrical conductivity, optical transparency and mechanical flexibility. Despite many efforts in this field, the optoelectronic performance of AgNW networks is still not sufficient to replace the present material, indium tin oxide (ITO), due to the high junction resistance. Also, the environmental stability and the mechanical properties need enhancement for future commercialization. Many studies have attempted to overcome such problems by tuning the AgNW synthesis and optimizing the film-forming process. In this chapter, we survey recent progresses of AgNWs in flexible electronics by describing both fabrication and applications of flexible transparent AgNW electrodes. The synthesis of AgNWs and the fabrication of AgNW electrodes will be demonstrated, and the performance enhanced by various methods to suit different applications will be also discussed. Finally, technical challenges and future trends are presented for the application of transparent electrodes in flexible electronics.

Keywords: flexible electronics, flexible transparent electrodes, silver nanowires, fabrication, application

1. Introduction

Flexible transparent electrodes are a crucial component in many devices, such as touch screen panels, solar cells, light emitting diodes (LEDs) and flexible sensors [1]. Although Indium tin oxide (ITO) is the dominant material with desirable performance for transparent electrodes currently, an alternative to ITO transparent electrodes has been widely studied in recent years

due to the increasing marketing demand for flexible devices and the brittleness and scarceness of ITO.

Recent studies have suggested carbon nanotubes (CNT) [2, 3], graphene [4] and silver nanowires (AgNWs) [5] as the alternatives. Though CNTs are reported to have good electrical, thermal and mechanical properties, the CNT electrodes show lower electrical conductivity than ITO electrodes due to large contact resistance and extensive bundling of CNTs. Graphene is reported to have high Fermi velocity of 106 m/s and high intrinsic in-plane conductivity. But the large-area production of high-performance graphene films remains a serious issue. Although chemical vapor deposition method has the ability of producing large-area high-performance graphene, the process costs a lot and needs extremely high temperature.

Metallic nanowire based electrodes, as the most promising alternative to ITO, have superior optical, electrical and mechanical properties. Both random and regular metallic nanowire networks have received an increasing interest from both academia and industry. Random metallic nanowires can be dispersed in the solvent and be deposited onto the substrates through low-cost solution-based processing [6]. This makes nanowire-based electrodes compatible for high-throughput and large-area production of the next generation flexible optoelectronic devices. Moreover, for regular metallic nanowire based electrodes, called metal mesh, the electrical conductivity and the optical transparency can be easily tuned by changing the geometry parameter of the nanowires. When the period of the metal mesh is in sub-micrometer scale and the line width is close to subwavelength, metal meshes can be considered as bulk materials to estimate the sheet resistance of the films. Various metallic materials, such as gold, silver and copper, are used to achieve different work functions and chemical properties for various applications. Silver, a material with high electrical conductivity and low price to some degree, is considered as the most suitable nanowire material. And the overall performance of AgNW electrodes has already surpassed that of ITO electrodes. **Table 1** shows the comparison of several transparent electrodes based on different materials.

The present chapter focuses on recent progresses in the fabrication techniques of flexible transparent AgNW electrodes. Firstly, we briefly introduce the requirements of electrical, optical, thermal and mechanical properties for flexible transparent electrodes in different applications. Then synthesis of AgNWs and film-forming techniques of flexible transparent AgNW

Properties	ITO	TCO	CNT	Graphene	AgNW	Ag mesh
Conductivity	++	++	—	—	++	+++
Transmittance	++	+	+++	++	+	+++
Haziness	+	+	++	++	—	—
Flexibility	—	—	+++	+++	+++	—
Stability	+	+	+	++	+++	+++
Large-scale	—	+	++	++	++	—
Low-cost	—	—	—	—	+++	—

Table 1. Comparison of several transparent electrodes.

electrodes will be introduced. Thirdly, recent investigations in optimizing all the properties of flexible transparent electrodes will be discussed in detail. Finally, the future challenges in the widespread adoption of flexible transparent AgNW electrodes will be proposed.

2. Requirements for flexible transparent electrodes in different applications

Flexible transparent electrodes can be applied in many cases. Different properties are required according to different applications subject to various problems, as shown in **Table 2**. In this section, we will introduce some applications such as touch panels, solar cells, flexible lighting, and flexible sensors.

2.1. Touch panels

Touch Display Research Inc. forecasted that the market of transparent electrodes without ITO will reach $13 billion by 2023. The surface area of manufactured touch panels will reach more than 80 km^2 in 2025, double of that in 2014, predicted by IDTechEx Ltd. [7]. Companies like Samsung, LG, Apple and Toshiba have all indicated the market trends for flexible displays. Touch screens can be divided into capacitive sensing and resistive sensing by different working principles. When fingers touch the screen, the capacitive sensing works on the change in capacitance instead of the change in resistance as the resistive sensing does. Resistive sensing is low-cost and high-resolution reported by S.H. Ko's team [8, 9]. With the durability and the compatibility of multi-touch features, the capacitive sensing arises many researchers' attention worldwide. Capacitive touch panels can now be divided into single [10–12] and double-sided sensors [13, 14] based on the number of transparent conductive layers. **Figure 1(a)** and **(b)** show the photograph of the working touch panel [10]. The resolution of single-sensor capacitive touch screen is required to be at the millimeter scale while that of double-sided ones is hundreds of micrometers. Not only the distribution but also the orientation and alignment will govern the performance of the AgNW networks. Patterning is also of prime importance for high performance. **Figure 1(c)** exhibits the design of touch sensors and the image

Properties	ITO	TCO	CNT	Graphene	AgNW	Ag mesh
Conductivity	++	++	-	---	++	+++
Transmittance	++	+	+++	++	+	+++
Haziness	+	+	++	++	---	---
Flexibility	---	---	+++	+++	+++	-
Stability	+	+	+	++	+++	+++
Large-scale	-	+	++	++	++	-
Low-cost	---	-	-	---	+++	---

Table 2. Comparison of performance requirements for different applications.

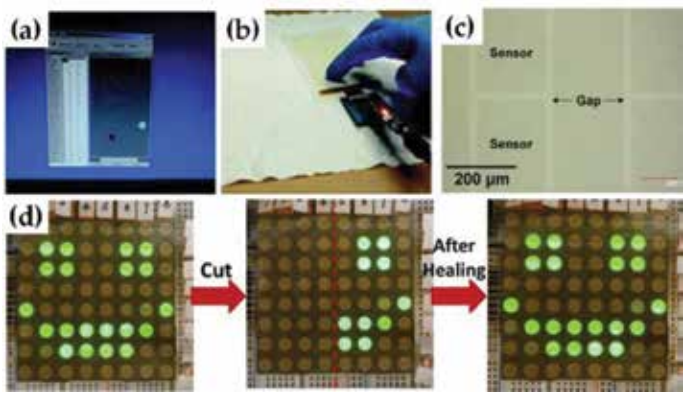

Figure 1. Photographs of touch panels: (a-b) photograph of working capacitive touch panels [10], (c) the patterned AgNW network [12], and (d) healable touch sensor [14].

of patterned AgNW networks respectively [12]. Interestingly, healable touchscreens were produced by Pei and co-workers through embedding AgNWs into the surface of healable polymer substrate [14], as shown in **Figure 1(d)**.

2.2. Solar cells

Flexible transparent electrodes as front electrodes is a crucial factor in determining photo-conversion efficiency of solar cells [15]. High electrical conductivity and high optical transparency of flexible transparent electrodes are required in order to lower the ohmic dissipation of heat and maximize the light absorption in the conversion layer. The band alignment and work function of the electrodes should also be considered. The most commonly used materials for solar cells are doped metal oxides. They are prone to cracking, costly and need high-temperature fabrication. Many researches have proved that AgNW networks are a promising alternative to ITO for both organic solar cells [16–18] and polymer solar cells [19]. AgNW networks have similar photovoltaic performances and excellent bending capacities as ITO and are compatible with solution-processed fabrication. And unlike doped metal oxides, AgNWs have high optical transparency in the IR range, leading to enhanced efficiency and the semi-transparency of solar cells. The performance comparison in solar cells using AgNW electrodes

PCE(%)	Jsc(mA/cm²)	Voc(V)	FF(%)	Ref
1.85	−7.22	0.5308	48.475	[20]
6.58	14.29	0.78	59	[1]
3.05	9.191	0.638	0.521	[21]
2.73	8.4	0.58	56.07	[22]
2.66	6.36	1.06	39.59	[19]

PCE: power conversion efficiency, Jsc: short-circuit current density, Voc: open-circuit voltage, FF: fill factor.

Table 3. Performance comparison in solar cells.

is shown in **Table 3**. Topics concerning the integration of transparent AgNW electrodes into flexible solar cells are as follows: one is the low-cost fabrication for the development of flexible solar cells and another one is the study of plasmonic effects to further control the optoelectronic properties.

2.3. Flexible lighting

AgNW electrodes can be integrated into LEDs. **Figure 2(a)** shows the schematic of AlGaN-based LEDs with AgNW/ITO electrodes [23]. The active layer of the light emitting devices mostly investigated can be organic materials (OLEDs) or polymer (PLEDs). The emulation of fully rollable lighting panels is time-to-market dependent on our ability to provide not only the active layer but also the interfaces and the transparent electrodes with high flexibility. In this case, it is essential for the transparent electrodes to have no alteration in optoelectronic properties under bending cycles. For conventional ITO-based OLEDs, the luminance and the efficiency of the devices would have a sharp decrease under mechanical stress due to the fracture of the brittle ITO electrodes. Thus the usage of AgNW electrodes with good optoelectronic and mechanical properties seems to be a good strategy to fulfill this demand. Polyvinyl alcohol (PVA) [24], polyacrylate [25], poly(methyl methacrylate) (PMMA) [26], colorless polyimide (cPI) [27] and poly(urethane acrylate) (PUA) [28, 29] are used to produce the transparent electrodes together with AgNWs to improve the performance of electrodes. For instance, AgNW/PMMA OLEDs show high luminous efficiency, the color-independent emission and the nearly perfect Lambertian emission [26], as depicted in **Figure 2(b)**. Many efforts have been done to decrease the current leakage [30, 31]. **Table 4** illustrates the performance comparison of LEDs produced by different researchers. The challenge of keeping the performance of AgNW-based OLEDs unchanged under deformation also arises many researchers' attention [28].

2.4. Flexible sensors

High sensitive and stretchable sensors can be used in both our daily life and large military projects, from the human health monitoring devices to the structural health monitoring of aircrafts and bridges [36–38]. **Figure 3(a)** shows a strain sensor attached to the neck to monitor human activities [39]. And as shown in **Figure 3(b)**, AgNW electrodes can be integrated

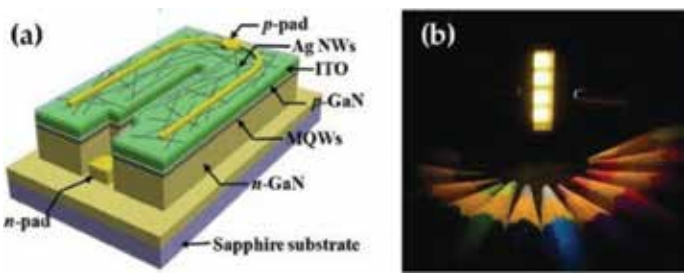

Figure 2. Light emitting diodes with AgNW electrodes: (a) the schematic of LEDs with AgNW/ITO electrodes [23], and (b) the angular dependence property of white OLEDs [26].

Category	Vc(V)	EQE(%)	CE(cd/A)	PE(lm/W)	Ref
OLED	NA	NA	58.2	NA	[32]
OLED	NA	18.7	68.6	62.8	[33]
OLED	6	24.3	49	30.3	[26]
PLED	0.6	NA	NA	NA	[34]
LED	2.72	NA	NA	NA	[35]
OLED	3.6	NA	44.5	35.8	[30]

Vc: turn on voltage, EQE: external quantum efficiency, CE: current efficiency, PE: power efficiency.

Table 4. Performance comparison in LEDs.

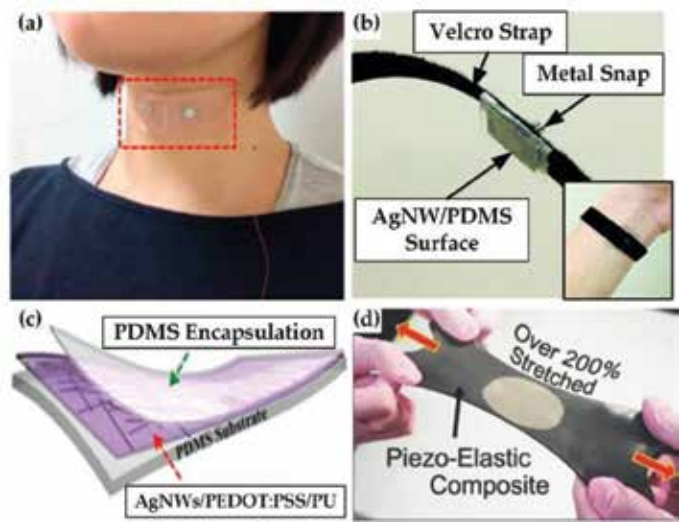

Figure 3. The schematic and photograph of flexible AgNW sensors: (a) photograph of strain sensor attached to the neck [39], (b) AgNW dry electrode for ECG measurements [38], (c) the schematic diagram of strain sensor [39], and (d) the schematic illustration of highly-stretchable nanocomposite generator [45].

into electrocardiogram (ECG) measurements [38]. Performances of flexible sensors concern about the linearity, sensitivity, detecting range, response time, stability and stretchability. Investigations using AgNW electrodes mainly concern about strain sensors [40, 41], pressure sensors [40] and electrochemical sensors [42]. Yao et al. presented wearable sensors based on highly stretchable AgNW electrodes enabling the detection of strain and pressure [40]. The strain sensors produced showed good linearity and reversibility even up to a large strain of 50%. At the same time, the pressure under detection ranged up to 1.2 MPa. Hwang et al. have recently developed a self-powered patchable platform to monitor human activities [39], as shown in **Figure 3(c)**. Usually, the stretchability of the transparent systems has been reported to be among 50–90% [43, 44]. The high stretchability is achieved by compositing AgNWs with a thin layer of elastomer [39, 41]. In particular, Jeong et al. integrated ultra-long AgNWs into an elastic-composite generator which exhibits hyper-stretchability up to 200% [45], as shown

in **Figure 3(d)**. In addition to stretchability, the sensitivity can be tuned by controlling the areal density and roughness of AgNW networks [46]. Further optimization of geometry and materials is needed in this field.

3. Fabrication of flexible transparent electrodes based on silver nanowires

3.1. Controllable synthesis of silver nanowires

Many approaches have been addressed to synthesize AgNWs, which can be mainly divided into two groups: template methods and polyol process [47]. Template methods are classified into two categories, in terms of hard templates and soft templates. Soft templates include polymer film of PVA and DNA chains [48, 49]. Hard templates include silicon wafer and aluminum oxide [50, 51]. Although many literatures have investigated template methods to synthesize AgNWs, these methods are incompatible for large-scale production. The preparation and removal of the templates are time consuming and high cost. Moreover, nanowires synthesized through template methods suffer from low aspect ratio, irregular morphology and low yield.

Different from template methods, polyol process provides high yield of nanowires with ideal morphology. As the most promising synthetic procedure, salt-mediated polyol method [52, 53] has good reproducibility and low cost. The usage of salts, such as NaCl [54], $CuCl_2$ [53], CuCl [53], $FeCl_3$ and $PtCl_2$, helps the mass synthesis of AgNWs. Metal seeds in the solution served as nuclei for subsequent growth of AgNWs, as depicted in **Figure 4(a)**. The dimensions of AgNWs can be kinetically controlled by temperature, seeding conditions, and the ratio between PVP and $AgNO_3$. High reaction temperature leads to the formation of nanowires with low aspect ratio. Increasing the concentration of metal seeds could slightly decrease the diameter of nanowires. Chen et al. [55] adjust the concentration of Na_2S to control the diameter of AgNWs. The aspect ratio of the nanowires is small, unable to meet the requirements for high aspect ratio nanowires. Microwave and UV irradiation have been adopted by researchers to assist the synthesis of AgNWs [56–58]. The controllable methods to fabricate high aspect ratio nanowires have received much attention. Long nanowires with length of over 300 μm were fabricated by Lee et al. [59] using a successive multistep growth method, as shown in **Figure 4(b)**. The fabrication process is time-consuming and complex. Then Andrés et al. [60] demonstrated a rapid synthesis of nanowires with the length reaching 190 μm to overcome this problem.

3.2. Coating techniques

Apart from the synthesis of AgNWs, coating and printing them onto the flexible plastic substrate is also an essential process in the fabrication of transparent electrodes. The performance of the electrodes varies according to different techniques and devices. The ideal process should meet three requirements: (1) the process should be free from toxic chemicals and costly materials; (2) the process should have a low environmental impact and can be recycled; (3) the process should meet the demand of the large-area, high-efficiency and high-quality production. Solution-processed fabrication can easily be surface scalable. Many solution processes have been reported to produce

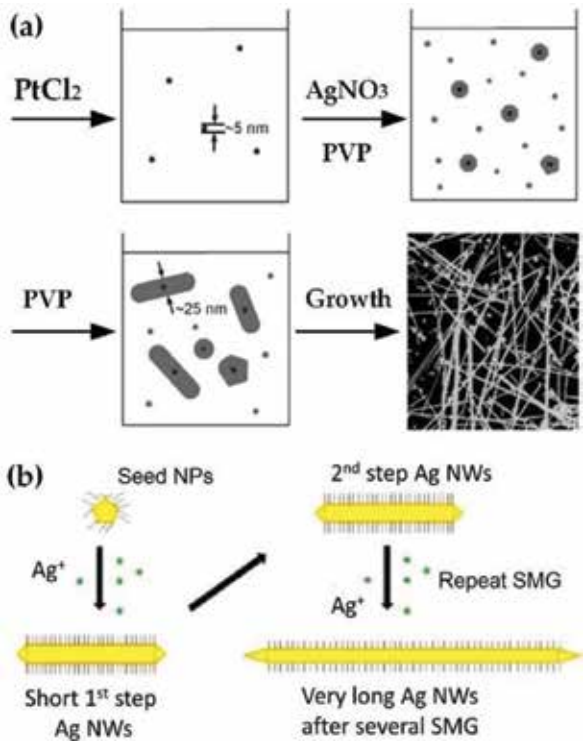

Figure 4. AgNW synthesis: (a) the polyol process of AgNW synthesis [61], and (b) the schematic diagram of a multistep synthesis of ultra-long AgNWs [59].

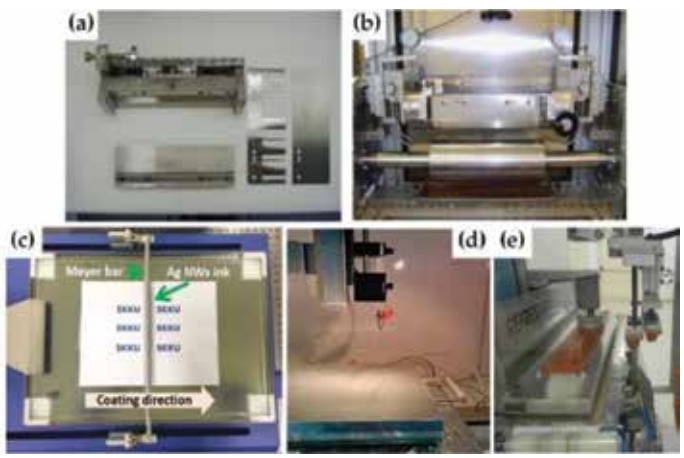

Figure 5. Equipments of different coating techniques: (a) parts of slot-die coating device [77], (b) slot-die coating device [77], (c) Meyer rod coating device [78], (d) electrostatic spray system [79], and (e) pad printer [80].

AgNW electrodes, including Meyer rod coating [5, 33, 62, 63], dip coating [64], spin coating [65–67], drop casting [68], spray coating [69], vacuum filtration [70], roll-to-roll printing [19, 71, 72] and transferring [73, 74]. **Figure 5(a)-(e)** show coating devices with different techniques. Most of the

techniques are compatible with low-energy deposition process and without any vacuum equipment. Direct laser ablation [13, 75], shadow mask [11], chemical etching using the photolithography process [76] are all the patterning strategies for flexible transparent electrodes.

3.2.1. Roll-to-roll techniques

The processability of AgNW networks by R2R was showed by many researchers due to their compatibility with large-area production [81–83]. The substrate in R2R coating system is required to have mechanical flexibility and in the form of a long sheet. Quite different from other solution-processed coating methods, the R2R process is continuous and is suitable for large-area production. During coating, the substrate is first unwound from a roll and then passed through the coating machine and finally rewound on another roll. Aside from the coating machine, some post-treatment may also be added into the process, such as compressing, heating, UV-curing, chemical welding and drying, as shown in **Figure 6(a)** [83]. Interestingly, Lai's team produced AgNW electrodes combined with moth-eye nanostructures using R2R techniques and greatly enhanced the transmittance [5, 81]. The quality of forming can be influenced by tension, speed, cleaning of the substrate and the removal of static electricity. Also, the pre-treatment and post-treatment can have a great impact on the performance of the coated AgNW films. Many laboratories have developed their own R2R system to study the coating process. **Figure 6(b)-(d)** show two laboratory-scale coating system [77, 84]. Hösel et al. have compared the performance of flexible electronics produced by R2R process [85]. The biggest challenge of R2R process is the unification problem [86]. The comparison between different printing methods for large-scale R2R production was reported in Roll-to-Roll Processing Technology Assessment by U.S. Department of Energy, as shown in **Table 5** [87].

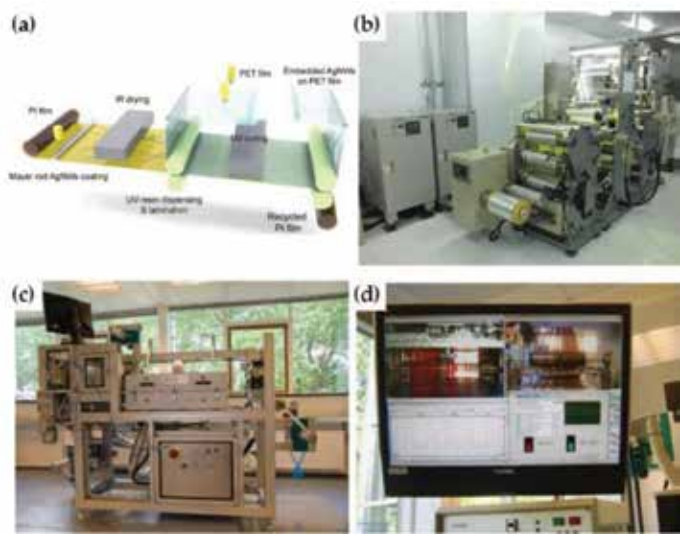

Figure 6. The schematic and equipment of roll-to-roll fabrication process: (a) the schematic [82], (b) photograph of the R2R system [84], (c) a laboratory-scale coating system from solar coating machinery GmbH, Germany [77], and (d) photograph of the monitoring during coating [77].

Printing method	Speed	Wet thickness	Resolution (μm)	Start/Stop	Complexity	Applicability
Flatbed Screen Printing	Low	5–100 μm	100 μm	Yes	Low	Limited
Rotary Screen Printing	High	3–500 μm	100 μm	Yes(a)	Medium	Very good
Inkjet Printing	Medium	1–5 μm	< 50 μm	Yes	High	Limited, materials must be jettable
Flexography	Very high	1–10 μm	< 50 μm	Yes(a)	Medium	Very good
Imprint or soft lithography	High (> 5m/min)	NA	0.1 μm	NA	NA	New technology
Laser ablation	Low	NA	~10	NA	NA	Thermal effect sensitivity
Gravure	High	NA	> 0.07 μm	NA	NA	Very good

(a)-Stopping should be avoided. Risk of registration lost and drying of ink in anilox cylinder. Short run-in length. NA-not available.

Table 5. Comparison between different printing methods in terms of their theoretical capacity and practical applicability for large-scale R2R production [87].

3.2.2. Drop casting

Drop casting is the simplest method to produce flexible transparent electrodes. The equipment needed is only a horizontal work platform. What we need to do is casting the coating solution onto the substrate followed by drying. However, problems exist due to the simple procedure. The thickness of the film is unable to be controlled. The effect of "coffee-ring" may be easily observed causing uneven distribution of nanowires due to the surface tension of the liquid and the self-aggregation of nanowires upon drying.

3.2.3. Spin coating

Spin coating is an important way to form homogeneous film. As illustrated in **Figure 7(a)**, the substrate is first accelerated to a chosen rotational speed and then the coating solution is applied onto the substrate [86]. Noticeably, most of the coating solution is ejected and only a little of the solution is left on the substrate to form a thin film. **Figure 7(b)-(f)** show the spin coating operation and the high speed images with different timing after the first drop [86]. Spin coating is high reproducible. The forming quality of spin coating can be measured by the thickness, morphology and the surface topography of the film coated. All these properties can be tuned by controlling the coating solution, the substrate and the rotational speed. Specially, the molecular weight, viscosity, diffusivity, volatility and concentration of the solutes all have impact on the final forming results.

3.2.4. Screen printing

Screen printing has a large wet film thickness. The coating ink used needs to have a high viscosity and low volatility. First, the screen should be under tension by being glued to a frame. Second, an emulsion is filled into the screen to obtain the pattern. Here the area of the emulsion should be with no print and the area of the pattern is open waiting for the coating ink.

http://dx.doi.org/10.5772/intechopen.77506

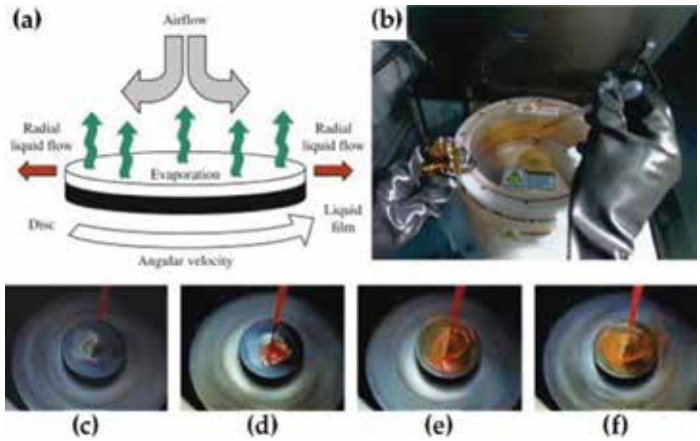

Figure 7. Spin coating: (a) the schematic, (b) photograph of the operation, and (c-f) high-speed images with the timing after the first drop of 17, 100, 137 and 180 ms [86].

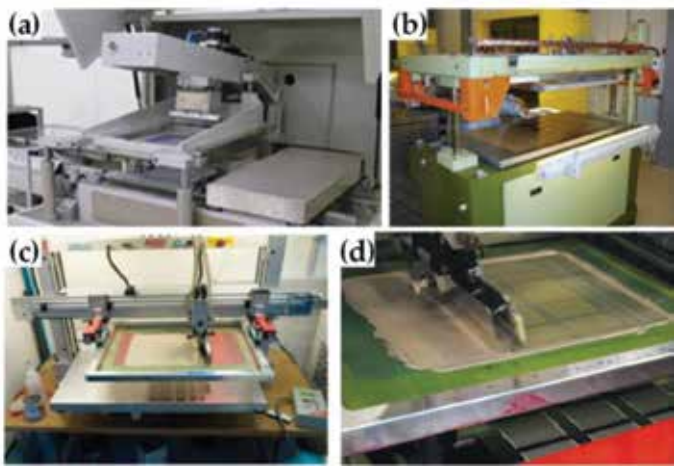

Figure 8. Photographs of screen printers and the coating process: (a-b) pictures of industrial screen printers [80, 86], (c) screen printing of silver nanowires in the laboratory [77], and (d) a close photograph showing screen printing [88].

Third, the patterned electrodes is obtained by filling the screen with coating ink. **Figure 8(a)-(c)** show screen printers both in laboratories and factories, while **Figure 8(d)** shows the screen printing process.

4. Performance enhancements of flexible transparent electrodes

4.1. Optoelectronic properties

The optimization of the optoelectronic properties has been studied for many years. Since junction resistance plays an important role in the electrical properties of the whole network, decreasing

the number of junctions and reducing the junction resistance between wires are two main ideas to lower the sheet resistance of the film. In order to decrease the number of junctions, some researchers have studied different approaches to synthesize nanowires with high aspect ratio [59, 60, 89], which have been introduced in Section 3.1. Researchers have also devoted great efforts to decrease the junction resistance between nanowires. Methods such as vacuum filtration [90], graphene coating [91, 92], electrochemical coating [93], modification with graphene oxide (GO) [29] and deposition of particles like Au, ZnO and TiO_2 [94] have been performed in the fabrication of transparent electrodes to reduce the resistance. Liang et al. wrapped the GO sheet around AgNW junctions and obtain a flexible transparent electrodes with the sheet resistance of 14 Ω/sq. and the transmittance of 88%, as shown in **Figure 9(a)** [29]. Many post-treatments such as thermal annealing [24], pressing [95], electrochemical annealing [96], salt treatment [83, 90], plasmonic welding [97], HCl vapor treatment, capillary-force-induced cold welding [63] and high intensity pulsed light technique(HIPL) [98, 99] have also been studied to reduce the junction resistance. **Figure 9(b)** and **(c)** show the obvious changes of AgNW junctions after hot-pressing. Lee et al. [6] demonstrated that annealing of the nanowire network at the temperature of 200°C causes the PVP to flow and partially decompose, leading AgNWs to fuse together. However, thermal annealing needs high temperature and long treatment time. It also cannot be employed with heat-sensitive substrates. Tokuno et al. [100] performed two steps to replace the heat treatment in the fabrication of transparent electrodes. The network was first rinsed with water and ethanol to remove the PVP followed by mechanical pressing to weld the wires. The sheet resistance was

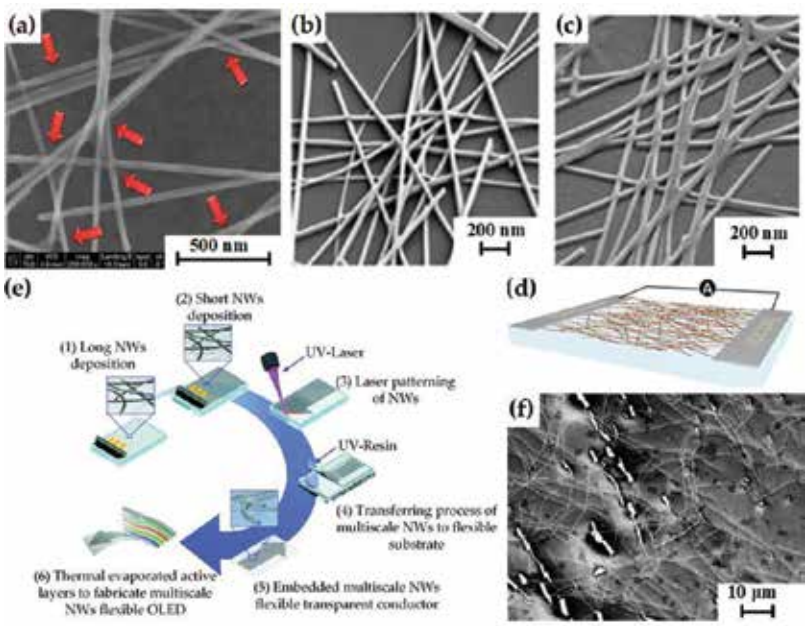

Figure 9. Different methods to improve the optoelectronic properties of flexible transparent AgNW electrodes: (a) SEM observation of AgNW networks with GO surrounding AgNW junctions [29], (b-c) SEM images of AgNW networks before and after hot-pressing [32], (d) a schematic diagram of electrowelding treatment [101], (e) illustration of the procedure used for the preparation of dual-scale nanowire networks [33], and (f) SEM image of AgNWs bridging graphene grains [104].

reduced from 6.9×10^6 to 1.8×10^4 Ω/sq. and then to 8.6 Ω/sq. However, mechanical pressing may not suitable for delicate substrates. Thus some other different approaches such as joule heating, HIPL, moisture-treating and hybridization with mesoscale wires, have been explored. Song et al. [101] apply the idea that joule heating can weld platinum wires and carbon nanotubes into the metallic nanowire networks. An approach with low additional power and short treatment durations is achieved by current-assisted localized joule heating accompanied by electromigration, as shown in **Figure 9(d)**. The resistance of individual nanowires is also investigated by researchers, such as the utilization of nanowires with large gain size [102] and the hybridization of different scale wires [33, 103]. **Figure 9(e)** shows the procedure used to produce dual-scale nanowire networks [33]. Many investigations also focus on hybridizing AgNWs with other conductive materials. AgNWs were treated as bridges for high resistance grain boundaries of graphene by Teymouri et al. to obtain highly transparent electrodes, as shown in **Figure 9(f)** [104].

Besides the electrical properties, many efforts have been done by researchers to improve the optical transparency of AgNW electrodes. Firstly, the dimensions of AgNWs are optimized for high transmittance. Nanowires networks with large aspect ratio show better optical property [105]. Secondly, different deposition process has been explored. Kim et al. [79] applied the electrostatic spray deposition to obtain electrodes with the transmittance of 92.1%. Thirdly, changing substrates into more transparent materials. Jiang et al. [106] changing the commonly used polyethylene terephthalate (PET) substrate into the flexible resin film and improve the transmittance by nearly 10%. Kim et al. integrated CNT into AgNW electrodes to reduce the haze factor by absorbing the scattered light from AgNWs [107]. **Table 6** illustrates the performance comparison in AgNW electrodes.

4.2. Environmental stability

Though environmental stability seems to be important for future application, few investigations have been reported so far on it compared to the optoelectronic performance. The

NW dimensions	Substrate	Rs (Ω/sq)	T (%)	Ref.
D 20–40 nm, L 20–40 μm	Glass/PET	91.3	97.9	[108]
D 35 nm, L 25 μm	PET	~50	94.5	[1]
D 25 nm, L 35 μm	PET	~20	86	[5]
D 20–90 nm, L 20–150 μm	PDMS	179	89.4	[63]
D 100 nm, L 100 μm and D 40 nm, L 10 μm	Resin	50	90	[33]
D 50–90 nm, L 15–25 μm	PEN	12	83	[32]
D 70 nm, L 8 μm	glass	6–21	70–85	[21]
D 70 nm, L 10–20 μm and D 85 nm, L 30–60 μm	PU	6	68	[98]
D 70 nm, L 200 μm	No data	<30	95	[104]
Not available	Glass	11	87	[34]
D 115 nm, L 20–50 μm	PET/PEN	5	92	[83]

Table 6. Performance comparison in AgNW electrodes.

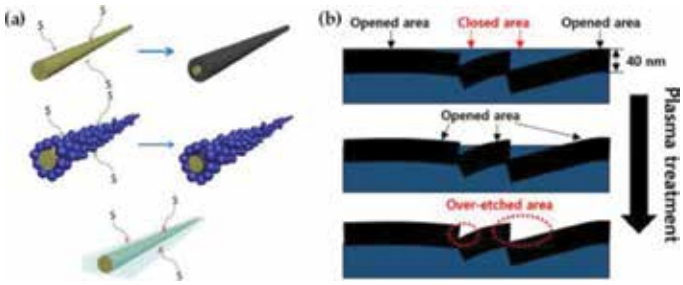

Figure 10. Schematic of the mechanism for treatments used to improve environmental stability and mechanical properties: (a) the protection mechanism for the nanoparticle coating and sol–gel TiO_2 coating [110], and (b) the conductive pathway enlarging mechanism for the plasma treatment on AgNW-cPI composite electrodes [27].

thermal conductivity of AgNWs and their degradation mechanism is lack of investigations. Mayousse et al. spend over 2 years to study the relationship between the stability of AgNW networks and the temperature, humidity, light, hydrogen sulfide and electrical stress [11]. Khaligh et al. [109] once modeled the random AgNW networks in MATLAB and analyzed the overall circuit with HSPICE. In their work, graphene can slow the degradation of AgNWs and uniform the surface temperature. In this case, the failure mechanism is not the nanowire degradation any more. It is changed into the melting of the substrate. Thus the most commonly used method is to use hybrid materials to improve both thermal and chemical stability. Also, the aging of flexible transparent electrodes under different working conditions is now lack of research. Song et al. compared the environmental stability of nanowires with nanoparticle coating and sol–gel TiO_2 coating [110]. As shown in **Figure 10(a)**, AgNWs can easily react with sulfur ions to form Ag_2S (dark gray). Nanoparticles can reduce the exposure area but are unable to diminish the whole area. AgNWs with nanoparticles coating can still react with sulfur ions. The sol–gel TiO_2 avoid AgNWs being exposed to sulfur ions and improve the chemical durability of AgNWs.

4.3. Mechanical properties

The sheet resistance of transparent AgNW electrodes shows negligible increase under bending test, quite different from that of ITO electrodes. AgNWs are able to conform to non-planar surface. They can easily fit to the surface, even the highly roughened surface. Though the flexibility makes AgNW a promising alternative to ITO, the high roughness of the network remains a serious problem which hinders the development of AgNW electrodes. The high roughness would lead to interlayer shorting, high leakage currents, and low quantum efficiency in OLEDs [33]. The buffer layer and the conductive material coating are investigated by many researchers to reduce the roughness of the networks [111–114]. Nevertheless, they would degrade the performance by increasing the driving voltage and the electron–hole imbalance [30]. Burying AgNW into polymer substrate is also a way to reduce the roughness, but the effective electrode areas decreased [33]. In order to overcome this problem, the plasma treatment was applied on AgNW-cPI composite electrodes to enlarge the conductive

pathways, as shown in **Figure 10(b)** [27]. Intense-pulsed-light irradiation and the UV-Ozone treatment are also ways to smooth the film without any severe deterioration in the optical performance [22, 115].

The poor adhesion to substrates, together with the roughness and reduced effective electrical area, hinders the widely application of AgNW electrodes. Strong bonding is essential to avoid detachment of AgNW networks and maintain electrical conductivity at high strain deformation. Modifying substrate surface [74, 116], applying strong conformal pressure, in situ polymerization [24, 25, 94] and surface encapsulation [71] can effectively improve the adhesion. These methods are complex and time consuming, together with changing the properties of the substrates. In recent papers, some new methods have also been put forward. It is a fast and simple method compared with conventional approaches embedding nanowires into polymers [98]. Khan et al. [117] proposed a facile method to make the nanowires a nail-like structure which can be fully embedded in plastic films, greatly enhancing the wire-substrate adhesion.

5. Conclusion

The aim of this chapter is to demonstrate the fabrication techniques of flexible transparent AgNW electrodes and the efforts made to enhance the performance. Though AgNW electrodes reported exhibit similar performances to ITO electrodes, there is still a long way to go for future commercialization. Firstly, new synthesis methods for fine-tuning the dimensions of AgNWs are needed. The performances of AgNW electrodes have a close relationship with the dimensions of AgNWs. Secondly, metals other than silver need investigations to reduce the cost of electrodes with similar performances, such as copper. Thirdly, the hybrid materials, such as core-shell Cu-Ni nanowires and sandwich structure, are also of interest. Fourthly, the stability optimization in real environments is lacking now. The evaluation of the intrinsic stability is an important value to prove the possibility of integrating nanowires into future devices. Finally, the toxicity of nanowires needs attention before being integrated into commercial devices.

Acknowledgements

This study was supported by the National Natural Science Foundation of China (51675334).

Conflict of interest

There are no conflicts of interest.

Author details

Peiyun Yi[1,2]*, Yuwen Zhu[1] and Yujun Deng[1]

*Address all correspondence to: yipeiyun@sjtu.edu.cn

1 State Key Laboratory of Mechanical System and Vibration, Shanghai Jiao Tong University, Shanghai, P.R. China

2 Shanghai Key Laboratory of Digital Manufacture for Thin-Walled Structures, Shanghai Jiao Tong University, Shanghai, P.R. China

References

[1] Wang J, Fei F, Luo Q, Nie S, Wu N, Chen X, et al. Modification of the highly conductive PEDOT:PSS layer for use in silver nanogrid electrodes for flexible inverted polymer solar cells. ACS Applied Materials & Interfaces. 2017;**9**(8):7834-7842. DOI: 10.1021/acsami.6b16341

[2] Zhu G, Wang H, Zhang L. A comparative study on electrosorption behavior of carbon nanotubes electrodes fabricated via different methods. Chemical Physics Letters. 2016;**649**:15-18. DOI: 10.1016/j.cplett.2016.02.027

[3] Imazu N, Fujigaya T, Nakashima N. Fabrication of flexible transparent conductive films from long double-walled carbon nanotubes. Science and Technology of Advanced Materials. 2016;**15**(2):025005. DOI: 10.1088/1468-6996/15/2/025005

[4] Kobayashi T, Bando M, Kimura N, Shimizu K, Kadono K, Umezu N, et al. Production of a 100-m-long high-quality graphene transparent conductive film by roll-to-roll chemical vapor deposition and transfer process. Applied Physics Letters. 2013;**102**(2):023112. DOI: 10.1063/1.4776707

[5] Zhang C, Zhu Y, Yi P, Peng L, Lai X. Fabrication of flexible silver nanowire conductive films and transmittance improvement based on moth-eye nanostructure array. Journal of Micromechanics & Microengineering. 2017;(7):27

[6] Lee JY, Connor ST, Cui Y, Peumans P. Solution-processed metal nanowire mesh transparent electrodes. Nano Letters. 2008;**8**(2):689-692. DOI: 10.1021/nl073296g

[7] Ghaffarzadeh K, Yamamoto Y, zervos H. Conductive Ink Markets 2016-2026. Boston, MA, USA: Forcasts, Technologies, Players, IDTechEx Ltd; 2016

[8] Lee J, Lee P, Lee HB, Hong S, Lee I, Yeo J, et al. Room-temperature nanosoldering of a very long metal nanowire network by conducting-polymer-assisted joining for a flexible touch-panel application. Advanced Functional Materials. 2013;**23**(34):4171-4176. DOI: 10.1002/adfm.201203802

[9] Lee J, Lee P, Lee H, Lee D, Lee SS, Ko SH. Very long ag nanowire synthesis and its application in a highly transparent, conductive and flexible metal electrode touch panel. Nanoscale. 2012;**4**(20):6408

[10] Kim Y, Song C-H, Kwak M-G, Ju B-K, Kim J-W. Flexible touch sensor with finely patterned ag nanowires buried at the surface of a colorless polyimide film. RSC Advances. 2015;**5**(53):42500-42505. DOI: 10.1039/c5ra01657f

[11] Mayousse C, Celle C, Moreau E, Mainguet JF, Carella A, Simonato JP. Improvements in purification of silver nanowires by decantation and fabrication of flexible transparent electrodes. Application to capacitive touch sensors. Nanotechnology. 2013;**24**(21):215501. DOI: 10.1088/0957-4484/24/21/215501

[12] Kim Y, Kim J-W. Silver nanowire networks embedded in urethane acrylate for flexible capacitive touch sensor. Applied Surface Science. 2016;**363**:1-6. DOI: 10.1016/j.apsusc.2015.11.052

[13] Cann M, Large MJ, Henley SJ, Milne D, Sato T, Chan H, et al. High performance transparent multi-touch sensors based on silver nanowires. Materials Today Communications. 2016;**7**:42-50. DOI: 10.1016/j.mtcomm.2016.03.005

[14] Li J, Liang J, Li L, Ren F, Hu W, Li J, et al. Healable capacitive touch screen sensors based on transparent composite electrodes comprising silver nanowires and a furan/maleimide Diels–Alder cycloaddition polymer. ACS Nano. 2014;**8**(12):12874-12882. DOI: 10.1021/nn506610p

[15] Yim JH, S-y J, Pang C, Lee KM, Jeong H, Park J-Y, et al. Fully solution-processed semitransparent organic solar cells with a silver nanowire cathode and a conducting polymer anode. ACS Nano. 2014;**8**(3):2857-2863. DOI: 10.1021/nn406672n

[16] Choi K-H, Kim J, Noh Y-J, Na S-I, Kim H-K. Ag nanowire-embedded ITO films as a near-infrared transparent and flexible anode for flexible organic solar cells. Solar Energy Materials and Solar Cells. 2013;**110**:147-153. DOI: 10.1016/j.solmat.2012.12.022

[17] Guo F, Zhu X, Forberich K, Krantz J, Stubhan T, Salinas M, et al. ITO-free and fully solution-processed semitransparent organic solar cells with high fill factors. Advanced Energy Materials. 2013;**3**(8):1062-1067. DOI: 10.1002/aenm.201300100

[18] Leem DS, Edwards A, Faist M, Nelson J, Bradley DD, de Mello JC. Efficient organic solar cells with solution-processed silver nanowire electrodes. Advanced Materials. 2011;**23**(38):4371-4375. DOI: 10.1002/adma.201100871

[19] Angmo D, Andersen TR, Bentzen JJ, Helgesen M, Søndergaard RR, Jørgensen M, et al. Roll-to-roll printed silver nanowire semitransparent electrodes for fully ambient solution-processed tandem polymer solar cells. Advanced Functional Materials. 2015;**25**(28):4539-4547. DOI: 10.1002/adfm.201501887

[20] Gupta R, Walia S, Hösel M, Jensen J, Angmo D, Krebs FC, et al. Solution processed large area fabrication of ag patterns as electrodes for flexible heaters, electrochromics and organic solar cells. Journal of Materials Chemistry A. 2014;**2**(28):10930-10937

[21] Karakawa M, Tokuno T, Nogi M, Aso Y, Suganuma K. Silver nanowire networks as a transparent printable electrode for organic photovoltaic cells. Electrochemistry. 2017; **85**(5):245-248. DOI: 10.5796/electrochemistry.85.245

[22] Wang D, Zhou W, Liu H, Ma Y, Zhang H. Performance improvement in flexible polymer solar cells based on modified silver nanowire electrode. Nanotechnology. 2016;**27**(33):335203. DOI: 10.1088/0957-4484/27/33/335203

[23] Park J-S, Kim J-H, Kim J-Y, Kim D-H, Kang D, Sung J-S, et al. Hybrid indium tin oxide/ag nanowire electrodes for improving the light output power of near ultraviolet AlGaN-based light-emitting diode. Current Applied Physics. 2016;**16**(5):545-548. DOI: 10.1016/j.cap.2016.03.004

[24] Zeng XY, Zhang QK, Yu RM, Lu CZ. A new transparent conductor: Silver nanowire film buried at the surface of a transparent polymer. Advanced Materials. 2010;**22**(40):4484-4488. DOI: 10.1002/adma.201001811

[25] Yu Z, Zhang Q, Li L, Chen Q, Niu X, Liu J, et al. Highly flexible silver nanowire electrodes for shape-memory polymer light-emitting diodes. Advanced Materials. 2011;**23**(5):664-668. DOI: 10.1002/adma.201003398

[26] Gaynor W, Hofmann S, Christoforo MG, Sachse C, Mehra S, Salleo A, et al. Color in the corners: ITO-free white OLEDs with angular color stability. Advanced Materials. 2013;**25**(29):4006-4013. DOI: 10.1002/adma.201300923

[27] Ok KH, Kim J, Park SR, Kim Y, Lee CJ, Hong SJ, et al. Ultra-thin and smooth transparent electrode for flexible and leakage-free organic light-emitting diodes. Scientific Reports. 2015;**5**:9464. DOI: 10.1038/srep09464

[28] Liang J, Li L, Niu X, Yu Z, Pei Q. Elastomeric polymer light-emitting devices and displays. Nature Photonics. 2013;**7**(10):817-824. DOI: 10.1038/nphoton.2013.242

[29] Liang J, Li L, Tong K, Ren Z, Hu W, Niu X, et al. Silver nanowire percolation network soldered with graphene oxide at room temperature and its application for fully stretchable polymer light-emitting diodes. ACS Nano. 2014;**8**(2):1590-1600

[30] Lee H, Lee D, Ahn Y, Lee EW, Park LS, Lee Y. Highly efficient and low voltage silver nanowire-based OLEDs employing a n-type hole injection layer. Nanoscale. 2014; **6**(15):8565-8570. DOI: 10.1039/c4nr01768d

[31] Lee Y, Suh M, Kim D, Lee D, Chang H, Lee HS, et al. Improved operational stability of polymer light-emitting diodes based on silver nanowire electrode through pre-bias conditioning treatment. Advanced Functional Materials. 2014;**24**(41):6465-6472. DOI: 10.1002/adfm.201401197

[32] Wei B, Wu X, Lian L, Yang S, Dong D, Feng D, et al. A highly conductive and smooth AgNW/PEDOT:PSS film treated by hot-pressing as electrode for organic light emitting diode. Organic Electronics. 2017;**43**:182-188. DOI: 10.1016/j.orgel.2017.01.030

[33] Lee J, An K, Won P, Ka Y, Hwang H, Moon H, et al. A dual-scale metal nanowire network transparent conductor for highly efficient and flexible organic light emitting diodes. Nanoscale. 2017;**9**(5):1978-1985. DOI: 10.1039/c6nr09902e

[34] Coskun S, Selen Ates E, Unalan HE. Optimization of silver nanowire networks for polymer light emitting diode electrodes. Nanotechnology. 2013;**24**(12):125202. DOI: 10.1088/0957-4484/24/12/125202

[35] Jeong G-J, Lee J-H, Han S-H, Jin W-Y, Kang J-W, Lee S-N. Silver nanowires for transparent conductive electrode to GaN-based light-emitting diodes. Applied Physics Letters. 2015;**106**(3). DOI: 031118, 10.1063/1.4906459

[36] Choi S, Park J, Hyun W, Kim J, Kim J, Lee YB, et al. Stretchable heater using ligand-exchanged silver nanowire nanocomposite for wearable articular thermotherapy. ACS Nano. 2015;**9**(6):6626-6633. DOI: 10.1021/acsnano.5b02790

[37] Lim S, Son D, Kim J, Lee YB, Song J-K, Choi S, et al. Transparent and stretchable interactive human machine interface based on patterned graphene heterostructures. Advanced Functional Materials. 2015;**25**(3):375-383. DOI: 10.1002/adfm.201402987

[38] Myers AC, Huang H, Zhu Y. Wearable silver nanowire dry electrodes for electrophysiological sensing. RSC Advances. 2015;**5**(15):11627-11632. DOI: 10.1039/c4ra15101a

[39] Hwang B-U, Lee J-H, Trung TQ, Roh E, Kim D-I, Kim S-W, et al. Transparent stretchable self-powered patchable sensor platform with ultrasensitive recognition of human activities. ACS Nano. 2015;**9**(9):8801-8810. DOI: 10.1021/acsnano.5b01835

[40] Yao S, Zhu Y. Wearable multifunctional sensors using printed stretchable conductors made of silver nanowires. Nanoscale. 2014;**6**(4):2345-2352. DOI: 10.1039/c3nr05496a

[41] Amjadi M, Pichitpajongkit A, Lee S, Ryu S, Park I. Highly stretchable and sensitive strain sensor based on silver nanowire–elastomer nanocomposite. ACS Nano. 2014;**8**(5):5154-5163. DOI: 10.1021/nn501204t

[42] Lee JH, Huynh-Nguyen B-C, Ko E, Kim JH, Seong GH. Fabrication of flexible, transparent silver nanowire electrodes for amperometric detection of hydrogen peroxide. Sensors and Actuators B: Chemical. 2016;**224**:789-797. DOI: 10.1016/j.snb.2015.11.006

[43] Hu W, Niu X, Zhao R, Pei Q. Elastomeric transparent capacitive sensors based on an interpenetrating composite of silver nanowires and polyurethane. Applied Physics Letters. 2013;**102**(8):083303. DOI: 10.1063/1.4794143

[44] Kim D-H, Yu K-C, Kim Y, Kim J-W. Highly stretchable and mechanically stable transparent electrode based on composite of silver nanowires and polyurethane–urea. ACS Applied Materials & Interfaces. 2015;**7**(28):15214-15222. DOI: 10.1021/acsami.5b04693

[45] Jeong CK, Lee J, Han S, Ryu J, Hwang GT, Park DY, et al. A hyper-stretchable elastic-composite energy harvester. Advanced Materials. 2015;**27**(18):2866-2875. DOI: 10.1002/adma.201500367

[46] Ho X, Cheng CK, Tey JN, Wei J. Tunable strain gauges based on two-dimensional silver nanowire networks. Nanotechnology. 2015;**26**(19):195504. DOI: 10.1088/0957-4484/26/19/195504

[47] Li X, Wang L, Yan G. Review: Recent research progress on preparation of silver nanowires by soft solution method and their applications. Crystal Research and Technology. 2011;**46**(5):427-438. DOI: 10.1002/crat.201100023

[48] Lazzara TD, Bourret GR, Lennox RB, van de Ven TGM. Polymer templated synthesis of AgCN and ag nanowires. Chemistry of Materials. 2009;**21**(10):2020-2026. DOI: 10.1021/cm802481v

[49] Ijiro K, Matsuo Y, Hashimoto Y. DNA-based silver nanowires fabricated by electroless plating. Molecular Crystals and Liquid Crystals. 2006;**445**(1):207/[497]-211/[501]. DOI: 10.1080/15421400500367132

[50] Za H, Xu T, Rj L, Hl L. Template preparation of high-density, and large-area ag nanowire array by acetaldehyde reduction. Materials Science and Engineering: A. 2004;**371**(1-2):236-240. DOI: 10.1016/j.msea.2003.11.050

[51] Zhang L, Zhang P, Fang Y. Magnetron sputtering of silver nanowires using anodic aluminum oxide template: A new active substrate of surface enhanced Raman scattering and an investigation of its enhanced mechanism. Analytica Chimica Acta. 2007;**591**(2):214-218. DOI: 10.1016/j.aca.2007.03.069

[52] Wiley B, Sun Y, Xia Y. Polyol synthesis of silver nanostructures: Control of product morphology with Fe(II) or Fe(III) species. Langmuir. 2005;**21**(18):8077-8080. DOI: 10.1021/la050887i

[53] Korte KE, Skrabalak SE, Xia Y. Rapid synthesis of silver nanowires through a CuCl- or $CuCl_2$-mediated polyol process. Journal of Materials Chemistry. 2008;**18**(4):437-441

[54] Gou L, Chipara M, Zaleski JM. Convenient, rapid synthesis of Ag nanowires. Chemistry of Materials. 2007;**19**(7):1755-1760. DOI: 10.1021/cm070160a

[55] Chen D, Qiao X, Qiu X, Chen J, Jiang R. Convenient synthesis of silver nanowires with adjustable diameters via a solvothermal method. Journal of Colloid and Interface Science. 2010;**344**(2):286-291. DOI: 10.1016/j.jcis.2009.12.055

[56] Spadaro D, Barletta E, Barreca F, Currò G, Neri F. PMA capped silver nanoparticles produced by UV-enhanced chemical process. Applied Surface Science. 2009;**255**(20):8403-8408. DOI: 10.1016/j.apsusc.2009.05.108

[57] Rakha SA, Ali N, Haleem YA, Alam F, Khurram AA, Munir A. Comparison of mechanical properties of acid and UV ozone treated nanodiamond epoxy nanocomposites. Journal of Materials Science & Technology. 2014;**30**(8):753-758. DOI: 10.1016/j.jmst.2013.12.011

[58] Nandikonda S, Davis EW. Parameters affecting the microwave-assisted polyol synthesis of silver nanorods. ISRN Nanotechnology. 2011;**2011**:1-7. DOI: 10.5402/2011/104086

[59] Lee JH, Lee P, Lee D, Lee SS, Ko SH. Large-scale synthesis and characterization of very long silver nanowires via successive multistep growth. Crystal growth & design. 2012;**12**(11):5598-5605. DOI: 10.1021/cg301119d

[60] Jose Andres L, Fe Menendez M, Gomez D, Luisa Martinez A, Bristow N, Paul Kettle J, et al. Rapid synthesis of ultra-long silver nanowires for tailor-made transparent conductive electrodes: Proof of concept in organic solar cells. Nanotechnology. 2015;**26**(26):265201. DOI: 10.1088/0957-4484/26/26/265201

[61] Sun Y, Yin Y, Mayers BT, Herricks T, Xia Y. Uniform silver nanowires synthesis by reducing $AgNO_3$ with ethylene glycol in the presence of seeds and poly(vinyl pyrrolidone). Chemistry of Materials. 2002;**14**(11):4736-4745. DOI: 10.1021/cm020587b

[62] Kiran Kumar ABV, wan Bae C, Piao L, Kim S-H. Silver nanowire based flexible electrodes with improved properties: High conductivity, transparency, adhesion and low haze. Materials Research Bulletin. 2013;**48**(8):2944-2949. DOI: 10.1016/j.materresbull.2013.04.035

[63] Liu Y, Zhang J, Gao H, Wang Y, Liu Q, Huang S, et al. Capillary-force-induced cold welding in silver-nanowire-based flexible transparent electrodes. Nano Letters. 2017;**17**(2):1090-1096. DOI: 10.1021/acs.nanolett.6b04613

[64] Duan SK, Niu QL, Wei JF, He JB, Yin YA, Zhang Y. Water-bath assisted convective assembly of aligned silver nanowire films for transparent electrodes. Physical chemistry chemical physics : PCCP. 2015;**17**(12):8106-8112. DOI: 10.1039/c4cp05989a

[65] Lee SH, Lim S, Kim H. Smooth-surface silver nanowire electrode with high conductivity and transparency on functional layer coated flexible film. Thin Solid Films. 2015;**589**:403-407

[66] Jung ED, Nam YS, Seo H, Lee BR, Yu JC, Lee SY, et al. Highly efficient flexible optoelectronic devices using metal nanowire-conducting polymer composite transparent electrode. Electronic Materials Letters. 2015;**11**(5):906-914. DOI: 10.1007/s13391-015-5120-z

[67] Nam S, Song M, Kim DH, Cho B, Lee HM, Kwon JD, et al. Ultrasmooth, extremely deformable and shape recoverable Ag nanowire embedded transparent electrode. Scientific Reports. 2014;**4**:4788. DOI: 10.1038/srep04788

[68] Lee P, Lee J, Lee H, Yeo J, Hong S, Nam KH, et al. Highly stretchable and highly conductive metal electrode by very long metal nanowire percolation network. Advanced Materials. 2012;**24**(25):3326-3332. DOI: 10.1002/adma.201200359

[69] Lee C, Kim C, Jeong M, Kim J, Lee J, Oh J-W, et al. Highly flexible and transparent metal grids made of metal nanowire networks. RSC Advances. 2015;**5**(94):77288-77295. DOI: 10.1039/c5ra14513a

[70] Miller MS, O'Kane JC, Niec A, Carmichael RS, Carmichael TB. Silver nanowire/optical adhesive coatings as transparent electrodes for flexible electronics. ACS Applied Materials & Interfaces. 2013;**5**(20):10165-10172. DOI: 10.1021/am402847y

[71] Hu L, Kim HS, Lee J-Y, Peumans P, Cui Y. Scalable coating and properties of transparent, flexible, silver nanowire electrodes. ACS Nano. 2010;**4**(5):2955-2963

[72] dos Reis Benatto GA, Roth B, Corazza M, Sondergaard RR, Gevorgyan SA, Jorgensen M, et al. Roll-to-roll printed silver nanowires for increased stability of flexible ITO-free organic solar cell modules. Nanoscale. 2016;**8**(1):318-326. DOI: 10.1039/c5nr07426f

[73] Im HG, Jin J, Ko JH, Lee J, Lee JY, Bae BS. Flexible transparent conducting composite films using a monolithically embedded AgNW electrode with robust performance stability. Nanoscale. 2014;**6**(2):711-715. DOI: 10.1039/c3nr05348b

[74] Madaria AR, Kumar A, Ishikawa FN, Zhou C. Uniform, highly conductive, and patterned transparent films of a percolating silver nanowire network on rigid and flexible substrates using a dry transfer technique. Nano Research. 2010;**3**(8):564-573. DOI: 10.1007/s12274-010-0017-5

[75] Hong S, Yeo J, Lee J, Lee H, Lee P, Lee SS, et al. Selective laser direct patterning of silver nanowire percolation network transparent conductor for capacitive touch panel. Journal of Nanoscience & Nanotechnology. 2015;**15**(3):2317-2323

[76] Jeon Y, Jin HB, Jung S, Go H, Lee I, Lee C, et al. Highly flexible touch screen panel fabricated with silver nanowire crossing electrodes and transparent bridges. Journal of the Optical Society of Korea. 2015;**19**(5):508-513. DOI: 10.3807/josk.2015.19.5.508

[77] Krebs FC. Polymer solar cell modules prepared using roll-to-roll methods: Knife-over-edge coating, slot-die coating and screen printing. Solar Energy Materials and Solar Cells. 2009;**93**(4):465-475. DOI: 10.1016/j.solmat.2008.12.012

[78] Menamparambath MM, Yang K, Kim HH, Bae OS, Jeong MS, Choi JY, et al. Reduced haze of transparent conductive films by smaller diameter silver nanowires. Nanotechnology. 2016;**27**(46):465706. DOI: 10.1088/0957-4484/27/46/465706

[79] Kim T, Canlier A, Kim GH, Choi J, Park M, Han SM. Electrostatic spray deposition of highly transparent silver nanowire electrode on flexible substrate. ACS applied materials & interfaces. 2013;**5**(3):788-794

[80] Mariani P, Vesce L, Di Carlo A. The role of printing techniques for large-area dye sensitized solar cells. Semiconductor Science and Technology. 2015;**30**(10):104003. DOI:10.1088/0268-1242/30/10/104003

[81] Yi P, Zhang C, Peng L, Lai X. Flexible silver-mesh electrodes with moth-eye nanostructures for transmittance enhancement by double-sided roll-to-roll nanoimprint lithography. RSC Advances. 2017;**7**(77):48835-48840. DOI: 10.1039/c7ra09149d

[82] Jung E, Kim C, Kim M, Chae H, Cho JH, Cho SM. Roll-to-roll preparation of silver-nanowire transparent electrode and its application to large-area organic light-emitting diodes. Organic Electronics. 2017;**41**:190-197. DOI: 10.1016/j.orgel.2016.11.003

[83] Lee SJ, Kim YH, Kim JK, Baik H, Park JH, Lee J, et al. A roll-to-roll welding process for planarized silver nanowire electrodes. Nanoscale. 2014;**6**(20):11828-11834. DOI: 10.1039/c4nr03771e

[84] Wang Z, Yi P, Peng L, Lai X, Ni J. Fabrication of metal mesh arrays using roll-to-roll UV-nanoimprint lithography for flexible transparent electrodes. 12th International Conference on Frontiers of Design and Manufacturing. 2016

[85] Hosel M, Angmo D, Sondergaard RR, Dos Reis Benatto GA, Carle JE, Jorgensen M, et al. High-volume processed, ITO-free superstrates and substrates for roll-to-roll development of organic electronics. Advanced science. 2014;**1**(1):1400002. DOI: 10.1002/advs.201400002

[86] Krebs FC. Fabrication and processing of polymer solar cells: A review of printing and coating techniques. Solar Energy Materials and Solar Cells. 2009;**93**(4):394-412. DOI: 10.1016/j.solmat.2008.10.004

[87] Roll to Roll (R2R) Processing Technology Assessment. https://www.energy.gov/sites/prod/files/2015/02/f19/QTR%20Ch8%20-%20Roll%20To%20Roll%20Processing%20TA%20Feb-13-2015.pdf

[88] Søndergaard R, Hösel M, Angmo D, Larsen-Olsen TT, Krebs FC. Roll-to-roll fabrication of polymer solar cells. Materials Today. 2012;**15**(1-2):36-49. DOI: 10.1016/s1369-7021(12)70019-6

[89] Araki T, Jiu J, Nogi M, Koga H, Nagao S, Sugahara T, et al. Low haze transparent electrodes and highly conducting air dried films with ultra-long silver nanowires synthesized by one-step polyol method. Nano Research. 2014;**7**(2):236-4235. DOI: 10.1007/s12274-013-0391-x

[90] Lee J, Lee I, Kim TS, Lee JY. Efficient welding of silver nanowire networks without post-processing. Small. 2013;**9**(17):2887-2894. DOI: 10.1002/smll.201203142

[91] Liu B-T, Kuo H-L. Graphene/silver nanowire sandwich structures for transparent conductive films. Carbon. 2013;**63**:390-396. DOI: 10.1016/j.carbon.2013.06.094

[92] Lee D, Lee H, Ahn Y, Lee Y. High-performance flexible transparent conductive film based on graphene/AgNW/graphene sandwich structure. Carbon. 2015;**81**:439-446. DOI: 10.1016/j.carbon.2014.09.076

[93] Aziz S, Zhao J, Cain C, Wang Y. Nanoarchitectured $LiMn_2O_4$/graphene/ZnO composites as electrodes for lithium ion batteries. Journal of Materials Science & Technology. 2014;**30**(5):427-433. DOI: 10.1016/j.jmst.2014.03.007

[94] Zhu R, Chung C-H, Cha KC, Yang W, Zheng YB, Zhou H, et al. Fused silver nanowires with metal oxide nanoparticles and organic polymers for highly transparent conductors. ACS Nano. 2011;**5**(12):9877-9882. DOI: 10.1021/nn203576v

[95] De S, Higgins TM, Lyons PE, Doherty EM, Nirmalraj PN, Blau WJ, et al. Silver nanowire networks as flexible, transparent, conducting films: Extremely high DC to optical conductivity ratios. ACS Nano. 2009;**3**(7):1767-1774

[96] Shin DY, Yi GR, Lee D, Park J, Lee YB, Hwang I, et al. Rapid two-step metallization through physicochemical conversion of Ag_2O for printed "black" transparent conductive films. Nanoscale. 2013;**5**(11):5043-5052. DOI: 10.1039/c3nr00962a\

[97] Garnett EC, Cai W, Cha JJ, Mahmood F, Connor ST, Greyson Christoforo M, et al. Self-limited plasmonic welding of silver nanowire junctions. Nature Materials. 2012;**11**(3):241-249. DOI: 10.1038/nmat3238

[98] Yang Y, Ding S, Araki T, Jiu J, Sugahara T, Wang J, et al. Facile fabrication of stretchable ag nanowire/polyurethane electrodes using high intensity pulsed light. Nano Research. 2016;**9**(2):401-414. DOI: 10.1007/s12274-015-0921-9

[99] Jiu J, Nogi M, Sugahara T, Tokuno T, Araki T, Komoda N, et al. Strongly adhesive and flexible transparent silver nanowire conductive films fabricated with a high-intensity pulsed light technique. Journal of Materials Chemistry. 2012;**22**(44):23561. DOI: 10.1039/c2jm35545k

[100] Tokuno T, Nogi M, Karakawa M, Jiu J, Nge TT, Aso Y, et al. Fabrication of silver nanowire transparent electrodes at room temperature. Nano Research. 2011;**4**(12):1215-1222

[101] Song TB, Chen Y, Chung CH, Yang YM, Bob B, Duan HS, et al. Nanoscale joule heating and electromigration enhanced ripening of silver nanowire contacts. ACS Nano. 2804;**8**(3):2014

[102] Sciacca B, van de Groep J, Polman A, Garnett EC. Solution-grown silver nanowire ordered arrays as transparent electrodes. Advanced Materials. 2016;**28**(5):905-909. DOI: 10.1002/adma.201504045

[103] Huh JW, Lee DK, Jeon HJ, Ahn CW. New approach for fabricating hybrid-structured metal mesh films for flexible transparent electrodes by the combination of electrospinning and metal deposition. Nanotechnology. 2016;**27**(47):475302

[104] Teymouri A, Pillai S, Ouyang Z, Hao X, Green M, editors. Promising hybrid graphene-silver nanowire transparent conductive electrode. Photovoltaic Specialists Conference; 2016

[105] Liu C-H, Yu X. Silver nanowire-based transparent, flexible, and conductive thin film. Nanoscale Research Letters. 2011;**6**(1):75

[106] Jiang Y, Xi J, Wu Z, Dong H, Zhao Z, Jiao B, et al. Highly transparent, conductive, flexible resin films embedded with silver nanowires. Langmuir. 2015;**31**(17):4950-4957

[107] Kim D, Zhu L, Jeong D-J, Chun K, Bang Y-Y, Kim S-R, et al. Transparent flexible heater based on hybrid of carbon nanotubes and silver nanowires. Carbon. 2013;**63**:530-536. DOI: 10.1016/j.carbon.2013.07.030

[108] Kim T, Kim YW, Lee HS, Kim H, Yang WS, Suh KS. Uniformly interconnected silver-nanowire networks for transparent film heaters. Advanced Functional Materials. 2013;**23**(10):1250-1255. DOI: 10.1002/adfm.201202013

[109] Khaligh HH, Xu L, Khosropour A, Madeira A, Romano M, Pradere C, et al. The joule heating problem in silver nanowire transparent electrodes. Nanotechnology. 2017;**28**(42):425703. DOI: 10.1088/1361-6528/aa7f34

[110] Song T-B, Rim YS, Liu F, Bob B, Ye S, Hsieh Y-T, et al. Highly robust silver nanowire network for transparent electrode. ACS Applied Materials & Interfaces. 2015;**7**(44):24601-24607. DOI: 10.1021/acsami.5b06540

[111] Chang JH, Chiang KM, Kang HW, Chi WJ, Chang JH, Wu CI, et al. A solution-processed molybdenum oxide treated silver nanowire network: A highly conductive

transparent conducting electrode with superior mechanical and hole injection properties. Nanoscale. 2015;**7**(10):4572-4579. DOI: 10.1039/c4nr06805j

[112] Y-s L, Feng J, Ou X-L, H-f C, Xu M, Sun H-B. Ultrasmooth, highly conductive and transparent PEDOT:PSS/silver nanowire composite electrode for flexible organic light-emitting devices. Organic Electronics. 2016;**31**:247-252. DOI: 10.1016/j.orgel.2016.01.014

[113] Duan Y-H, Duan Y, Wang X, Yang D, Yang Y-Q, Chen P, et al. Highly flexible peeled-off silver nanowire transparent anode using in organic light-emitting devices. Applied Surface Science. 2015;**351**:445-450. DOI: 10.1016/j.apsusc.2015.05.161

[114] Zhang M, Hofle S, Czolk J, Mertens A, Colsmann A. All-solution processed transparent organic light emitting diodes. Nanoscale. 2015;**7**(47):20009-20014. DOI: 10.1039/c5nr05820a

[115] Song C-H, Ok K-H, Lee C-J, Kim Y, Kwak M-G, Han CJ, et al. Intense-pulsed-light irradiation of ag nanowire-based transparent electrodes for use in flexible organic light emitting diodes. Organic Electronics. 2015;**17**:208-215. DOI: 10.1016/j.orgel.2014.12.015

[116] Zhu R, Jiang C-Y, Liu X-Z, Liu B, Kumar A, Ramakrishna S. Improved adhesion of interconnected TiO_2 nanofiber network on conductive substrate and its application in polymer photovoltaic devices. Applied physics Letters. 2008;**93**(1):013102

[117] Khan A, Lee S, Jang T, Xiong Z, Zhang C, Tang J, et al. High-performance flexible transparent electrode with an embedded metal mesh fabricated by cost-effective solution process. Small. 2016;**12**(22):3021-3030. DOI: 10.1002/smll.201600309

Chapter 3

Printing Technologies on Flexible Substrates for Printed Electronics

Sílvia Manuela Ferreira Cruz, Luís A. Rocha and Júlio C. Viana

Additional information is available at the end of the chapter

http://dx.doi.org/10.5772/intechopen.76161

Abstract

Printing technologies have been demonstrated to be highly efficient and compatible with polymeric materials (both inks and substrates) enabling a new generation of flexible electronics applications. Conductive flexible polymers are a new class of materials that are prepared for a wide range of applications, such as photovoltaic solar cells, transistors molecular devices, and sensors and actuators. There are many possible printing techniques. This chapter provides an opportunity to review the most common printing techniques used at the industrial level, the most commonly used substrates and electronic materials, giving an overall vision for a better understanding and evaluation of their different features. Several technological solutions (contact/noncontact) and its critical challenges are also presented. Inkjet Printing Technology (IPT) has been receiving a great attention and therefore higher focus is given to this technology. An overview of IPT is presented to evidence its importance and potential as a key-technology on the research field for printed electronics development, as well as on large scale industrial manufacturing. A background and a review on prior work are presented along with used materials, developed applications and potential of IPT technology. The main features of the different printing technologies, advantages and main challenges are also compared.

Keywords: printing techniques, flexible polymers, conductive inks

1. Introduction

When an electrical device is created through a printing process, it is designated Printed Electronics (PE). Over 20 years, the manufacturing industry has been using various printing techniques to produce, e.g., antennas, sensors, membrane switches, etc. [1]. This list is

continuously increasing. Today users' demands (for lower cost, flexible and smarter products) are a decisive factor for the selection of PE fabrication technologies, therefore, contributing to novel and better products. The interest on flexible electronic systems to be used, for example, on non-planar surfaces grew tremendously in recent years, [2] in areas such as aerospace and automotive, [3] biomedical, [4] robotics, [5] and health applications [6]. This is possible thanks to the combination of different polymeric materials (compared to traditional silicon substrates) with new coating and printing techniques able to work at temperatures compatible with the polymeric substrate, or even the manufacturing of non-planar surfaces otherwise impossible with old-fashioned fabrication techniques. The use of flexible polymers has many advantages compared to traditional hard substrates including: higher contact area, capability to fold/roll, lightweight, etc., therefore, they have a key role in the development of new conductive circuits.

Thanks to better and flexible materials combined with PE, commercial applications diversity will continue to emerge. According to Markets and Markets latest report, the progress of flexible applications based on PE market will worth $12.1B by 2022. According to Electronics.ca Publications, Printed organic & flexible electronics market will be worth over $73B by 2027.

Each technology is selected according to the type of electronic components or devices (e.g., small, thin, lightweight, flexible, inexpensive and disposable, etc.), the production cost and volume. The essential aspects for the success of any type of PE device is the processability, performance and long-term reliability [1] of the materials used [7]. The pastes, inks or coatings can be based both on organic and inorganic materials [7]. Inorganic inks normally contain metallic (e.g., copper, gold, silver, aluminum) nanoparticles dispersed in a retaining matrix and they are used, for example, in the fabrication of passive components and transistor electrodes [7]. Organic inks are based on organic materials, such as polymers (conductors, semiconductors and dielectrics). The inks based on high conductive polymers are employed in batteries, electromagnetic shields, capacitors, resistors and inductors, sensors, etc., while inks based on organic semiconductors are employed as active layers of active devices such as, Organic PhotoDiodes (OPDs), Organic Light Emitting Diodes (OLEDs), Organic Field-Effect Transistors (OFETs), organic solar cells (OSC), sensors, etc. [7]. Due to the wide range of printing technologies, the materials must meet certain requirements depending on the type of printing being performed and on the application.

PE technologies can be divided in contact and non-contact techniques as shown on **Figure 1**:

- contact techniques (e.g., screen printing, flexography, gravure printing and soft lithography), in which the printing plate is in direct contact with the substrate;
- non-contact techniques (e.g., laser direct writing, aerosol printing, inkjet printing), where only the deposition material get in contact with the substrate.

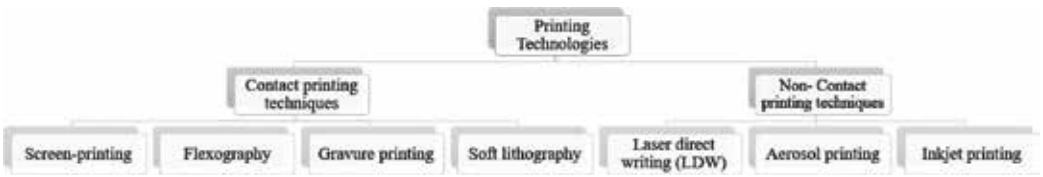

Figure 1. Printing technologies classification.

This chapter reviews simultaneously the most used techniques at the research and industrial level, substrates and electronic materials for an overall vision and a better understanding and evaluation of its different features. Their main features and examples of PE applications are discussed with greater focus on Inkjet Printing Technology.

2. Printing technologies

2.1. Contact printing technologies

The contact printing technologies are the predominant printing processes in the current days. They involve high material waste and limitations around the resolution and range of the materials used (substrates, inks, solvents). Main contact printing technologies are described in the following.

2.1.1. Screen printing

Screen printing (SP) is a mature printing technique that may be performed in a planar system or in a roll-to-roll (R2R) process (**Figure 2**). The planar system uses a SP mesh, which is in direct contact with the substrate; the blade moves, distributes the ink and helps filling the mesh. The ink passes into the standard image in the mesh to the substrate and defines the final image. The substrates could be epidermis [8], paper, glass, metal [9], ceramic, [10] wood, textiles [10], polymers [10]. Webb et al. [11] describes a SP functional ink, comprising a combination of semiconducting acicular particles, electrically insulating nanoparticles and a base polymer ink, that exhibits pronounced pressure sensitive electrical properties for applications in sensing and touch sensitive surfaces.

In the R2R process, the squeegee is replaced by a roller and the ink and the blade are placed inside. The blade forces the ink through the mesh. The process is continuous, contrary to the planar system, allowing high speeds production, although rotary setup is expensive and hard to clean.

SP is a technology that has been often used for PE [12]. This technique produces large waste of production material (including the ink). The biggest limitation is reflected in the level of resolution. Also, the planar system speed is low in comparison to other conventional printing processes [13].

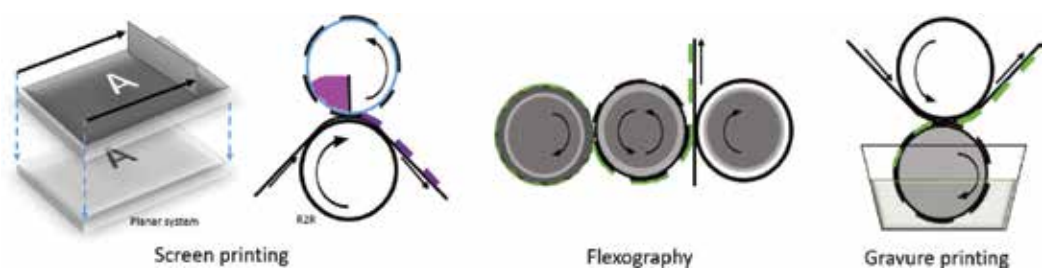

Figure 2. Schematic of contact printing techniques.

2.1.2. Flexography

The flexography is a R2R direct printing technology, where the final pattern stands out from the ink transfer. A ceramic anilox roller, covered with micro-cavities on its surface, allows the collection of ink, and then is transferred to the printing plate cylinder (**Figure 2**). A closed chamber supplies the ink to the anilox roller [13]. A doctor blade removes excess ink from the cylinder and prevents the output from the ink supply chamber. The printing plate continuously rotates in contact with the substrate ensuring a continuous high speed printing process.

However, situations such as the Halo effect (patterns with excess of ink) occur due to the compression between the printing plate and the substrate, despite the low pressure applied. This leads to limitations on image size stability and resolution [13]. This technology is commonly used for the fabrication of on-label battery testers, drug delivery patches, printed batteries and other e-label applications [1]. Julin used flexography to produce flexible piezoelectric pressure sensors [14]. They investigated the suitability of flexography printing and new electrode materials in their manufacture, developing a flexo-printed piezoelectric PolyVinyliDene Fluoride (PVDF) pressure sensor. Although the sheet resistance of the fabricated samples presented high values and a lot of variability, the devices showed a non-uniform structure and some difficulties were reported on achieving a uniform pressure sensor.

2.1.3. Gravure printing

The gravure printing technology is the reverse process of flexography, where the image to be printed is negative (**Figure 2**). The ink is received directly by the ink supplier container or by an additional roller to the gravure plate, where the pattern image is located. A flexible metal blade removes the excess ink. The ink is transferred through capillary action from the small engraved cavities on the cylinder surface to the substrate. This technology is capable of producing high quality patterns in a cost-effective manner and is suitable for printing with inks of low viscosity, and high manufacturing speeds (up to 0.1 m/s [15]) can be achieved. A careful optimization of the process and of the materials is important because the final print quality is highly dependent upon:

- inks properties, i.e., its rheological behavior (viscosity), solvent evaporation rate and curing;
- proper cell spacing (1.06–1.4 μm) for print quality [16, 17];
- feature dimensions on gravure cylinder for proper cell emptying capability [16] are very important;
- shear force in the printing mechanism [17].

Widely used in magazine production, gravure printing is also highly employed for certain electronics products such as medical Electrocardiography (ECG or EKG) pads and high-volume Radio-Frequency Identification devices (RFID) [1], Thin-Film-Transistors (TFT) [16], solar cells [18] and sensors [19]. However, this process presents two main limitations: the printing image is built from separate cells, and when printing a straight line, a jagged line is observed [13], which represents a major obstacle when high resolution is need, e.g., less

than 20 μm size is required for electronic structures [15], and the parasitic capacitances are to be avoid; the proper layer deposition alignment, e.g., in electronic applications, repeating conductive film deposition is sometimes required in order to reduce sheet resistance. When it comes to R2R techniques (e.g., screen-printing, flexography and gravure printing) another level of complexity is added to these technologies. Also, frequent replacements of the gravure cylinders are needed, which adds a maintenance cost.

2.1.4. Soft lithography

Soft lithography technology encompasses several printing techniques (**Figure 3**), such as microcontact printing (μCP) [20], replica molding (REM), micro transference molding (μTM), micromolding in capillaries (MIMIC), and solvent assisted micromolding (SAMIM) [21]. It provides a convenient, effective method for the manufacturing of high quality micro- and nanostructured systems [22]. In this set of technologies, an elastomeric (commonly of poly (dimethylsiloxane) (PDMS)) stamp or mold with patterned relief structures on its surface is used to transfer patterns and structures with feature sizes ranging from 30 nm to 100 μm [21]. Usually the master is prepared using either e-beam or photolithography. From this master, several stamps can be molded. The material of interest is deposited on the stamp and transferred on the substrate. However, soft lithography does not offer better economic advantages when compared to R2R printing techniques due to the rapid throughput [7]. The fabrication includes several manufacture steps with the involvement of photolithographic technology [5, 23]. Other challenges rely on a proper adjustment of the surface energies of substrates and inks for efficient transfer to the substrate to be printed, on common swelling of transferring materials, resulting on increased features size.

2.1.5. Comparing contact printing technologies

Tables 1 and **2** summarize qualitatively the mechanisms, the process requirements, material and critical limitations of the contact printing technologies, highlighting their main features. These tables also provide the possibility of merging the different techniques in order to combine technologies to overcome one technology limitation with another technology.

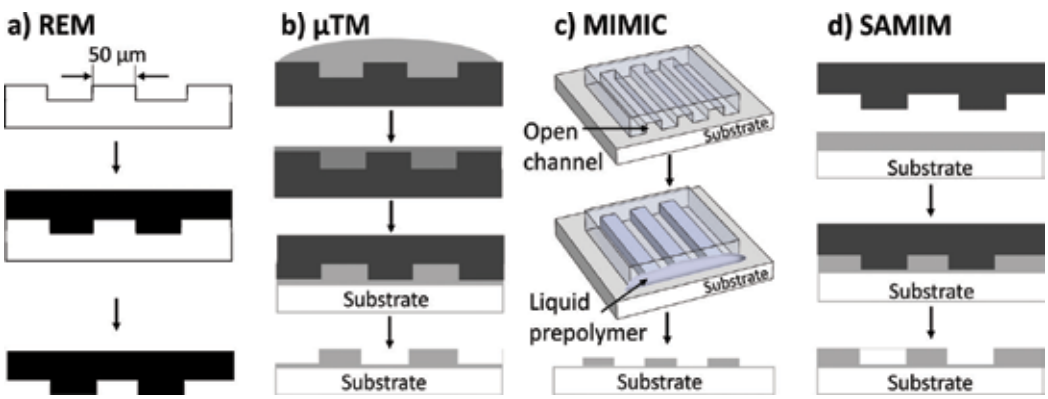

Figure 3. Major steps in soft lithography technologies.

2.2. Non-contact printing technologies

Compared to the contact printing technologies, the non-contact has the advantage of the substrate only getting in contact with the deposition material. This lowers the risks of contamination, of damaging the substrate and the patterns alignment is more accurate. This last issue is an indispensable functionality to pattern multilayered devices. For non-contact printing techniques there is no need for physical mask of the to-be-printed image, only requiring a digital image, simplifying the switching process without no additional cost. However, the non-contact technologies also stumble upon some difficulties when completing multilayered devices [23] are needed. They work with all kinds of substrates, such as, wood, glass, metals and most interesting, rubbers, polymers, which require low processing temperatures, and risk to be damaged and deformed when subjected to thermal stresses and high temperature processes. Main non-contact printing techniques are described in the following.

2.2.1. Laser direct writing

Laser direct-writing (LDW) techniques enable the realization of 1D to 3D structures by laser-induced deposition of metals, semiconductors, polymers and ceramics, without using masks and without physical contact between a tool or nozzle and the substrate material. Operated by a computer, the laser pulses are manipulated to control the composition, structure, and properties of individual three-dimensional volumes of materials, across length-scales spanning six orders of magnitude from nanometers to millimeters [25]. The ability to process complex

Print technique	Mechanisms and features	Challenges
Screen printing [13–15]	Most used and mature printing technique; planar or R2R system; speed and versatile.	Hard to clean; solvents deteriorate mask patterns; high resolution of uniform line patterns are not possible under 30 μm; Unfeasible use of low viscosity inks to prevent spreading and bleed out; material wastage.
Flexography [13]	High speed printing process; low-cost patterns plate; high flexibility and low pressure printing; better vertical and horizontal pattern quality compared to gravure.	Halo effect (patterns with excess of ink) due to printing plate compression to the substrate, despite the low pressure applied; marbling effect; complex multi layers alignment.
Gravure printing [13, 15, 17, 24]	High quality patterns in a cost-effective manner; high speed; low viscosity inks.	Cylinder life and high cost; demanding and careful optimization of the process (several variables) influence final print quality representing a major obstacle where high resolution is required (e.g., PE).
Soft lithography [20–22]	Encompasses several printing techniques (μCP, REM, μTM, MIMIC, SAMIM); fabrication of micro-and nanostructures of high quality; convenient, effective method; mostly used by the biological science area.	Proper adjustment of the surface energies for efficient transfer to the substrate to be printed; common swelling of transferring materials, resulting an increased features size; pattern reproduction and resolution is a challenge due to used forces on stamp; costly solution.

Table 1. Summary of contact printing techniques: mechanisms, features and main challenges.

Technique	Solution types	Solution viscosity (Pa.s)	Print thickness (μm)	Resolution (μm)	Surface tension (mN/m)
Screen printing	Water based, solvent based, UV or electron beam curable	0.1–10	0.02–100 [12, 13]	30–100	38–47
Flexography	Water based, solvent based, UV curable	0.01–0.1	0.17–8	30–80	13.9–23
Gravure printing	Water based, solvent based, UV curable	0.01–1.1 [14]	0.02–12 [13, 24]	50–200	41–44
Soft lithography	Water based, solvent based, UV curable	~0.10	0.18–0.7	0.03–100	22–80

Table 2. Comparison between main contact printing techniques.

or delicate material systems and the achieved resolutions enable LDW to fabricate structures that are not possible to generate using other techniques. Within LDW, there are three writing techniques:

i. LDW addition (LDW+) technique, where the material can be deposited from gaseous, liquid and solid precursors (e.g., Laser Chemical Vapor Deposition (LCVD)) or by transfer, by laser beam, from an optically transparent support onto a parallel substrate (e.g., Laser-induced forward transfer (LIFT) [7], **Figure 4**). These techniques entail high cost due to the sophisticated equipment (e.g., reaction chamber associated with vacuum equipment); it does not allow to deposit organic substrates; and it can only print on flat substrates, parallel to the support material.

ii. LDW subtraction (LDW-) technique, where the material is removed by ablation (e.g., photochemical, photothermal, or photophysical ablation [26], laser scribing, cutting, drilling, or etching [27]). An industrial application example is the high-resolution manufacturing and texturing of stents or other implantable biomaterials.

iii. LDW Modification (LDWM) technique, where the material is modified thermally or chemically [25] (e.g., Laser-Enhanced Electroless Plating, LEEP). The substrate is submerged in a chemical solution that contains the metallic ions required for the deposition. A laser beam is responsible for local temperature rise, decomposing the liquid and leading to the deposition of a metallic layer on the substrate surface. The main disadvantage relies in its disability to create 3D structures.

2.2.2. Aerosol jet printing

Aerosol jet printing (**Figure 4**), also known as Maskless Mesoscale Materials Deposition (M3D) is another material deposition technology for printed electronics [28] developed by Optomec [29]. The ink (solutions and nanoparticle suspensions based on metals, alloys, ceramics, polymers, adhesives or biomaterials) is placed into an atomizer where it aerosolizes in liquid

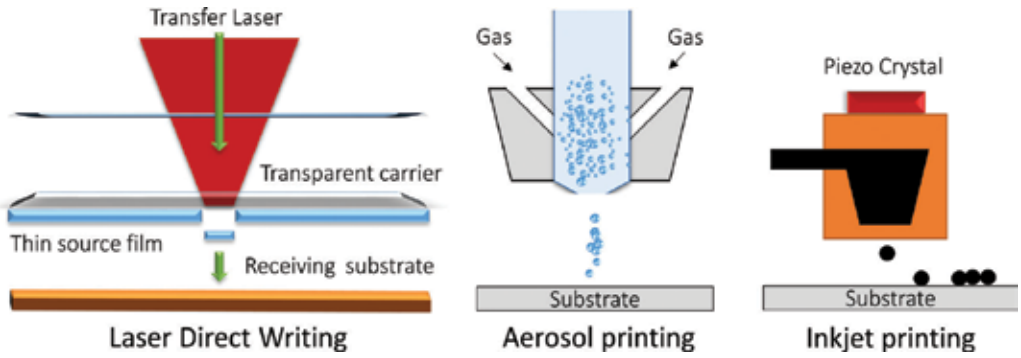

Figure 4. Schematic of non-contact printing.

particles of diameter between 20 nm and 5 μm, depending on the ink viscosity. Then, the ink is transported into the deposition head by a nitrogen flow, the aerosol being focused by jet stream onto the substrate. As being a low-temperature process, many materials and substrates can be handled by Aerosol Jet printing. The technique is also scalable to support high volume production needs. It is suitable for non-planar capability and complex designs could be printed (e.g., displays, thin film transistors, TFT, and solar cells) [29]. Complex conformal surfaces (3D printed electronics) are also possible, thanks to the ability to control the position in z-direction of the writing head over the substrate. This technique also stumbles upon some difficulties. The droplet carrier creates a cloud of powder in the surroundings of the print area. The sheath gas creates a localized crystallization/solidification phase at the trace pattern, reducing the localized bonding layer quality.

2.2.3. Inkjet printing

Inkjet printing is new technology with a grown interest from the scientific community and is considered to be in an early stage of development [2]. In Inkjet printing technology (IPT), a content stored in a digital format is transferred by a direct deposition (from small openings in print-heads, without the use of masks and without contact between the print-head and the substrate) of droplet fluid or powder, proteins or minerals [30, 31], conductive polymers [32], nanoparticles [33, 34] and a wide range of materials (e.g., bioactive fluids, which cannot tolerate exposure to photolithography and etching chemicals present in conventional techniques [32]). Under the print-head ejection, the gravity force, and air resistance, the ink is project into a specified position of the substrate creating the printing patterns (**Figure 4**).

In the case of fluids, it dries through the evaporation of the solvent, by chemical changes (e.g., cross-linking of polymers) or crystallization. Eventually, a post-processing treatment is required, as thermal annealing or sintering [35]. When compared to other deposition methods, IPT is adaptable for patterning on a high variety (rigid or flexible, smooth or rough surfaces [2, 36]) of substrates (glass, plastic [36], paper [37], textile [38], etc.), with low consumption of raw materials [36] and low levels of waste production harmful to the environment [2]. IPT is intended for a wide range of applications: transducers [32], transistors [39], structural polymers and ceramics [30], biomimetic and biomedical materials [31], printed scaffolds for growth

of living tissues [30], as well as for building 3D electric circuits [40], MEMS [34], and sensors [37]. No special processing conditions are needed. IPT stands out for being a one-step process, with a simple operating principle, reduced number of manufacturing steps, with the possibility of using low cost raw materials [41]. Thickness around nanometer range is easily achieved by increasing the electric field value along with the distance between the print head and substrate. The used inks have a particular set of physical specifications in particular its viscosity, the superficial tension [36], and the amount of humectant (10–20%) [42]. Sometimes, modifications on the ink viscosity, concentration and solvent system are necessary for proper droplet injection without blocking the nozzle. Although the low process velocity and possible clogging of the nozzles, presenting a challenge to the industrial production, IPT becomes ideal for laboratory research providing innovative fabrication, high quality and low cost productions.

2.2.4. Comparing non-contact printing techniques

Tables 3 and **4** summarize the mechanisms, the process requirements, material and critical limitations of the non-contact printing technologies, highlighting their main features.

2.3. IPT mode technology systems

The IPT can operate in two different modes: Continuous InkJet (CIJ) and Drop-On-Demand (DoD) [36]. The method for controlling the droplet movement is quite different between the two systems.

2.3.1. Continuous inkjet (CIJ) mode

In the CIJ system, the ejection of the droplet is continuous in all nozzles of the printer. In the traditional CIJ, a piezoelectric transducer is coupled to the print head to provide a periodic excitation [38]. After leaving the nozzle, an electric field determines and controls the trajectory of the droplet to the desired position on the substrate (**Figure 5**).

Printing technique	Mechanisms and features	Challenges
LDW [7, 25–27]	1D to 3D structures; nm to mm magnitude; no mask; three writing techniques (LDW+, LDW−, LDWM)	High cost equipment; not possible to deposit organic substrates, printing only on flat substrates, parallel to the substrate
Aerosol [28–43]	Complex design could be printed; complex conformal surfaces; many materials and substrates; non-planar; low-temperature processing, local sintering	Droplet carrier creates a cloud of powder in surrounding printed area; sheath gas creates a localized crystallization/ solidification phase at the trace pattern reducing the quality of the localized bonding layer
IPT [30–42]	Low viscosity; deposition of many types of droplets; droplets ejection through different actuation phenomena; all type of substrates; low material wastage; environmentally friendly	Slow printing speed compared to other techniques; nozzle clogging

Table 3. Summary of non-contact printing techniques and challenges.

Technique	Solution types	Solution viscosity (Pa.s)	Thickness (μm)	Resolution (μm)	Surf. tension (mN/m)
LDW	Solid film (donor substrate)	–	>10	ca. 0.7	–
Aerosol	Solutions and nanoparticle suspensions based on metals, alloys, ceramics, polymers, adhesives or biomaterials	0.001–1	>0.1	10–250	–
IPT	Water based, solvent based, UV curable	0.002–0.1	0.01–0.5	15–100	15–35

Table 4. Comparison between main non-contact printing techniques.

Within this technology, the droplets can be diverted by binary or multiple deflection systems. On the binary systems, the droplets are directed to a single pixel location on the substrate or to the gutter, for later recycling of the ink. In the multiple deflection system, the droplets are charged and deflected to the substrate at different levels, this way creating multiple pixels. Hertz et al. [43] used the binary CIJ and developed a method consisting in the formation of a layer of irregularly droplets of ink size. In the Hertz method, the droplets are dispersed in a straight line to a gutter so as to converge into the recirculation system. This method also introduced a new procedure and methodology relatively to the use of volatile solvents that allows a quick drying of the ink and the adhesion to the substrate materials. The CIJ system benefits from the ability to combine the printing speed (on the order of 25 m/s) with the possibility of achieving extended distances and the ability to divert droplets independent of gravity [44].

CIJ technology is typically used for large industrial productions of bar codes and labels of food products or medicines. This process can be comparatively fast, with the advantage of circumscribing large printing areas with a single pass and its printing heads have a long duration. The droplet size can reach values such as 20 μm, with a standard size of 150 μm [45]. However, in the manufacture of electronic products, the CIJ produces droplets of inadequate resolution due to the long distance between the print-head and the substrate [13]. Other less positive factors are the high cost of initial investment in such equipment, the lower resolution compared to some DoD systems, the need to use low viscosity electrolyte inks (in the range of 3–6 mPa.s), resulting in some final ink waste [46].

2.3.2. Drop-on-demand (DoD) mode

In the DoD system, the print-head ejects a single droplet only when activated (**Figure 5**). The printer is based on several injector nozzles in the print-head and, at each pulse, the droplets are ejected in parallel to each other. The image is constructed from successive pulses, which largely differentiates from CIJ. The DoD is a high speed method, of high scalability that uses high frequency multiple nozzles. The method that is used to generate these pulses defines the subcategories of the primary DoD, namely: the acoustic, the electrostatic, the thermal, the piezoelectric, and an additional method, sometimes controversial, the MEMS [47] method. This last method is more related to the fabrication process, since the drop generation is based on thermal or piezo print-heads.

http://dx.doi.org/10.5772/intechopen.76161

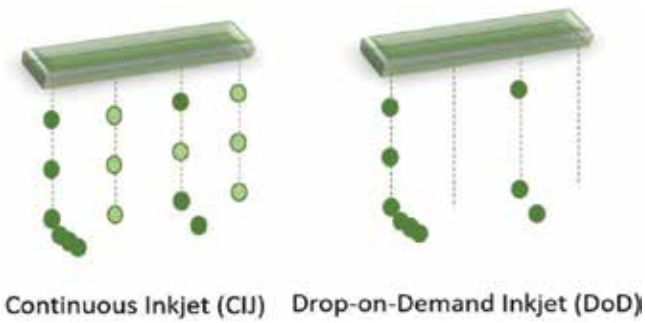

Figure 5. IPT mode technology systems.

2.3.3. Main influencing factors

The control of ink drop, the print-head temperature, the sintering or cure of the ink, and the printing control of each layer are key parameters to ensure the quality of a multilayer printed structure. Also important is to evaluate the properties of the substrate, such as, the service temperature, its barrier properties against humidity, electrical, optical, mechanical and chemical properties. Equally important is consider the receptivity of the ink by the substrate or with previously printed layers, in the case where a different ink has been used. The droplet size can vary depending on the interactions between the ink and the substrate. The droplet size sets the width of the printed line, establishing the pattern space and the electric design limits, and defines the final specifications of the printed pattern and application system (e.g., resolution, bandwidth in the case of a PE). Thereby, during the manufacturing step, the printed pattern characteristics are dependent on the materials and their interaction (i.e., the properties of the ink must be chosen in advance to understand its behavior during and after the printing process over a given substrate). Sintering and cure of conductive materials are essential because it defines its chemical, electrical and physical performance and the reliability of the printed layers over the long term.

3. Printable materials for PE

The printable materials are selected depending on the type of substrate, the type of ink, the type of printing technology and final PE application.

The conductive inks are gathering increasingly attention over the past two decades, and are revolutionizing the industry. Elected due to their attributes, such as, conductivity, suitability for printing substrates, its processing simplicity and mechanical flexibility, but also due to its ability to assign new properties, capabilities and complex functionalities. These emerging inks are penetrating the market with an opportunity to reach $400 m by 2027, according to IDTechEX report "Condutive Ink Market 2017-2027". A large variety of materials, organic and inorganic, conductors and semiconductors, have been explored for electronics applications. The most common types of inks are water, oil or solvents based. The general form of the ink consist of a mixture of compounds (pigments or dyes, resins, solvents, fillers, humectant and

additives), in liquid or solid state, with specific proprieties adapted to the printing technology characteristic, such as viscosity, surface tension, etc., to be easily printed in a large variety of substrates. What makes conductive inks electrically conductive is the fact that it contains in the composition conductive nanoscale particles. The incorporation of conductive polymers [48], carbon (C) [49] or metallic particles (e.g., silver (Ag) [8, 36], copper (Cu) [50], and gold (Au) [51]) are the most common selections. **Table 5** shows the resistivity of the bulk metal particles and the sintered metal ink form. Commonly, the metallic nanoparticles are stabilized in ink solutions by organic ligand shells, i.e., the nanoparticles are encapsulated with an organic material, called a capping agent, to form a uniform and stable dispersion, preventing particles agglomeration. This capping agent can be removed after printing through curing or sintering to allow physical contact between nanoparticles, forming continuous connectivity, i.e., a percolation path for electrical conductivity. Thus, sintering consist on welding the particles to each other below their melting point [2], and this particle welding could be achieved by exposure of the printed pattern to laser sintering [52], to microwave radiation [53], by applying an electrical voltage [54], by a chemical agent at room temperature (RT sintering) [55], or, the most conventional approach, by heating (thermal sintering) [33, 56]. In the case of thermal sintering, the temperature (typically between 100 to 400°C) must be below the softening temperature of the substrate. The presence of a few nanometers organic layer between the conductive particles is enough to block the movement of electrons from one particle to the other [33], thus reducing electrical conductivity. If this happens, the removal of this organic layer is required at high temperatures. For this reason, the sintering temperature of the nanoparticle based inks has extreme importance in plastic electronic applications, where materials, such as polyethylene terephthalate [56] and polycarbonate [56], are widely used as substrates, but have low T_g (98 and 148°C, respectively). The electrical conductivity of a printed nanoparticles based ink layer also depends on the shape and size of the nanoparticles. The amount of sintering temperature and time required depend upon how easy the organic encapsulation breaks, the particle dimensions and upon the thickness of the ink film. The smaller the particle size (2–10 nm) the lower the temperature required to sinter the particles, the short is the process and a higher electrical conductivity is achieved. Typically, the nanoparticle loading inks is higher than 20 wt%. Metal nanoparticles hold the highest electrical conductivity, although, the use of the above categorized precious metals hardly fits in the so called low cost PE.

Conductive polymers are classified into two different categories: extrinsically or intrinsically conductive polymers. The extrinsically conductive polymers normally involve a blend of conductive or nonconductive polymers, and a highly conductive additive (e.g., metallic particles) suspended in the polymer matrix [57], meaning that they are extrinsically enhanced to be conductive. Relatively to the intrinsically conductive polymer, they consist simply in a network

Metal	**Ag**	**Cu**	**Au**
Pure state (Ω.m)	1.59×10^{-8}	1.68×10^{-8}	2.44×10^{-8}
Printed ink (μΩ.cm)*	10–50	5–7	8

*Dependent on sintering temperature and time-higher temperature.

Table 5. Metal resistivity [33].

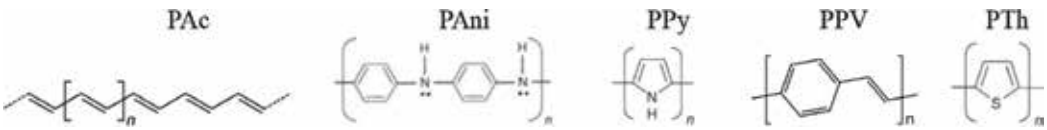

Figure 6. Chemical structure of conductive polymers.

of alternating single and double carbon bonds. It's this alternation of bonds that produces conjugated π-bonds, resulting in an intrinsically conductive material [58]. Polyacetylene (PAc), Polyaniline (PAni), polypyrrole (PPy), polyphenylene vinylene (PPV), polythiophene (PTh) are intrinsically conductive polymers (**Figure 6**).

Within the intrinsically conductive materials, the regioregular PTh has a tremendous potential for applications in flexible organics electronics because of its low cost and specific properties, such us, solubility (thanks to the three-substituents alkyl-chain in the PTh core [59]), spectroscopic and electronic properties, low-temperature process [60], highly ordered structure and semi-crystallinity state in its solid states [61], regioregular compatibility to large-area fabrications and industrial mass production technologies. In the chemical structure of the regioregular PThs, the backbone of the polymer is formed by thiophene rings and a chemical side-chain group can be attached on each thiophene ring along the polymer (**Figure 7**). An end-group or a secondary copolymer chain can be added to each end of the PTh.

Within the PTh and its derivatives, the poly(3-hexylthiophne) (P3HT) and poly (3,4-ethylenedioxythiophene) (PEDOT) [62] are the most well-known. The P3HT is a reference material in organic electronic, physics and chemistry to which any new p-type or donor conjugate molecule should be compared and evaluated. The PEDOT is the most widely used [63] intrinsically conductive polymer. PEDOT stands out for its high transparency [64] when deposited in thin oxidized films, high electrical conductivity [64], very high chemical stability in the oxidized state, processability and simplicity of production [65]. All these features make them suitable for several printing technologies, such as, spin coating [66], screen printing [67] and inkjet printing [68]. These unique properties make intrinsically conductive polymers excellent for various applications, such as, electrochromic devices [69], sensors [60], biosensors [68], actuators [70], capacitors [70], and photovoltaic cells [70], thin film diode [71]; organic thin film transistors (OTFTs) [72], photodiodes, Organic Field-Effect Transistor (OFETs) [52], organic light-emitting diodes (OLEDs) [73], etc., with a growing interest in PE due to its relatively low cost [74].

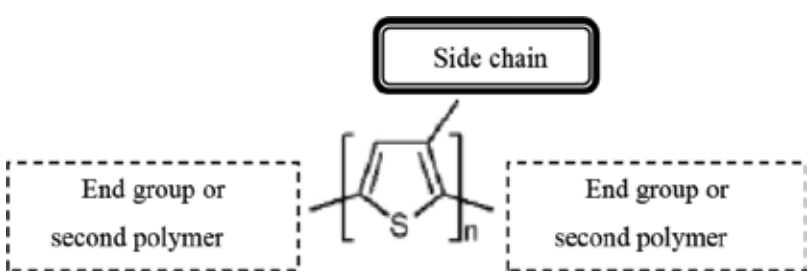

Figure 7. Schematic diagram of a regioregular polythiophene based polymers.

4. Flexible and extensible substrate for PE

There are three types of substrates that may be used on electronic devices: glass; metal and polymers. The first two are rigid material. The glass is non flexible. The metal foil is flexible and sustain high temperature, although, is limited on the freedom of design and is high cost. Polymers composites, such as, glass-reinforced epoxy laminates with flame retardant (FR-4) have been largely used in rigid printed circuit boards (PCB). Non-reinforced polymers are flexible materials, are more economically processed, and gives greater freedom of design, providing studies with increasingly intelligent PE applications, able to be integrated in complex systems and environments [34]. Their major drawback lies on the low surface energy, which, normally requires a prior surface treatment before printing and low processing temperatures. Their selection must meet a series of physical, mechanical, chemical, thermal and optical requirements, and also important, the compatibility with the conductive inks.

Various types of polymers (semi-crystalline and amorphous) have been proposed as flexible substrates (e.g., polyimide [5, 12, 74], polyethylene terephthalate [11], polyethylene naphthalate [75], PVDF [14], polycarbonate [14]), and both flexible and extensible substrates (e.g., poly (PDMS) [4, 5, 75, 76], polyurethane [76], thermoplastic polyurethanes (TPU) [77, 78]), etc. **Table 6** shows the main properties of flexible polymeric substrates.

Substrate	PI	PET	PC	PEN	PDMS	TPU
Tg (°C)	155–270	70–110	145	120–155	−125	80
Tm (°C)	250–452	115–258	115–160	269	–	180
Density (g/cm^3)	1.36–1.43	1.39	1.20–1.22	1.36	1.03	1.18
Vol.Res.(Ω.cm)	1.5×10^{17}	1.0×10^{19}	10^{12}–10^{14}	10^5	1.2×10^{14}	3.0×10^{14}
Modulus (MPa)	2.5×10^3	2–4.1×10^3	2.0–2.6×10^3	0.1–0.5×10^3	1	7
WorkTemp. (°C)	Up to 400	−50 to 150	−40 to 130	–	−45 to 200	130
CTE (ppm/°C)	8–20	15–33	75	20	310	153
Water absorption (%)	1.3–3.0	0.4–0.6	0.16–0.35	0.3–0.4	>0.1	0.2
Solvent resistance	Good	Good	Poor	Good	Poor	Good
Dimensional stability	Fair	Good	Fair	Good	Good	Good-

Tg – glass transition temperature, Tm – melting temperature, CTE – coefficient of thermal expansion.

Table 6. Comparison between flexible polymeric substrates.

5. Printing technologies challenges

Understanding the printing process and relationships between process parameters and printing quality (e.g., print resolution, uniformity and electrical conductivity of printed layer) is necessary for process optimization, as well as the suitability of the selected material in terms of adhesion and final applications; the appropriateness of the printed technology and ink

properties, the process deposition rate, etc. It will be a commitment between several criteria that will allow achieve the desired PE performance, functionalities and requirements. The main challenges are summarized in **Table 7**.

5.1. Compatibility between printable material and substrate

Most polymers have low surface energy (SE). The transfer and distribution of the ink on a substrate depends on the wettability and adhesion capabilities. The adhesion between two materials is the sum of a number of mechanical, physical, and chemical forces between them, at the interface, and depend on the mechanism of adhesion involved, that include mainly:

- Substrate properties (chemical composition, surface topography and porosity, etc.).
- Conductive ink properties (chemical composition, rheological behavior, the rate of solvent evaporation, etc.).
- The superficial tension (ST) of the ink and the SE of the substrate that will receive the ink, i.e., the difference between them.
- Functional groups and their intermolecular forces present in the ink/polymer system.

Surface wettability, spreadability and adhesion are the most important requirements in the printing process, and both are directly dependent on the fluid contact angle (**Figure 8**). When a fluid spreads evenly over the surface without the formation of droplets, the surface is said to be wettable. When a droplet is formed, the surface is said to be non-wettable, implying that cohesive forces associated with the fluid are greater than the forces associated with the interaction of the fluid with the surface. ST refers to the amount of cohesive forces between liquid molecules. The SE describes the degree of energy with which the molecules of the surface of a solid draw and allow adherence of a fluid. Often, ST and SE are interrelated, since both measure the ability of molecules to attract and to adhere to each other. In IPT, the spheroidal shape of the liquid emerging from the nozzle is defined by the ST of the liquid. The adhesion between two surfaces (ink, substrate) occurs when these droplets come into contact and develop strength in order to maintain a stable interface solid–liquid. Adhesion between a solid and a liquid exists when the solid SE exceeds the liquid ST.

The polymer low SE represents a great challenge in PE. In this situation, surface treatments are required to increasing the SE of the polymer, although implies an extra step in the

Flexible substrates	Printable inks	Equipment
• Flexible substrates encapsulation • Cost effective barrier encapsulation material • Scalability to large area (e.g., OLEDs) • Adhesion • Long time reliability	• Development of new inks formulation • Adhesion • Scalability to large area • Lifetime and stability	• Appropriate, affordable • High volumes • Resolution

Table 7. Main challenges.

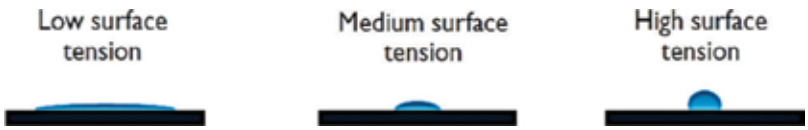

Figure 8. Ink behavior on a substrate.

manufacturing process, increases the time and cost of production. Adhesion-enhancing techniques such as: chemical [79] or mechanical induced roughening of the surface [77], or resorting to a primer (e.g., silane coupling agents [80]), corona discharge [81], plasma treatment [82], and flame treatment [81] are some examples. The most common techniques are plasma, flame and chemical treatment. With plasma and flame treatment, the substrate SE is changed by creating functional groups on the surface and eliminating surface contaminants. Although, the surface treatment is temporary, i.e., the treatment enhances the compatibility of the surface with the ink, but the exposure to air induces hydrophobic recovery [83]. Therefore, it is recommended to print after surface treatment. Chemical treatment is another option. The chemical treatment changes the surface characteristics (physical and chemical) by increasing the total area of interface between both layers leading to structural changes (by increasing the interface roughness) and interactions between the fluid molecules and the substrate.

5.2. Printable materials compatibility

Another aspect that can pose a problem during printing is the incompatibility between different inks used in multilayered structures or between layers of the same ink, which can cause dissolution or resuspension of the previously deposited layer of ink, depriving uniform and uncontaminated layers [42]. The morphology and uniformity of the printed pattern depends on the contained deposited drop in the determined spatial printing area.

The optimization of the ink and interaction between ink and the substrate strongly affects the final resolution and constitutes a main research challenge in order to achieve repeatability of printed patterns and devices. An optimized ink formulation, according to equipment and target application, as well as the substrate treatment processes constitute the main successful factors to achieve high resolution and repeatability of the printed patterns and devices.

Equally relevant are the different post-processing treatments, such as, sintering, annealing or simply drying in air required for each ink, which defines the final morphology and uniformity of the printed pattern and the manufacturing time [32].

6. Applications of IPT to flexible PE

The increase of the printing resolution leads to an increased number of applications. Lee et al. [84] developed a flexible capacitive pressure sensor for plantar pressure measurement, using a flexible printed circuit film as a sensor substrate and PDMS as dielectric layer. Cheng et al. [5] developed a tactile sensor with PDMS using a highly reliable capacitive mechanism. However, the required manufacturing process involved multiple factoring steps and the use

of several material layers, which consequently leads to time consumption, large material waste and high manufacturing costs, preventing the process automation to an industrial level. When the goal is large area sensing platforms, manufacture premium prices constitute a problem. In recent years, the interest for IPT to sensor fabrication has attracted attention [39, 85]. First IPT prototypes start to appear and has already been selected to step in the production of several devices, such as, integrated circuits [30, 33], transistors [32, 86], conducting polymer devices [30], structural polymers and ceramics [85], biomaterials, and printed scaffolds for growth of living tissues [30, 31]. In the field of flexible sensors, IPT it is just taking the first steps. IPT of an intrinsically conducting polymer [87] onto a flexible substrate for humidity and gas sensing applications [88] are two of many of the rapidly emerging IPT examples. Only a few examples of IPT sensors combining IPT polymer conductive ink (PEDOT:PSS and P3HT) [79, 89] or silver ink [90], printed on polymer substrate have been reported so far. Someya et al. [91] has developed flexible pressure sensors with a complex designed structure using OFET active matrices manufactured by IPT and screen printing technology. Basiricó et al. [92] have proposed a totally IPT flexible OFET assembled on plastic films as sensors for mechanical variables using a PEDOT:PSS as electrodes and a P3HT as a semiconductor. The results obtained were promising despite the lower charge carrier mobility measured. Cruz et al. [89] have developed a inkjet printed pressure sensing platform capable of measuring the central plantar pressure (CPP). The use of PEDOT:PSS for definition of the electrodes over a TPU substrate resulted in pressure sensors with higher sensitivities and better linearity. Good performance results (comparable with existing solutions) were achieved, with the particularity of offering a low-cost alternative. The printed substrate presented high flexibility, was able to follow and deform along with the substrate, without breaking or losing adhesion and its conductivity properties. The ink piezo-resistive effect and high gauge factors (>300) were demonstrated (higher than the typical value of flexible metallic strain gauges) showing the potential of the material to be used in several sensing applications [79].

7. Final remarks

The PE technology is not a replacement for conventional electronics, however, allows free design and unlimited applications areas. The PE benefits from new printing technologies, new material solutions, and by the combination of other manufacturing processes. The increase of research and development is reflecting a growing interest in the new generation of flexible and PE applications for, space and weight reduction. The PE had an undeniable impact on the electronic industry, economics and on the human life, revolutionizing the electronic applications, otherwise impossible to achieve with the conventional techniques and materials.

This chapter made an overview of the most important printing techniques and material solutions for the PE, with particular attention to the IPT. For the different printing technology, the process requirements, the materials and their critical limitations, highlighting their main features, were summarized. The possibility of combining technologies to overcome one technology limitation with another technology was also presented. Moreover, IPT is a promising technology which main advantages lies on its simplicity and low cost operating principle, overcoming the flaws of traditional technologies. Also, the main printing challenges are addressed, in terms

of compatibility between printable material and substrate. At the end, examples of IPT flexible PE are presented. A breakthrough is expected in the next years which potentially will reduce cost with mass production applications. So far, there are other issues that need to be discussed and practical questions start to arise once the industry gets more involved and focused in developing commercial products, such us, market trend, recycling, and return of the investment.

Acknowledgements

TSSiPRO – Technologies for Sustainable and Innovative Products, NORTE-01-0145-FEDER-00 0015, supported by the NORTE 2020, under the terms of Notice of Appeal No. NORTE-45-2015-2102 "Structured R&D&I Projects", framed in the IPC/i3N Research Unit.

Author details

Sílvia Manuela Ferreira Cruz[1]*, Luís A. Rocha[2] and Júlio C. Viana[1]

*Address all correspondence to: s.cruz@dep.uminho.pt

1 IPC/I3N – Institute of Polymers and Composites/Institute for Nanostructures, Nanomodelling and Nanofabrication, Polymer Engineering Department, Campus of Azurém, University of Minho, Portugal

2 CMEMS, University of Minho, Guimarães, Portugal

References

[1] Adcock T, Fenner D. Printed Electronics Traditional Technology Addresses Today's Smaller, Faster, Lower Cost Requirements [Internet]. 2012. Available from: http://www.henkel.com/electronics.htm [Accessed: Feb 20, 2018]

[2] Nir M et al. Electrically conductive inks for inkjet printing. In: Magdassi S, editor. Handbook of Chemistry of Inkjet Inks. Jerusalem: World Scientific Publishing; 2010. pp. 225-254. DOI: 10.1142/9789812818225_0012

[3] Engel J et al. Flexible multimodal tactile sensing system for object identification. In: Proceedings of the IEEE Sensors; Oct 22-25, 2006. Exco, Daegu, Korea: IEEE; 2007. pp. 563-566

[4] Chiang C-C, Lin C-C K, Ju M-S. An implantable capacitive pressure sensor for biomedical applications. Sensors Actuators A: Physical. 2007;**134**:382-388. DOI: 10.1016/j.sna.2006.06.007

[5] Cheng MY, Lin CL, Yang YJ. Tactile and shear stress sensing array using capacitive mechanisms with floating electrodes. In: Proceedings of the IEEE 23rd International Conference on Micro Electro Mechanical Systems (MEMS). Wanchai, Hong Kong, China: IEEE; Feb 2010. pp. 228-231

[6] Pritchard E, Mahfouz M, Evans B, Eliza S, Haider M. Flexible capacitive sensors for high resolution pressure measurement. Sensors IEEE. 2008;**1484**:1484-1487. DOI: 10.1109/ICSENS.2008.4716726

[7] Basiricó L. Inkjet printing of organic transistor devices [thesis]. University of Cagliari; 2012

[8] Li M, Li Y-T, Li D-W, Long Y-T. Recent developments and applications of screen-printed electrodes in environmental assays-review. Analytica Chimica Acta. 2012;**734**:31-44. DOI: 10.1016/j.aca.2012.05.018

[9] Li J, Peng T, Fang C. Screen-printable sol–gel ceramic carbon composite pH sensor with a receptor zeolite. Analytica Chimica Acta. 2002;**455**:53-60. DOI: 10.1016/S0003-2670(01)01540-9

[10] Metters JP, Kadara RO, Banks CE. Fabrication of co-planar screen printed microband electrodes. The Analyst. 2013;**138**:2516-2521. DOI: 10.1039/C3AN00268C

[11] Webb AJ et al. A multi-component nanocomposite screen-printed ink with non-linear touch sensitive electrical conductivity. Nanotechnology. 2013;**24**:165501. DOI: 10.1088/0957-4484/24/16/165501

[12] Ochoteco E et al. Tactile sensors based on conductive polymers. Microsystems Technology. 2010;**16**:765-776. DOI: 10.1117/12.821627

[13] Blayo A, Pineaux B. Printing processes and their potential for RFID printing. In: Proceedings of the 2005 Joint Conference on Smart Objects and Ambient Intelligence: Innovative Context-Aware Services: Usages and Technologies. Grenoble, France: ACM; 2005. pp. 27-30

[14] Julin T. Flexo-printed piezoelectric PVDF pressure [thesis]. Tampere University of Technology; 2011

[15] Clark DA, Major Trends in Gravure Printed Electronics [Internet]. 2010. Available from: http://digitalcommons.calpoly.edu/grcsp/26 [Accessed: Nov 23, 2017]

[16] Sung D, Fuente VA, Subramanian V. Scaling and optimization of gravure-printed silver nanoparticle lines for printed electronics. IEEE Transactions on Components and Packaging Technologies. 2010;**33**:105-114. DOI: 10.1109/TCAPT.2009.2021464

[17] Lee T-M et al. The effect of shear force on ink transfer in gravure offset printing. Journal of Micromechanics and Microengineering. 2010;**20**:125026. DOI: 10.1088/0960-1317/20/12/125026

[18] Yang J et al. Organic photovoltaic modules fabricated by an industrial gravure printing proofer. Solar Energy Materials and Solar Cells. 2013;**109**:47-55. DOI: 10.1016/j.solmat.2012.10.018

[19] Reddy A et al. Fully printed flexible humidity sensor. In: Proc. Eurosensors XXV, Sep 4-7, 2011. Athens, Greece: Procedia Engineering; 2011. pp. 120-123

[20] Liu C-X, Choi J-W. Patterning conductive PDMS nanocomposite in an elastomer using microcontact printing. Journal of Micromechanics and Microengineering. 2009;**19**:85019. DOI: 10.1088/0960-1317/19/8/085019

[21] Xia Y, Whitesides GM. Soft lithography. Annual Review of Materials Science. 1998;**37**:550. DOI: 0084-6600/98/0801-0153$08.00

[22] Qin D, Xia Y, Whitesides GM. Soft lithography for micro- and nanoscale patterning. Nature Protocols. 2010;**5**:491-502. DOI: 10.1038/nprot.2009.234

[23] Kawase T et al. Inkjet printing of polymer thin film transistors. Thin Solid Films. 2003; **438**:279-287. DOI: 10.1016/S0040-6090(03)00801-0

[24] Khan S, Lorenzelli L, Dahiya R. Technologies for printing sensors and electronics over large flexible substrates: A review. IEEE Sensors Journal. 2015;**15**:3164-3185. DOI: 10. 1109/JSEN.2014.2375203

[25] Arnold CB, Piqué A. Laser direct-write processing. MRS Bulletin. 2007;**32**:9-15

[26] Bauerle D. Handbook of Laser Processing and Chemistry. 3rd ed. Physics and Astronomy. Berlin Heidelberg: Springer-Verlag; 2000. 19p

[27] Steen W, Mazumder J. Handbook of Laser Material Processing. 4th ed. London: Springer-Verlag; 2010. 558 p. DOI: 10.1007/978-1-84996-062-5

[28] Christenson KK et al. Direct printing of circuit boards using Aerosol Jet. In: Technical Program and Proceedings. NIP 27 Digital Fabrication. Springfield, Va: IS&T–the Society for Imaging Science and Technology; 2011. pp. 433-436

[29] Optomec [Internet]. 2018. Available from: https://www.optomec.com/ [Accessed: Jan 2, 2018]

[30] Calvert P. Inkjet printing for materials and devices. Chemistry of Materials. 2001;**13**: 3299-3305. DOI: 10.1021/cm0101632

[31] Calvert P, Yoshioka Y, Jabbour G. Inkjet printing for biomimetic and biomedical materials. In: Reis RL, Weiner S, editors. Handbook of Learning from Nature How to Design New Implantable Biomaterials. Netherlands: Kluwer Academic Publishers; 2004. pp. 169-180

[32] Al-chami H. Inkjet printing of transducers [thesis]. University of British Columbia; 2010

[33] Kamyshny A, Steinke J, Magdassi S. Metal-based inkjet inks for printed electronics. The Open Applied Physics Journal. 2011;**4**:19-36. DOI: 10.2174/1874183501104010019

[34] Fuller SB, Wilhelm EJ, Jacobson JM. Ink-jet printed nanoparticle microelectromechanical systems. Journal of Microelectromechanical Systems. IEEE. 2002;**11**:54-60. DOI: 10.1109/84.982863

[35] Perelaer J, Schubert US. Inkjet printing and alternative sintering of narrow conductive tracks on flexible substrates for plastic electronic applications. In: Turcu C, editor.

Handbook of Radio Frequency Identification Fundamentals and Applications Design Methods and Solutions. Croatia: InTech; 2010. pp. 265-286. DOI: 10.5772/7983

[36] Gans BJ, Duineveld PC, Schubert US. Inkjet printing of polymers: State of the art and future developments. Advanced Materials. 2004;**16**:203-213. DOI: 10.1002/adma.200300385

[37] Hadimioglu B et al. Acoustic ink printing. In: Ultrasonics Symposium. Tucson, AZ, USA: IEEE; 1992. pp. 929-936. DOI: 10.1109/ULTSYM.1992.275823

[38] Ujiie H. Handbook of Digital Printing of Textiles. 1st ed. Cambridge, London: Woodhead Publishing; 2006. 384 p

[39] Paul KE, Wong WS, Ready SE, Street RA. Additive jet printing of polymer thin-film transistors. Applied Physics Letters. 2003;**83**:2070-2072. DOI: 10.1063/1.1609233

[40] Junfeng M, Lovell MR, Mickle MH. Formulation and processing of novel conductive solution inks in continuous inkjet printing of 3-D electric circuits. IEEE Transactions on Electronics Packaging Manufacturing. 2005;**28**:265-273. DOI: 10.1109/TEPM.2005.852542

[41] Andò B, Baglio S. Inkjet-printed sensors: A useful approach for low cost, rapid prototyping. IEEE Instrumentation & Measurement Magazine. 2011;**14**:36-40. DOI: 10.1109/MIM.2011.6041380

[42] Caglar U. Studies of inkjet printing technology with focus on electronic materials [thesis]. Tampere University; 2009

[43] Hertz [Internet]. 2015. Available from: https://www.google.com/patents/US6509917 [Accessed: Nov 6, 2018]

[44] Smith L et al. Continuous ink-jet print head utilizing silicon micromachined nozzles. Sensors and Actuators A: Physoical. 1994;**43**:311-316. DOI: 10.1016/0924-4247(93)00707-b

[45] Piqué A, Chrisey DB. Handbook of Direct-Write Technologies for Rapid Prototyping Applications: Sensors, Electronics, and Integrated Power Sources. New York: Academic Press; 2002. 726 p

[46] Cabbill V. Introduction to Digital Printing Technology. Graphic Artists: Pre-Press Personnel; 1998

[47] Hudd A. Inkjet printing technologies. In: Magdassi S, editor. Handbook of The Chemistry of Inkjet Inks. Singapore: World Scientific Publishing; 2010. pp. 3-18. DOI: 10.1142/9789812818225_0001

[48] Lin C-T, Hsu C-H, Lee C-H, Wu W-J. Inkjet-printed organic field-effect transistor by using composite semiconductor material of carbon nanoparticles and poly(3-Hexylthiophene). Journal of Nanotechnology. 2011;**2011**:1-7. DOI: 10.1155/2011/142890

[49] Lin C-T, Hsu C-H, Chen I-R, Lee C-H, Wu W-J. Enhancement of carrier mobility in all-inkjet-printed organic thin-film transistors using a blend of poly(3-hexylthiophene) and carbon nanoparticles. Thin Solid Films. 2011;**519**:8008-8012. DOI: 10.1016/j.tsf.2011.05.071

[50] Haffarzadeh K, Zervos H. Conductive Ink Markets 2012-2018 Silver & Copper Inks & Pastes and Beyond. USA: IDTechEX; 2012

[51] Molesa S, Redinger DR, Huang DC, Subramanian V. High-quality inkjet-printed multilevel interconnects and inductive components on plastic for ultra-low-cost RFID applications. In: Materials Research Society Symposia Proceedings. Vol. 769. Cambridge, Boston, USA: Materials Research Society; 2003. pp. 1-6

[52] Ko SH et al. All-inkjet-printed flexible electronics fabrication on a polymer substrate by low-temperature high-resolution selective laser sintering of metal nanoparticles. Nanotechnology. 2007;**18**:345202. DOI: 10.1088/0957-4484/18/34/345202

[53] Perelaer J, Gans B-J, Schubert US. Ink-jet printing and microwave sintering of conductive silver tracks. Advanced Materials. 2006;**18**:2101-2104. DOI: 10.1002/adma.200502422

[54] Xie G, Ohashi O, Yamaguchi N, Wang A. Effect of surface oxide films on the properties of pulse electric-current sintered metal powders. Metallurgical and Materials Transactions A. 2003;**34**:2655-2661. DOI: 10.1007/s11661-003-0024-1

[55] Wakuda D, Hatamura M, Suganuma K. Novel method for room temperature sintering of Ag nanoparticle paste in air, Chemical Physics Letters. 2007;**441**:305-308. DOI: 10.1016/j.cplett.2007.05.033

[56] Perelaer J et al. One-step inkjet printing of conductive silver tracks on polymer substrates. Nanotechnology. 2009;**20**:165303. DOI: 10.1088/0957-4484/20/16/165303

[57] Mcbride JW, Lam L. A review of conducting polymers in electrical contact applications. In: International Conference of Polymeric Materials in Power Engineering ICPMPE-07 I-3, University of Southampton Institutional Repository; Oct 4-6, 2007. p. 9

[58] Elschner A et al. PEDOT – Principles and Applications of an Intrinsically Conductive Polymer 2010. New York: Taylor and Francis Group, CRC Press; 2011. 377 p

[59] Li B et al. Inkjet printed chemical sensor array based on polythiophene conductive polymers. Sensors and Actuators B: Chemical. 2007;**123**:651-660. DOI: 10.1016/j.snb.2006.09.064

[60] Bernardo G et al. Solid-state low-temperature extrusion of P3HT ribbons. Applied Physics A: Materials Science and Processing. 2014;**117**:2079-2086. DOI: 10.1007/s00339-014-8622-x

[61] Chen T-A, Wu X, Rieke RD. Regiocontrolled synthesis of poly(3-alkylthiophenes) mediated by Rieke Zinc: Their characterization and solid-state properties. Journal of American Chemical Society. 1995;**117**:233-244. DOI: 10.1021/ja00106a027

[62] Bai H, Shi G. Gas sensors based on conducting polymers. Sensors. 2007;**7**:267-307

[63] Chen JH, Dai C-A, Chiu W-Y. Synthesis of highly conductive EDOT copolymer films via oxidative chemical *in situ* polymerization. Journal of Polymer Science-Part A: Polymer Chemistry. 2008;**46**:1662-1673. DOI: 10.1002/pola.22508

[64] Kim YH, Sachse C, Machala ML, May C, Müller-Meskamp L, Leo K. Highly conductive PEDOT:PSS electrode with optimized solvent and thermal post-treatment for ITO-free organic solar cells. Advanced Functional Materials. 2011;**21**:1076-1081. DOI: 10.1002/adfm.201002290

[65] Groenendaal JR, Jonas L, Freitag F, Pielartzik D, Reynolds H. Poly(3,4-ethylenedioxythiophene) and its derivatives: Past, present, and future. Advanced Materials. 2000;**12**:481-494. DOI: 10.1002/(SICI)1521-4095(200004)12:73.3.CO;2-3

[66] Greco F et al. Ultra-thin conductive free-standing PEDOT/PSS nanofilms. The Royal Society of Chemistry. 2011;**7**:10642-10650. DOI: 10.1039/c1sm06174g

[67] Zirkl M et al. An all-printed ferroelectric active matrix sensor network based on only five functional materials forming a touchless control interface. Advanced Materials. 2011;**23**:2069-2074. DOI: 10.1002/adma.201100054

[68] Phongphut A et al. A disposable amperometric biosensor based on inkjet-printed au/PEDOT-PSS nanocomposite for triglyceride determination. Sensors Actuators B: Chemistry. 2013;**178**:501. DOI: 10.1016/j.snb.2013.01.012

[69] Deutschmann T, Oesterschulze E. Micro-structured electrochromic device based on poly(3,4-ethylenedioxythiophene). Journal of Micromechanics and Microengineering. 2013;**23**:065032. DOI: 10.1088/0960-1317/23/6/065032

[70] Wang Y. Research progress on a novel conductive polymer–poly(3,4-ethylenedioxythiophene) (PEDOT). Journal of Physics Conference Series. 2009;**152**:12023. DOI: 10.1088/1742-6596/152/1/012023

[71] Speakman SP et al. High performance organic semiconducting thin films: Ink jet printed polythiophene [rr -P3HT]. Organic Electronics. 2001;**2**:65-73

[72] Molina-Lopez F, Briand D, Rooij NF. All additive inkjet printed humidity sensors on plastic substrate. Sensors Actuators B: Chemical. 2012;**212**:212-222. DOI: 10.1016/j.snb.2012.02.042

[73] Xie G, et al. Fabrication and properties of an OLED-based gas sensor with poly(3-hexylthiophene) sensing film. In: IMCS 2012 – 14th Int. Meet. Chem. Sensors, AMA Services Gmbh; 2012. pp. 1130-1133

[74] Kang BJ, Lee CK, Oh JH. All-inkjet-printed electrical components and circuit fabrication on a plastic substrate. Microelectronic Engineering. 2012;**97**:251. DOI: 10.1016/j.mee.2012.03.032

[75] Caglar U et al. Analysis of mechanical performance silver inkjet-printed structures. In: 2nd IEEE Int. Nanoelectron. Conf. INEC 2008. Shanghai, China: IEEE; 2008. pp. 851-856

[76] Suzuki M, Takahashi T, Aoyagi S. Flexible tactile sensor using polyurethane thin film. Micromachines. 2012;**3**:315. DOI: 10.3390/mi3020315

[77] Cruz S, Rocha LA, Viana JC. Enhanced printability of thermoplastic polyurethane substrates by silica particles surface interactions. Applied Surface Science. 2016;**360**:198. DOI: 10.1016/j.apsusc.2015.10.094

[78] Cruz S, Rocha LA, Viana JC. Piezo-resistive behaviour at high strain levels of PEDOT:PSS printed on a flexible polymeric substrate by a novel surface treatment. Journal of Materials Science: Materials in Electronics. 2017;**28**:2563-2573. DOI: 10.1007/s10854-016-5832-3

[79] Siau S, Vervaet A, Van Calster A, Swennen I, Schacht E. Influence of wet chemical treatments on the evolution of epoxy polymer layer surface roughness for use as a build-up layer Appl. Surface Science. 2004;**237**:457. DOI: 10.1016/j.apsusc.2004.06.111

[80] Arkles B, Pan Y, Kim YM. The role of polarity in the structure of silanes employed in surface modification. In: Mittal KL, editor. Handbook of Silanes and Other Coupling Agents. Vol. 5. Leiden, The Netherlands: Taylor & Francis Group; 2009. p. 14

[81] Strobel M, Jones V, Lyons CS, Ulsh M, Kushner MJ, Dorai R, Branch MC. A comparison of corona-treated and flame-treated polypropylene films. Plasmas and Polymers. 2003;**8**:61-95

[82] Morent R, Geyter N, Leys C. Effects of operating parameters on plasma-induced PET surface treatment. Nuclear Instruments and Methods in Physics Research Section B. 2008;**266**:3081. DOI: 10.1016/j.nimb.2008.03.166

[83] McDonald JC, Whitesides GM. Poly(dimethylsiloxane) as a material for fabricating microfluidic devices. Accounts of Chemical Research. 2002;**35**:491. DOI: 10.1021/ar010110q

[84] Lei KF, Lee K-F, Lee M-Y. Development of a flexible PDMS capacitive pressure sensor for plantar pressure measurement. Microelectronic Engineering. 2012;**99**:1-5. DOI: 10.1016/j.mee.2012.06.005

[85] Griggs C, Sumerel J, Ph D, Industrial + Speccialty Printing [Internet]. 1899. Available from: http://www.industrial-Printing.net [Accessed: Dec 21, 2017]

[86] Meixner RM, Cibis D, Krueger K, Goebel H. Characterization of polymer inks for drop-on-demand printing systems. Microsystem Technologies. 2008;**4**:1137. DOI: 10.1007/s00542-008-0639-7

[87] Kulkarni MV et al. Ink-jet printed conducting polyaniline based flexible humidity sensor. Sensors and Actuators B: Chemical. 2013;**178**:140-143. DOI: 10.1016/j.snb.2012.12.046

[88] Matic V et al. Inkjet printed differential mode touch and humidity sensors on injection molded polymer packages. IEEE Sensors 2014 Proc. 2234.Valencia, Spain: SENSORS, IEEE; 2014. DOI: 10.1109/ICSENS.2014.6985485

[89] Cruz S, Dias D, Viana J, Rocha LA. Inkjet printed pressure sensing platform for postural imbalance monitoring. IEEE Transactions on Instrumentation and Measurement. 2015;**64**:2813. DOI: 10.1109/TIM.2015.2433611

[90] Li Y et al. An all-inkjet printed flexible capacitor for wearable applications. In: Design, Test, Integration and Packaging of MEMS/MOEMS (DTIP), 2012 Symposium. Apr 25-27, 2012. Cannes, France: IEEE, 2012. pp. 25-28

[91] Someya T et al. Printed organic transistors for large-area electronics. In: 6th Int. Conf. Polymers & Adhesives in Microelectronics & Photonics, 2007. Polytronic. Japan: IEEE; 2007. pp. 6-11

[92] Basiricò L et al. Inkjet printed arrays of pressure sensors based on all-organic field effect transistors. In: 32nd Annual Int. Conf. IEEE EMBS Buenos Aires, Argentina. Engineering in Medicine and Biology Society (EMBC), 2010 Annual International Conference of the IEEE. 2010. pp. 2111-2114

Chapter 4

Direct Growth of Graphene on Flexible Substrates toward Flexible Electronics: A Promising Perspective

Viet Phuong Pham

Additional information is available at the end of the chapter

http://dx.doi.org/10.5772/intechopen.73171

Abstract

Graphene has recently been attracting considerable interest because of its exceptional conductivity, mechanical strength, thermal stability, etc. Graphene-based devices exhibit high potential for applications in flexible electronics, optoelectronics, and energy harvesting. In this paper, we review various growth strategies including metal-catalyzed transfer-free growth and direct-growth of graphene on flexible insulating substrates which are "major issues" for avoiding the complicated transfer process that cause graphene defects, residues, tears and performance degradation of its functional devices. Recent advances in practical applications based on "direct-grown graphene" are discussed. Finally, several important directions, challenges and perspectives in the commercialization of 'direct growth of graphene' are also discussed and addressed.

Keywords: graphene, direct-growth, flexible substrate, flexible electronic, chemical vapor deposition (CVD)

1. Introduction

Single-layer graphene (SLG) and few-layer graphene (FLG) films have been regarded as ideal materials for electronics and optoelectronics due to their excellent electrical properties and their ability to integrate with current top-down device fabrication technology [1–20]. Since the beginning of the twenty-first century, the interest in graphene materials has drastically increased, which is apparent in the number of annual publications on graphene (**Figure 1**). Until now, various strategies, including chemical vapor deposition (CVD) [21], liquid and mechanical exfoliation from graphite [16, 22, 23], epitaxial growth on crystal substrate [24–27], or solution-based processes on graphene oxides [28–34]. have been investigated for obtaining graphene layers. In particular, recent advances in CVD growth have successfully led to large-scale graphene

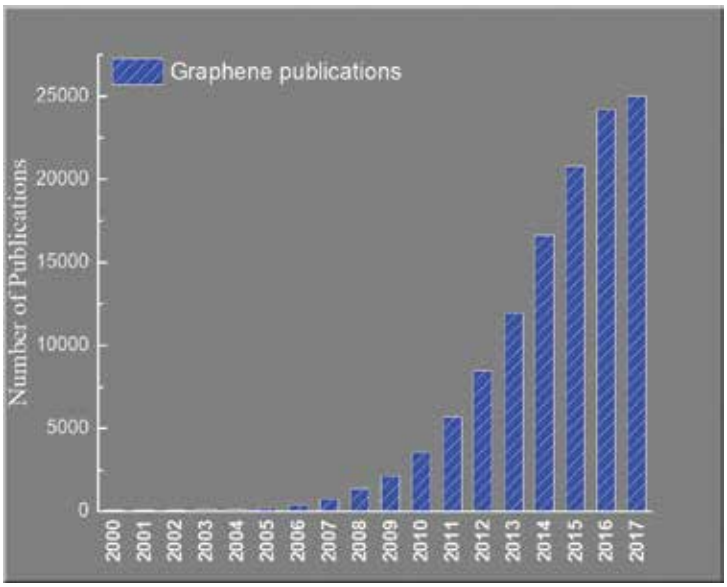

Figure 1. Publications on Graphene from 2000 to 2017. Source: ISI web of science (search: Topic = Graphene).

production on metal substrates [1, 21, 35–41], driven by the high demand for utilizing graphene in possible applications of current complementary metal-oxide-semiconductor (CMOS) technology such as radio-frequency transistors, optical devices, and deposition processes [2].

In these days, high-quality large-area graphene has been well synthesized on conducting metal substrates by using the catalytic CVD growth approach, which promoted a wide range of graphene-based device applications [1, 21, 35–42]. However, graphene grown on a metal substrate needs to be transferred onto dielectric substrates for electronic applications. Although various approaches, such as wet etching/transfer [38], mechanical exfoliation/transfer [16, 22, 23], bubbling transfer [43], electrochemical delamination [44–46], for transferring from the catalytic metal growth substrates to dielectric device substrates have been developed, none of these approaches is free from degradation of the transferred graphene. For example, 'wet etching and transfer', the most widely used transfer approach, is a serial process, which includes encapsulation the graphene surface with polymer supporting layer, subsequent chemical etching of the underlying metal substrate, transferring of the polymer/graphene film onto a dielectric substrate and removal of the polymer supporting layer [42]. Unfortunately, the transfer process is not just inconvenient but also causes various chemical and mechanical defects in the transferred graphene layer. CVD graphene grown on arbitrary substrates contains various defects, such as point defects, dislocation-like defects, cracks, wrinkles, and grain boundaries [47]. Because carbon atoms at such defect sites are chemically less stable than the carbon in defect-free graphene [47], the defect sites exposed to unavoidable surface/interface contaminants during the graphene transfer process are chemically damaged by bonding to oxygen, hydrogen, etc. Similarly, CVD graphene can be contaminated by metallic impurities from the growth substrate, which influences the electrochemical and electronic properties of graphene [48, 49]. CVD graphene never has 100% coverage and there are defects and holes which can

be determined electrochemically [50]. In addition, transfer of ultrathin graphene layer on to target substrates leave unavoidable mechanical defects in the transferred graphene, such as cracks, tears and wrinkles. Thus, it leads to high deterioration in the performance of the resulting graphene-based devices, such as inducing a gradual reduction in the electrical conductivity of the devices or reducing the stability or increasing the leakage current of the devices.

Recently, significant efforts have been made to obtain graphene on semiconductor and dielectric substrates to avoid the problematic wet-transfer process. For example, a graphene was directly grown on a quartz substrate using a thin-layer Cu (100–450 nm thick) on the substrate as catalytic layer [51]. After growth on the Cu layer and the graphene layer could be transferred directly on the underlying dielectric surface through de-wetting and evaporating of Cu layer. Furthermore, the graphene on Cu was patterned for facile transfer to the underlying dielectric substrate after etching of the metal layer underneath the graphene [52]. However, the above transfer methods may only be suitable for small-size lateral graphene. Recently, Byun et al. have obtained FLG directly on SiO_2 using organic-polymer-coated insulators and thermal encapsulation of the Ni layer [53]. Lee et al. have observed the formation of FLG at the interfaces of Ni and SiO_2 using plasma-enhanced CVD (PECVD); however, the interface FLG was defective and thick [54]. The graphene formation on Ni is due to the dissociation and precipitation processes of the carbon species in Ni [54]. Consequently, the carbon precipitation is a non-equilibrium process and might be a major challenge for obtaining homogeneous graphene based on an Ni catalyst [36, 55]. The drawback of the metal catalyzed-CVD process is defects and tears unavoidably during the transfer process [56]. To avoid these drawbacks, two growth approaches have been suggested for the direct formation of graphene on flexible and rigid insulating substrates: (1) metal-catalyzed direct growth without transfer to external substrates [51], and (2) direct growth of graphene on a dielectric substrate without metal catalyst [57–59]. A recent report demonstrated graphene synthesized by metal-free CVD process on sapphire for forming large-scale highly crystalline SLG; however, it still has high wrinkles or ripples [60], similar to the situation in case of graphene pads/exfoliated h-BN [61]. Consequently, the metal-free CVD growth is not yet applicable to amorphous flexible and rigid substrates. A promising approach for increasing the graphene quality and minimizing the amount of metal catalyst is by evaporation and reaction with carbon-based gas precursors on the substrate surface. The formation of SLG and FLG on amorphous oxide substrates has been described in a previous report [62]. However, there are still many drawbacks that need to be addressed, particularly the amount of defects and non-uniform graphene due to imperfect nucleation and catalytic reactions. To the best of our understanding, there is no uniform high-quality SLG directly grown on dielectric substrates.

Considering that the mechanical transfer of graphene to the device substrates inevitably causes serious degradation in the performance of the resulting graphene devices, direct growth of graphene in a simple way on the flexible organic (e.g. polyimide (PI), PDMS, and Willow glass, mica) or rigid inorganic (e.g. glass, AlN, GaN, sapphire, quartz, Si, textured Si, SiO_2, SiC, fused silica, MgO, h-BN, MnO_2, TiO_2, and HfO_2) insulating substrates is highly desirable. The direct growth approach for device applications enables avoiding complex transfer process and transfer-induced defects. Moreover, it enables conformal growth of graphene on three-dimensional (3D) surfaces, which is necessary for various functional

devices, such as sensors [63–65], black silicon solar cells [66], cambered micro-optics [67], 3D microelectromechanical system (MEMS) [68], or CMOS technology-based applications [2]. Here, we present an overview of various recently reported strategies for direct graphene growth on flexible substrates. In addition, a wide-range of applications as well as the perspectives and challenges are also addressed.

2. Generally growth mechanism of CVD-based graphene

CVD growth of graphene is a chemical process for the formation of SLG or FLG on an arbitrary substrate by exposing the substrate to the gas-phase precursors at controlled reaction conditions [69]. Owing to the versatile nature of CVD, intricately mixed homogeneous gas-phase and heterogeneous surface reactions are involved [70]. In general, as the partial pressure and/or temperature in the reaction substances are increased, homogeneous gas-phase reactions and the resulting homogeneous nucleation become significant [80]. To grow a high-quality graphene layer, this homogeneous nucleation needs be minimized [70]. A general mechanism for CVD-based graphene growth on catalytic metal substrates, for the growth of uniform and highly crystalline graphene layer on the surface, includes eight steps as follow: (1) mass transport of the reactant, (2) reaction of the film precursor, (3) diffusion of gas molecules, (4) adsorption of the precursor, (5) diffusion of the precursor into substrate, (6) surface reaction, (7) desorption of the product, and (8) removal of the by-product (**Figure 2**) [71].

Typically, CVD growth of 2D materials (e.g. graphene) involves catalytic activation of chemical reactions of precursors at the growth substrate surface/interface in a properly designed

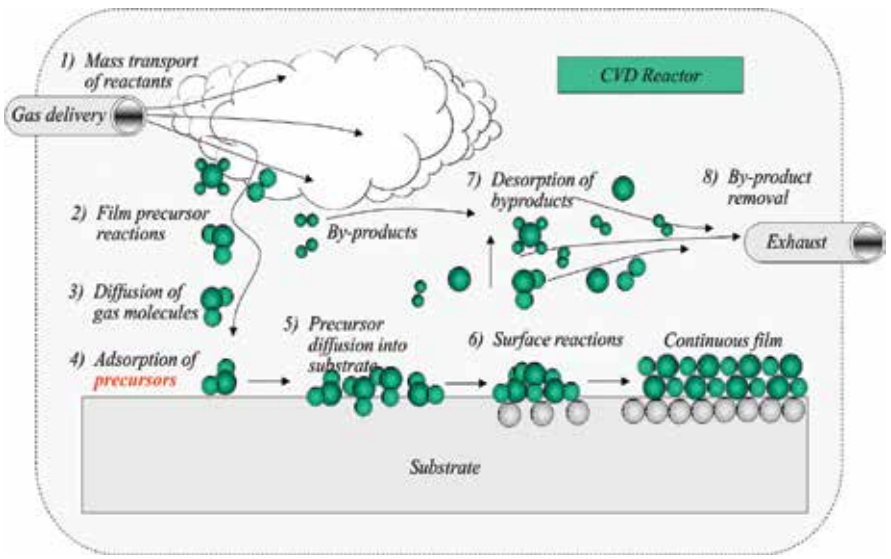

Figure 2. Diagram of generally growth mechanism of CVD-based graphene: Transport and reaction processes. Reproduced with permission from [71]. Copyright 2011, Freund Publishing.

environment. Generally speaking, the roles of precursors, conditions (e.g. fast growth rates, large domain size, or very high crystalline quality), atmosphere, substrates and catalysts are the key factors affecting the final quality of the grown 2D materials. So far, significant efforts have been made to prepare highly crystalline 2D materials (e.g. graphene), but many challenges are still ahead. For example, due to the rough feature of catalytic metal surface, growth of uniform and high quality graphene is considerably difficult. The 2D material research community is also interested in new precursors (e.g. solid precursor only, gas precursor or solid precursor mixed with certain solvents) that could induce the formation of high-quality uniform graphene with minimal defect density. Another question is the effect of growth rate on the catalytic metal surface on the quality of graphene. Currently, it is difficult to give an exact answer, as investigations are progressing at an exponential rate.

However, non-catalytic direct-growth of graphene on semiconducting and dielectric rigid and flexible substrates follows different mechanisms according to our best insights. To date, the understanding of the concept of the general mechanism of the direct growth of graphene is still not yet adequate, neither experimentally nor theoretically, with many proposed possible growth mechanisms, e.g. vapor-solid-solid [72], or vapor-solid [73], or solid-liquid-solid [74]. There has been arguments on the direct-growth mechanism of graphene domains on dielectric rigid and flexible substrates or non-catalytic substrates in previous reports [59, 60, 75], but the mechanism for the entire process of the carbon precursor transformation to the crystalline graphene structures has not yet been fully understood. Thus, understanding the graphene growth mechanism and the effect of various growth conditions will be of significant interest to the 2D material research community to obtain large-scale, high-quality graphene.

3. Direct growth of graphene on flexible organic substrates at low temperature

To avoid the problems arising in the graphene transferring process, two growth approaches have been suggested for the direct formation of graphene on flexible insulating substrates without additional transfer processes: (i) catalytic growth with the help of an external metal catalyst [51], and (ii) non-catalytic direct growth of graphene on a dielectric substrate without a metal catalyst [57–59].

The direct growth of graphene is a process on flexible substrates (PI, PDMS and Willow glass, mica) and rigid substrates (glass, AlN, GaN, sapphire, quartz, Si, textured Si, SiO_2, SiC, fused silica, MgO, h-BN, MnO_2, TiO_2, and HfO_2) without transfer processes [6, 52–63, 74, 76–100], compared with conventional indirect growth processes on metal substrates (Cu, Ni, Ge, etc.) which need additional transfer processes onto arbitrary substrates [1–5, 8–51]. Using this method, we can avoid the complicated transfer process, which induces the defects, residues, and tears that degrade the performance of graphene-based devices. Various approaches for direct growth of graphene were classified into three major types: (i) catalyst-free and polymer-free, (ii) based on both catalyst and polymer, and (iii) based on metal catalyst (**Figure 3**).

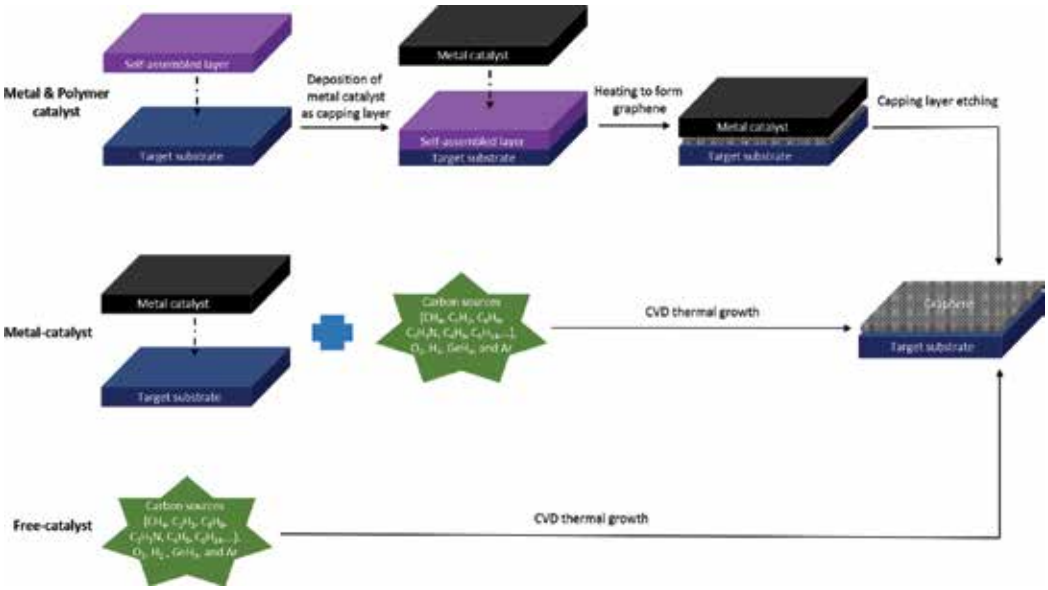

Figure 3. Generally methods for direct-growth of graphene onto target insulating substrate.

Compared with the conventional catalytic growth approach, the direct growth of graphene on dielectric substrate without any external catalysts has various advantages, such as low process cost, and the shorter experimental processes. However, the drawback of this method is that without using catalysts, the chemical reactions for the excitation of the kinetic energy of the graphene growth process is not sufficient to obtain high quality direct-grown graphene for commercialization, compared with the catalytic direct growth described in previous sections.

Direct growth of graphene on flexible organic substrates has a huge potential in applications related to flexible and stretchable electronics, such as e-skin and health monitoring on the human body [101–103]. However, the limited thermal stability of organic substrates, which can be easily melted, deformed or damaged at high temperatures (>300°C), leads to a serious limitation in direct growth of graphene on the flexible substrates, because the quality of graphene grown at low temperatures (<400°C) is much lower than that of the one at high temperatures (~1000°C). Owing to these constraints, graphene growth on flexible substrates is only recently being studied [77, 78]. To reduce the process temperature, most of the studied growth methods involve the catalytic conversion of organic precursors to graphitic layers on the flexible organic substrates with the help of catalytic metal layers.

In 2012, Kim et al. reported a low-temperature (300°C) growth of graphene-graphitic carbon (G-GC) films on Cu layer deposited on polyimide (PI) substrate using inductively coupled plasma-enhanced CVD (ICP-CVD), and a direct transfer of the G-GC films onto a underlying flexible PI substrate using wet etching of Cu layer (**Figure 4a–f**) [77]. The optical and electrical characteristics of G-GC are affected by the varying growth temperature, plasma power and growth time. More recently, in 2016, Seo et al. revealed a simple, inexpensive, scalable

http://dx.doi.org/10.5772/intechopen.73171

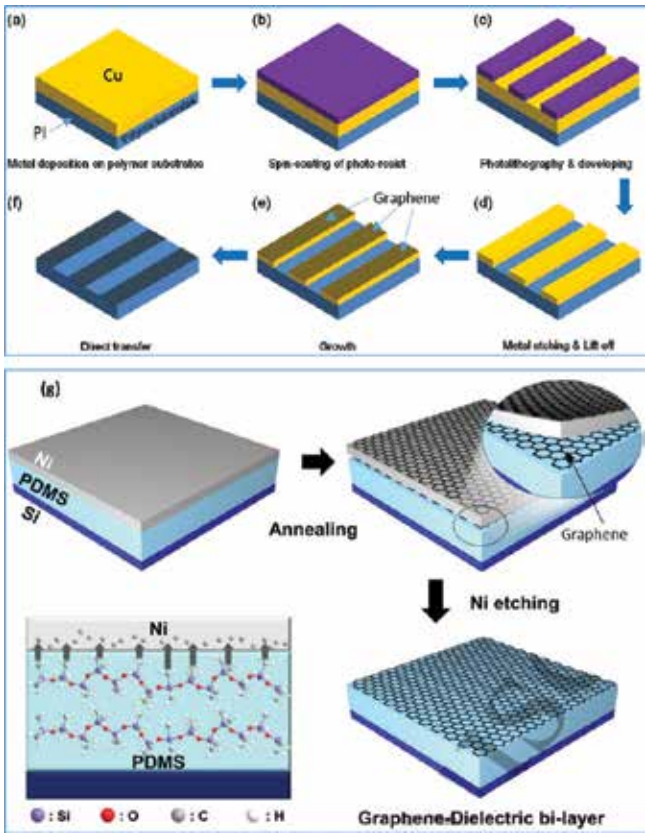

Figure 4. Diagram of direct-growth of graphene onto flexible substrates: (a–f) PI, and (g) PDMS. (a–f) Reproduced with permission from [77], copyright 2012, IOP publishing. (g) Diagram of direct-growth of bilayer graphene on PDMS substrate based on Ni catalyst (reproduced with permission from [78], copyright 2017, IOP Publishing).

and patternable process to synthesize graphene-dielectric bi-layer (GDB) films on solution-processed polydimethylsiloxane (PDMS) under a Ni capping layer (**Figure 4g**) [78]. Seo et al. deposited the Ni film as the catalyst and encapsulation layer on a PDMS layer that was a few micrometer thick; this layer enabled direct growth of GDB between the substrate and Ni layer. PDMS (4 μm)/Ni (400 nm) films on the substrate were thermally annealed under vacuum, forming a PDMS/MLG/Ni/MLG structure. At the interface of the PDMS layer and the Ni film, the carbon atoms in the PDMS surface diffused into the Ni layer under high temperature, and carbon atoms were released to form MLG on both sides of the Ni layer during cooling. With this method the GDB structure was fabricated simultaneously and directly on the substrate, by thermal conversion of the PDMS without using additional graphene transfer and patterning process or formation of an expensive dielectric layer, which makes the device fabrication process much easier.

In 2015, Sun et al. revealed a growth method of graphene-graphitic carbon (G-GC) at the growth conditions (low-temperature range 400–600°C, CH_4 gas, pressure 100 W, and growth time in 1 h) using PECVD system as depicted in **Figure 5** [108]. The advantage of direct PECVD process is that graphene films could be formed on flexible substrate, e.g.

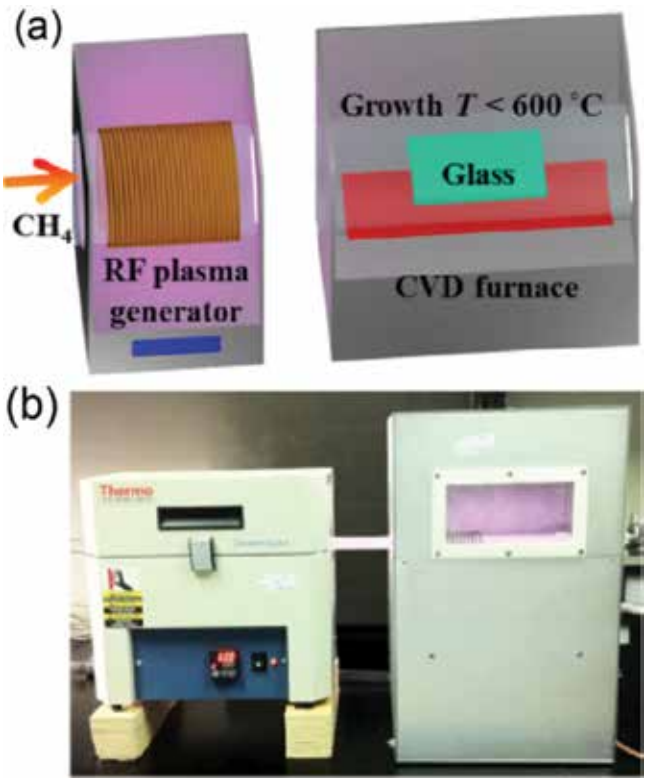

Figure 5. (a) Diagram of direct-growth of graphene onto flexible mica glass substrate: (b) PECVD system utilized in this graphene growth with a single-zone electrical chamber (left) and RF plasma source (right). (a, b) reproduced with permission from [100], copyright 2015, Springer and Tsinghua University Press.

mica substrate. The uniform and high-quality graphene films directly integrated with low-cost used flexible mica glass will unlock a promising perspective in fabrication of multi-functional electrodes in solar cell, smart window, and transparent electronic.

4. Application of direct-grown graphene on flexible electronics

A wide range of functional devices (transistors, solar cells, sensors, resistors, diffusion barriers, heat-resistant devices, photocatalytic plates and energy-saving smart windows) of graphene directly grown on various dielectric substrates using different growth methods, catalysts and device performances to date have been introduced, as briefly classified in **Table 1**.

4.1. Transistors (FETs)

The transfer-free growth of graphene will provide a new way to fabricate the FET-based electronic applications of graphene simply and inexpensively, while avoiding the transfer process. In general, FETs based on transfer-free direct graphene growth on various substrates (PDMS, sapphire, quartz, SiO_2 and h-BN), have been investigated thoroughly in previous studies [1, 6, 52, 59, 60, 62, 78, 82, 86, 88, 90, 92, 95, 97]. In particular, direct-grown graphene

Substrate	Property	Method	Catalyst	Applications of direct-grown graphene	Results	Ref.
PI	Flexible	ICP-CVD	Cu	Strain sensor	Transmittance (%T) (77% at 550 nm) Sheet resistance (R_s) (80 KΩ/sq)	[77]
PDMS	Flexible	Spin coat and thermal annealing, CVD	Ni	FET	Electron mobility μ_e = 0.01 cm^2/Vs On/off ratio (1.1×10^4)	[78]
Flexible Willow Glass	Flexible	CVD	Ni	Graphene pattern	High flexibility pattern	[98]
Mica	Flexible	PECVD		Transparent circuit for LED	High transparent and flexibility	[100]

Note: "NA" means "not applicable".

Table 1. A brief classification of direct-grown graphene on various flexible substrates and their applications to date.

on flexible PDMS-based FET device (**Figure 6**) will be a promising potential in future flexible electronics [78].

4.2. Strain sensor

Graphene can be used as 3D structured electrodes in multifunctional devices, such as pressure sensors [59], black silicon solar cells [66], cambered micro-optics [67], and MEMS sensors [68]. In general, graphene grown on catalytic metal substrate is almost impossible to be

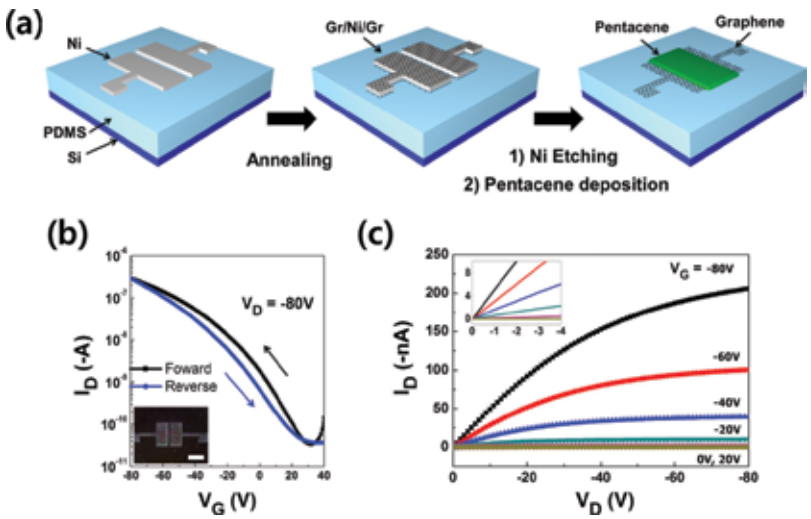

Figure 6. (a) Schematic of flexible PDMS-based FET device. (b) I-V curves of this FET device (black: Forward bias, blue: Reverse bias). Inset: Optical image of patterned source/drain graphene electrodes on a-PDMS. Scale bar: 1 mm. (c) Output characteristics of this FET device (channel length: 100 μm). Inset: Output characteristics at low voltage. (a-c) Reproduced with permission from [88], copyright 2017, IOP Publishing.

conformally transferred onto the 3D structural surface without mechanical damages [104]. Therefore, the direct growth of graphene on the 3D structured device surface can be a potential way to solve the limitations and problems above.

In 2012, by using CVD growth at low-temperature (300°C) for graphene films on a dielectric PI flexible substrate, Kim et al. successfully fabricated a graphene-based strain sensor on a PI substrate, and demonstrated the resistance modulation at different strains [77]. The resistance of graphene films showed a gradually increasing tensile strain of ~0.8% for 340 s (**Figure 7a**). Particularly, it linearly increased in the range of 31.64–31.69 MΩ with the applied strains of 0.1–0.8% (**Figure 7b**).

4.3. Strain pattern

To demonstrate the potential for applications of Ni-catalyzed direct-grown graphene on Willow flexible glass, Marchena et al. successfully produced ribbons and a square pattern of graphene (**Figure 8**) [98]. In particular, growing graphene directly on an ultrathin flexible Willow glass has huge potential in future flexible electronics.

4.4. Transparent circuit for green LED device

The directly grown graphene/glass sample, for the use in a range of transparent conductive applications (like transparent circuit) in industry, requires uniformity, low-cost, flexibility and good quality graphene on transparent flexible substrates (Corning Willow glass, or mica). It is currently in high demand to explore the novel functions of circuits on flexible glass, which may have application potentials in optoelectronics, gas/moisture/bio sensors etc. For instance, the resistances of the pattern graphene within circuit devices, would show a noticeable change without the harmful wet transfer graphene process applied directly on devices. In addition, regarding the potential for integration into flexible electronic devices, mechanical durability of the directly grown graphene is an important factor. To the best of our knowledge, such properties have not been studied so far.

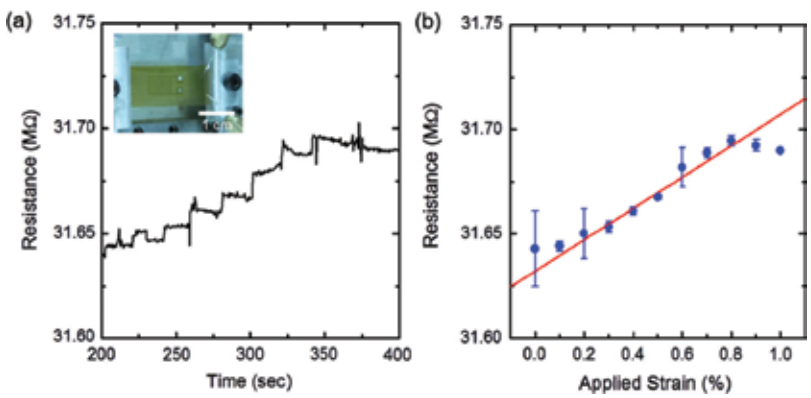

Figure 7. (a) Resistance changes of flexible strain sensor assisted direct-grown graphene on PI flexible substrate at various treatment time. The inset is strain-applied sensor. (b) Resistance changes of this device under applied strains. (a, b) reproduced with permission from [77], copyright 2012, IOP Publishing.

http://dx.doi.org/10.5772/intechopen.73171

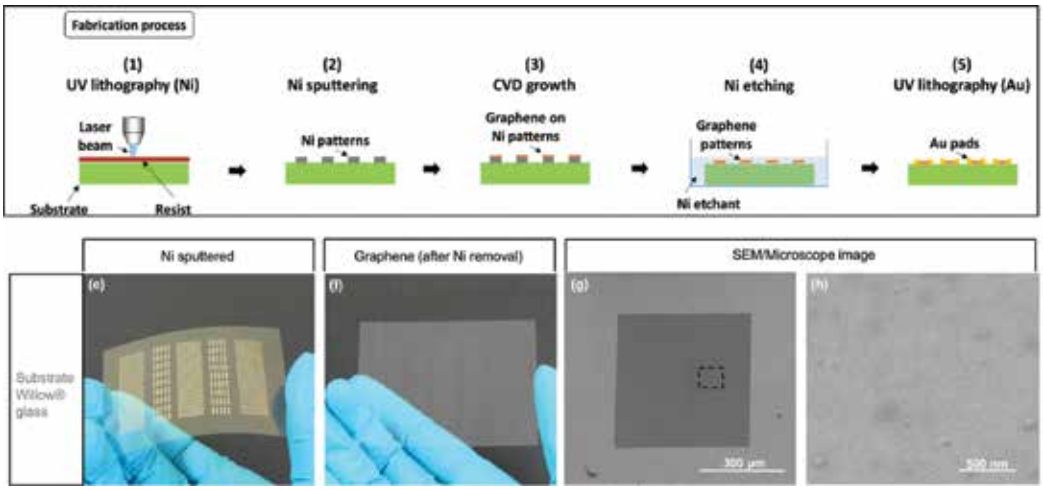

Figure 8. Sequences of direct-grown graphene pattern fabrication on willow flexible glass using Ni catalyst by UV lithography. Reproduced with permission from [98], copyright 2016, OSA Publishing.

Recently, Sun et al. fabricated and designed a transparent circuit based on PECVD direct-grown graphene on flexible mica glass sheet (2 × 8 cm) by utilizing photolithography, as shown in **Figure 9a** [100]. The results showed the patterned graphene electrode on a flexible mica glass can lighten up a green light-emitting diode (LED) indicator (**Figure 9b**). They also

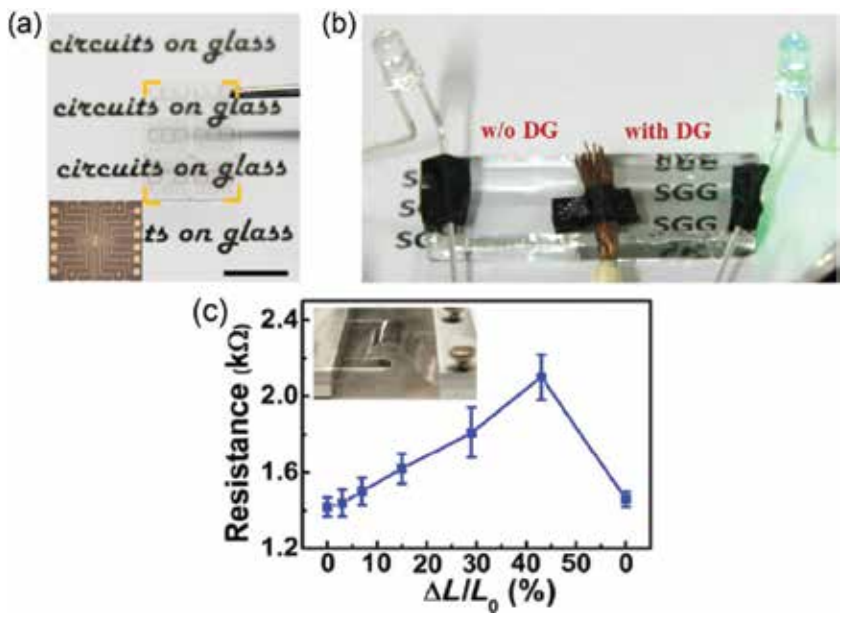

Figure 9. (a) Photograph of transparent circuit based on PECVD direct-grown graphene/flexible mica glass. The inset shows OM image of this device. (b) Photograph of patterned PECVD graphene on white glass showing the transparent conductivity to lighten up a green LED device. (c) Resistance with various bending values of direct-grown graphene film on mica glass. The inset shows the bending test. Reproduced with permission from [100], copyright 2015, Springer and Tsinghua University Press.

synthesized graphene directly on flexible mica glass and measured the change of the resistance through bending tests, with a bending variation of ~45%, and the full recovery after bending indicates good mechanical stability and flexibility of the graphene electrode (**Figure 9c**).

5. Conclusions, perspectives, and challenges

Strategies for direct graphene growth on arbitrary dielectric flexible substrates using the CVD method without metal catalyst at low temperature have been briefly reviewed. In addition, a wide range of device applications of the direct-grown graphene has been also discussed. The prospects of direct-grown transfer-free graphene are bright and currently receiving considerable attention from the 2D material research community. By discovering new methods for obtaining transfer-free graphene, the direct fabrication of a wide-range of various hetero-structured devices can be achieved. However, understanding the growth process and conditions that affect the quality of graphene is still very poor. So far, graphene grown directly on an insulating substrate is generally of low quality (**Table 1**). Because the direct growth relies on the thermal decomposition of carbon resources, the growth rate is usually low and size of the graphene domain is small, resulting in growth of defective graphene layer. Until now, many challenges remain in this direction and large-area high-quality graphene production is still very difficult. In order to obtain more advanced results, an in-depth understanding of the mechanism of graphene growth on insulating substrates is essential.

Direct graphene growth at low temperatures is an important research issue, because high growth temperatures are not allowed on many device substrates, such as flexible polymer and Si substrates. Direct growth of graphene at low- or near-room temperature [57, 77, 86], has been carried out. However, the results to date have not yet met the expectations. Given the practical application of graphene, several directions to pursue in direct graphene growth include low-temperature growth, high-speed growth of highly crystalline graphene, and direct growth on other two-dimensional materials (e.g. h-BN) located on flexible substrate (e.g. polyethylene terephthalate (PET), PDMS, PI, or mica). This issue also a very interesting issue toward future flexible electronic applications. The direct growth of large-scale graphene on h-BN is also an attractive topic [61, 83, 88–90, 105–107]. Graphene on h-BN can have excellent electrical properties, because h-BN is an ideal dielectric substrate for graphene devices, owing to its ultra-smooth, ultra-flat surface, insulation properties, chemical inertness and small lattice misfit compared to SiO_2 [111]. In theory, graphene synthesized could synthesize at low temperature on as-grown h-BN/flexible substrate exhibits better properties than that grown on transferred h-BN because of the transfer-induced contamination and defects on h-BN substrates. The transfer-free grown graphene on ultra-flat h-BN/flexible substrate, which could preserve the pristine properties of graphene, enables further promising flexible device applications based on vertically stacked 2D materials located on above flexible substrates.

Ultrafast direct growth of single-crystal graphene on flexible substrates is another fascinating and challenging topic, as ultrafast conventional indirect growth on copper has been investigated thoroughly and has progressed in recent years [108]. Further studies are required for obtaining faster direct growth and larger graphene single crystals on insulating flexible substrates. Several

possible strategies are proposed: (i) to explore a more efficient way to reduce the reaction barrier for graphene direct growth; (ii) to obtain epitaxial, direct-grown well-aligned graphene domains and seamlessly stitch them together into a complete single-crystal film. One potential way to realize strategy (i) is probably to introduce a gas phase catalyst enhancing the catalytic conversion of carbon precursors to graphene layer. In fact, strategy (ii) has been implemented for conventional indirect-grown graphene on catalytic single-crystal substrates such as Ge (110) [5], or Cu (111) [109, 110]. However, the single-crystal graphene layer has limited size due to the limited single-crystal substrate size, and often the quality is less satisfactory owing to the imperfect alignment of individual graphene islands. Thus, to achieve a large-area, high-quality direct-grown graphene film, preparation of the large-area flexible substrate for releasing larger graphene nucleation seeds and an improvement in graphene alignment are critical issues in future works.

In addition, direct-growth of graphene on flexible substrate assisted by metal powder precursors (solid, diluted solution) contained inside a sub-chamber (as high temperature region) for a direct evaporation process into an innovative and re-designed-CVD main-chamber (containing flexible substrate as low temperature region) in order to allow graphene formation on dielectric substrates is an attractive topic and currently under investigation.

Acknowledgements

This work is supported by the research and development grant, South Korea.

Conflict of interest

There are no conflicts of interest to declare.

Author details

Viet Phuong Pham

Address all correspondence to: pvphuong85@ibs.re.kr

SKKU Advanced Institute of Nano Technology, Sungkyunkwan University, Suwon, South Korea

References

[1] Kim KS, Zhao Y, Jang H, Lee SY, Kim JM, Kim KS, Ahn JH, Kim P, Choi JY, Hong BH. Large-scale pattern growth of graphene films for stretchable. Nature. 2009;**457**:706-710. DOI: 10.1038/nature07719

[2] Kim K, Choi JY, Kim T, Cho SH, Chung HJ. A role for graphene in silicon-based semiconductor devices. Nature. 2011;**479**:338-344. DOI: 10.1038/nature10680

[3] Duong DL, Han GH, Lee SM, Gunes F, Kim ES, Kim ST, Kim H, Ta QH, So KP, Yoon SJ, Chae SJ, Jo YW, Park MH, Chae SH, Lim SC, Choi JY, Lee YH. Probing graphene grain boundaries with optical miscroscopy. Nature. 2012;**490**:235-239. DOI: 10.1038/nature11562

[4] Choi JY. Graphene transfer: A stamp for all substrates. Nature Nanotechnology. 2013;**8**:311-312. DOI: 10.1038/nnano.2013.74

[5] Lee JH, Lee EK, Joo WJ, Jang Y, Kim BS, Lim JY, Choi SH, Ahn SJ, Ahn JR, Park MH, Yang CW, Choi BL, Hwang SW, Whang D. Wafer-scale growth of single-crystal monolayer graphene on reusable hydrogen-terminated germanium. Science. 2014;**344**:286-289. DOI: 10.1126/science.1252268

[6] Shin HJ, Choi WM, Yoon SM, Han GH, Woo YS, Kim ES, Chae SJ, Li XS, Benayad A, Loc DD, Gunes F, Lee YH, Choi JY. Transfer-free growth of few-layer graphene by self-assembled monolayers. Advanced Materials. 2011;**23**:4392-4397. DOI: 10.1002/adma.201102526

[7] Chae SJ, Güneş F, Kim KK, Kim ES, Han GH, Kim SM, Shin H, Yoon SM, Choi JY, Park MH, Yang CW, Pribat D, Lee YH. Synthesis of large-area graphene layers on poly-nickel substrate by chemical vapor deposition: Wrinkle formation. Advanced Materials. 2009;**21**:2328-2333. DOI: 10.1002/adma.200803016

[8] Güneş F, Shin HJ, Biswas C, Han GH, Kim ES, Chae SJ, Choi JY, Lee YH. Layer-by-layer doping of few-layer graphene film. ACS Nano. 2010;**4**:4595-4600. DOI: 10.1021/nn1008808

[9] Pham VP, Jang HS, Whang D, Choi JY. Direct growth of graphene on rigid and flexible substrates: Progress, applications, and challenges. Chemical Society Reviews. 2017;**46**:6276-6300. DOI: 10.1039/c7cs00224f

[10] Pham VP, Nguyen MT, Park JW, Kwak SS, Nguyen DHT, Mun MK, Phan HD, Kim DS, Kim KH, Lee J, Lee NE, Yeom GY. Chlorine-trapped CVD bilayer graphene for resistive pressure sensor with high detection limit and high sensitivity. 2D Materials. 2017;**4**:025049. DOI: 10.1088/2053-1583/aa6390

[11] Pham VP, Mishra A, Yeom GY. The enhancement of hall mobility and conductivity of CVD graphene through radical doping and vacuum annealing. RSC Advances. 2017;**7**:16104-16108. DOI: 10.1039/c7ra01330b

[12] Pham VP, Kim DS, Kim KS, Park JW, Yang KC, Lee SH, Kim KN, Yeom GY. Low energy BCl3 plasma doping of few-layer graphene. Science of Advanced Materials. 2016;**8**:884-890. DOI: 10.1166/sam.2016.2549

[13] Kim KN, Pham VP, Yeom GY. Chlorine radical doping of a few layer graphene with low damage. ECS Journal of Solid State Science and Technology. 2015;**4**:N5095-N5097. DOI: 10.1149/2.0141506jss

[14] Pham VP, Kim KN, Jeon MH, Kim KS, Yeom GY. Cyclic chlorine trap-doping for transparent, conductive, thermally stable and damage-free graphene. Nanoscale. 2014;**6**:15301-15308. DOI: 10.1039/c4nr04387a

[15] Pham VP, Kim KH, Jeon MH, Lee SH, Kim KN, Yeom GY. Low damage pre-doping on CVD graphene/cu using a chlorine inductively coupled plasma. Carbon. 2015;**95**:664-671. DOI: 10.1016/j.carbon.2015.08.070

[16] Geim AK, Novoselov KS. The rise of graphene. Nature Materials. 2007;**6**:183-191. DOI: 10.1038/nmat1849

[17] Neto AHC, Guinea F, Peres NMR, Novoselov KS, Geim AK. The electronic properties of graphene. Reviews of Modern Physics. 2009;**81**:109-162. DOI: 10.1103/RevModPhys.81.109

[18] Schwierz F. Graphene transistor. Nature Nanotechnology. 2010;**5**:487-496. DOI: 10.1038/nnano.2010.89

[19] Wilson NR, Macpherson JV. Carbon nanotube tips for atomic force microscopy. Nature Nanotechnology. 2009;**4**:483-491. DOI: 10.1038/nnano.2009.154

[20] Lin YM, Dimitrakopoulos C, Jenkins KA, Farmer DB, Chiu HY, Grill A, Avouris P. 100GHz transistor from wafer-scale epitaxial graphene. Science. 2010;**327**:662. DOI: 10.1126/science.1184289

[21] Yan Z, Peng Z, Tour JM. Chemical vapor deposition of graphene single crystals. Accounts of Chemical Research. 2014;**47**:1327-1337. DOI: 10.1021/ar4003043

[22] Su CY, Lu AY, Xu Y, Chen FR, Khlobystov AN, Li LJ. High-quality thin graphene films from fast electrochemical exfoliation. ACS Nano. 2011;**5**:2332-2339. DOI: 10.1021/nn200025p

[23] Hernandez Y, Nicolosi V, Lotya M, Blighe FM, Sun Z, De S, McGovern I, Holland B, Byrne M, Gun'Ko YK. High-yield production of graphene by liquid-phase exfoliation of graphite. Nature Nanotechnology. 2008;**3**:563-568. DOI: 10.1038/nnano.2008.215

[24] Sutter PW, Flege JI, Sutter EA. Epitaxial graphene on ruthenium. Nature Materials. 2008;**7**:406-411. DOI: 10.1038/nmat2166

[25] Berger C, Song Z, Li X, Wu X, Brown N, Naud C, Mayou D, Li T, Hass J, Marchenkov AN. Electronic confinement and coherence in patterned epitaxial graphene. Science. 2006;**312**:1191-1196. DOI: 10.1126/science.1125925

[26] Emtsev KV, Speck F, Seyller T, Ley L, Riley JD. Interaction, growth, and ordering of epitaxial graphene on SiC{0001} surfaces: A comparative photoelectron spectroscopy study. Physical Review B. 2008;**77**:155303. DOI: 10.1103/PhysRevB.77.155303

[27] Hass J, Heer WA, Conrad EH. The growth and morphology of epitaxial multilayer graphene. Journal of Physics. Condensed Matter. 2008;**20**:323202. DOI: 10.1088/0953-8984/20/32/323202

[28] Su CY, Xu Y, Zhang W, Zhao J, Liu A, Tang X, Tsai CH, Huang Y, Li LJ. Highly efficient restoration of graphitic structure in graphene oxide using alcohol vapors. ACS Nano. 2010;**4**:5285-5292. DOI: 10.1021/nn10169m

[29] Williams G, Seger B, Kamat PV. TiO_2-graphene nanocomposites UV-assisited photocatalytic reduction of graphene oxide. ACS Nano. 2008;**2**:1487-1491. DOI: 10.1021/nn800251f

[30] Green AA, Hersam MC. Solution phase production of graphene with controlled thickness via density differentiation. Nano Letters. 2009;**9**:4031-4036. DOI: 10.1021/nl902200b

[31] Cote LJ, Kim F, Huang J. Langmuir-Blodgett assembly of graphite oxide single layers. Journal of the American Chemical Society. 2008;**131**:1043-1049. DOI: 10.1021/ja806262m

[32] Li D, Müller MB, Gilje S, Kaner RB, Wallace GG. Processable aquaous dispersions of graphene nanosheets. Nature Nanotechnology. 2008;**3**:101-105. DOI: 10.1038/nnano.2007.451

[33] Gao W, Alemany LB, Ci L, Ajayan PM. New insights into the structure and reduction of graphite oxide. Nature Chemistry. 2009;**1**:403-408. DOI: 10.1038/nchem.281

[34] Joshi RK, Alwarappan S, Yoshimura M, Sahajwalla V. Graphene oxide: The new membrane material. Appl. Mater. Today. 2015;**1**:1-12. DOI: 10.1016/j.apmt.2015.06.002

[35] Coraux J, Diaye ATN, Busse C, Michely T. Structural coherency of graphene on Ir(111). Nano Letters. 2008;**8**:565-570. DOI: 10.1021/nl0728874

[36] Lee Y, Bae S, Jang H, Jang S, Zhu SE, Sim SH, Song YI, Hong BH, Ahn JH. Wafer-scale synthesis and transfer of graphene films. Nano Letters. 2010;**10**:490-493. DOI: 10.1021/nl903272n

[37] Reina A, Jia X, Ho J, Nezich D, Son H, Bulovic V, Dresselhaus MS, Kong J. Large area, few-layer graphene films on arbitrary substrates by chemical vapor deposition. Nano Letters. 2008;**9**:30-35. DOI: 10.1021/nl801827v

[38] Li X, Cai W, An J, Kim S, Nah J, Yang D, Piner R, Velamakanni A, Jung I, Tutuc E. Large-area synthesis of high-quality and uniform graphene films on copper foils. Science. 2009;**324**:1312-1314. DOI: 10.1126/science.1171245

[39] Lee S, Lee K, Zhong Z. Wafer scale homogeneous bilayer graphene films by chemical vapor deposition. Nano Letters. 2010;**10**:4702-4707. DOI: 10.1021/nl1029978

[40] Yan K, Peng H, Zhou Y, Li H, Liu Z. Formation of bilayer Bernal graphene: Layer-by-layer epitaxy via chemical vapor depostion. Nano Letters. 2011;**11**:1106-1110. DOI: 10.1021/nl104000b

[41] Sun Z, Yan Z, Yao J, Beitler E, Zhu Y, Tour JM. Growth of graphene from solid carbon sources. Nature. 2010;**468**:549-552. DOI: 10.1038/nature09579

[42] Chen Y, Gong XZ, Gai JG. Progress and challenges in transfer of large-area graphene films. Advancement of Science. 2016;**3**:1500343. DOI: 10.1002/advs.201500343

[43] Sun J, Deng S, Guo W, Zhan Z, Deng J, Xu C, Fan X, Xu K, Guo W, Huang Y, Liu X. Electrochemical bubbling transfer of graphene using a polymer support with encapsulated air gap as permeation stopping layer. Journal of Nanomaterials. 2016;**2016**:1-7. DOI: 10.1155/2016/7024246

[44] Cherian CT, Giustiniano F, Martin-Fernandez I, Andersen H, Balakrishnan J, Özyilmaz B. Bubble-free electrochemical delamination of CVD graphene films. Small. 2015;**11**:189-194. DOI: 10.1002/smll.201402024

[45] Mafra D, Ming T, Kong J. Facial graphene transfer directly to target substrates with a reusable metal catalyst. Nanoscale. 2015;**7**:14807-14812. DOI: 10.1039/C5NR3892H

[46] Wang Y, Zheng Y, Xu X, Dubuisson E, Bao Q, Lu J, Loh KP. Electrochemical delamination of CVD-grown graphene film: Toward the recyclable use of copper catalyst. ACS Nano. 2011;**5**:9927-9933. DOI: 10.1021/nn203700w

[47] Terrones H, Lv R, Terrones M, Dresselhaus MS. The role of defects and doping in 2D graphene sheets and 1D nanoribbons. Reports on Progress in Physics. 2012;**75**:062501. DOI: 10.1088/0034-4885/75/6/062501

[48] Ambrosi A, Pumera M. The CVD graphene transfer procedure introduces metallic impurities which alter the graphene electrochemical properties. Nanoscale. 2014;**6**:472-476. DOI: 10.1039/C3NR05230C

[49] Lupina G, Kitsmann J, Costina I, Lukosius M, Wenger C, Wolff A, Vaziri S, Ostling M, Pasternak I, Krajewska A, Strupinski W, Kataria S, Gahoi A, Lemme MC, Ruhl G, Zoth G, Luxenhofer O, Mehr W. ACS Nano. 2015;**9**:4776-4785

[50] Ambrosi A, Bonanni A, Sofer Z, Pumera M. Large-scale quantification of CVD graphene surface coverage. Nanoscale. 2013;**5**:2379-2387. DOI: 10.1039/C3NR33824J

[51] Ismach A, Druzgalski C, Penwell S, Schwartzberg A, Zheng M, Javey A, Bokor J, Zhang Y. Direct chemical vapor deposition of graphene on dielectric surfaces. Nano Letters. 2010;**10**:1542-1548. DOI: 10.1021/nl9037714

[52] Levendorf MP, Ruiz-Vargas CS, Garg S, Park J. Transfer-free batch fabrication of single layer graphene transistors. Nano Letters. 2009;**9**:4479-4483. DOI: 10.1021/nl902790r

[53] Byun SJ, Lim H, Shin GY, Han TH, Oh SH, Ahn JH, Choi HC, Lee TW. Graphenes converted from polymers. Journal of Physical Chemistry Letters. 2011;**2**:493-497. DOI: 10.1021/jz200001g

[54] Lee CS, Baraton L, He Z, Maurice JL, Chaigneau M, Pribat D, Cojocaru CS. Dual graphene films growth process based on plasma-assisted chemical vapor deposition. Proceedings of SPIE. 2010;**7761**:77610P. DOI: 10.1117/12.861866

[55] Li X, Cai W, Colombo L, Ruoff RS. Evolution of graphene growth on Ni and cu by carbon isotope labeling. Nano Letters. 2009;**9**:4268-4272. DOI: 10.1021/nl902515k

[56] Li X, Zhu Y, Cai W, Borysiak M, Han B, Chen D, Piner RD, Colombo L, Ruoff RS. Transfer of large-area graphene films for high-performance transparent conductive electrodes. Nano Letters. 2009;**9**:4359-4363. DOI: 10.1021/nl902623y

[57] Rummeli MH, Bachmatiuk A, Scott A, Borrnert F, Warner JH, Hoffman V, Lin JH, Cuniberti G, Buchner B. Direct low-temperature nanographene CVD synthesis over a dielectric insulator. ACS Nano. 2010;**4**:4206-4210. DOI: 10.1021/nn100971s

[58] Zhang L, Shi Z, Wang Y, Yang R, Shi D, Zhang G. Ctalyst-free growth of nanographene films on various substrates. Nano Research. 2011;**4**:315-321. DOI: 10.1007/s12274-010-0086-5

[59] Chen J, Wen Y, Guo Y, Wu B, Huang L, Xue Y, Geng D, Wang D, Yu G, Liu Y. Oxygen-aided synthesis of polycrystalline graphene on silicon dioxide substrates. Journal of the American Chemical Society. 2011;**133**:17548-17551. DOI: 10.1021/ja2063633

[60] Song HJ, Son M, Park C, Lim H, Levendorf MP, Tsen AW, Park J, Choi HC. Large scale metal-free synthesis of graphene on sapphire and transfer-free device fabrication. Nanoscale. 2012;**4**:3050-3054. DOI: 10.1039/C2NR30330B

[61] Son M, Lim H, Hong M, Choi HC. Direct growth of graphene pad on exfoliated hexagonal boron nitride surface. Nanoscale. 2011;**3**:3089-3093. DOI: 10.1039/C1NR10504C

[62] Teng PY, Lu CC, Akiyama-Hasegawa K, Lin YC, Yeh CH, Suenaga K, Chiu PW. Remote catalyzation for direct formation of graphene layers on oxides. Nano Letters. 2012;**12**:1379-1384. DOI: 10.1021/nl204024

[63] Song X, Sun T, Yang J, Yu L, Wei D, Fang L, Lu B, Du C, Wei D. Direct growth of graphene films on 3D grating structural quartz substrates for high-performance pressure-sensitive sensors. ACS Applied Materials & Interfaces. 2016;**8**:16869-16875. DOI: 10.1021/acsami.6b04526

[64] Ambrosi A, Pumera M. Electrochemistry at CVD grown multilayer graphene transferred onto flexible substrates. Journal of Physical Chemistry C. 2013;**117**:2053-2058. DOI: 10.1021/jp311739n

[65] Loo AH, Ambrosi A, Bonanni A, Pumera M. CVD graphene based immuosensor. RSC Advances. 2014;**4**:23952-23956. DOI: 10.1039/c4ra03506b

[66] Jiao T, Liu J, Wei D, Feng Y, Song X, Shi H, Jia S, Sun W, Du C. Composite transparent electrode of graphene nanowalls and silver nanowires on micropyramidal Si for high-efficiency schottky junction solar cells. ACS Applied Materials & Interfaces. 2015;**7**:20179-20183. DOI: 10.1021/acsami.5b05565

[67] Steingrüber R, Ferstl M, Pilz W. Micro-optical elements fabricated by electron-beam lithography and dry etching technique using top conductive coatings. Microelectronic Eng. 2001;**57**:285-289. DOI: 10.1016/S0167-9317(01)00497-X

[68] Mannsfeld SC, Tee BC, Stoltenberg RM, Chen CVH, Barman S, Muir BV, Sokolov AN, Reese C, Bao Z. Highly sensitive flexible pressure sensors with microstructured rubber dilectric layers. Nature Materials. 2010;**9**:859-864. DOI: 10.1038/nmat2834

[69] Gogotsi Y. Nanomaterials Handbook: Florida, USA: CRC Press, Taylor & Francis Group; 2006. 800 p. https://www.crcpress.com/Nanomaterials-andbook/Gogotsi/p/book/9780849323089

[70] Davis RF, Palmour III H, Porter RL. Emergent Process Methods for High-Technology Ceramics: New York, USA: Springer; 1984. 834 p. http://www.springer.com/gp/book/9781468482072

[71] (a) Morosanu CE. Thin Films by Chemical Vapour Deposition: Amsterdam, Netherlands: Elsevier; 1990. p. 717. https://www.elsevier.com/books/thin-films-by-chemical-vapour-deposition/morosanu/978-0-444-98801-0. (b) Hess DW, Jensen KF, Anderson TJ. Chemical Vapor Deposition: A Chemical Engineering Perspective: Freund Publishing; 2011. DOI: 10.1515/REVCE.1985.3.2.97

[72] Liu B, Tang DM, Sun C, Liu C, Ren W, Li F, Yu WJ, Yin LC, Zhang L, Jiang C. Importance of oxygen in the metal-free catalytic growth of single-walled carbon nanotubes from SiOx by a vapor-solid-solid mechanism. Journal of the American Chemical Society. 2010;**133**:197-199. DOI: 10.1021/ja107855q

[73] Chen Y, Zhang J. Diameter controlled growth of single-walled carbon nanotubes from SiO_2 nanoparticles. Carbon. 2011;**49**:3316-3324. DOI: 10.1016/j.carbon.2011.04.016

[74] Vishwakarma R, Rosmi MS, Takahashi K, Wakamatsu Y, Yaakob Y, Araby MI, Kalita G, Kitazawa M, Tanemura M. Transfer free graphene growth on SiO_2 substrate at 250 °C. Scientific Reports. 2017;**7**:43756. DOI: 10.1038/srep43756

[75] Saito K, Ogino T. Direct growth of graphene films on sapphire (0001) and (1120) surfaces by self-catalytic chemical vapor deposition. Journal of Physical Chemistry C. 2014;**118**:5523-5529. DOI: 10.1021/jp408126e

[76] Kang J, Shin D, Bae S, Hong BH. Graphene transfer: Key for applications. Nanoscale. 2012;**4**:5527-5537. DOI: 10.1039/C2NR3131K

[77] Kim YJ, Kim SJ, Jung MH, Choi KY, Bae S, Lee SK, Lee Y, Shin D, Lee B, Shin H. Low-temperature growth and direct transfer of graphene-graphitic carbon films on flexible plastic substrates. Nanotechnology. 2012;**23**:344016. DOI: 10.1088/0957-4484/23/34/344016

[78] Seo HK, Kim K, Min SY, Lee Y, Park CE, Raj R, Lee TW. Direct growth of graphene-dilectric bi-layer structure on device substrates from Si-based polymer. 2D Mater. 2017;**4**:024001. DOI: 10.1088/2053-1583/aa5408

[79] Yamada J, Ueda Y, Maruyama T, Naritsuka S. Direct growth of multilayer graphene by precipitation using W capping layer. Japanese Journal of Applied Physics. 2016;**55**:100302. DOI: 10.7567/JJAP.55.100302

[80] Su CY, Lu AY, Wu CY, Li YT, Liu KK, Zhang W, Lin SY, Juang ZY, Zhong YL, Chen FR. Direct formation of wafer scale graphene thin layers on insulating substrates by chemical vapor deposition. Nano Letters. 2011;**11**:3612-3616. DOI: 10.1021/nl201362n

[81] Peng Z, Yan Z, Sun Z, Tour JM. Direct growth of bilayer graphene on SiO_2 substrates by carbon diffusion through nickel. ACS Nano. 2011;**5**:8241-8247. DOI: 10.1021/nn202923y

[82] Min M, Seo S, Yoon Y, Cho K, Lee SM, Lee T, Lee H. Catalyst-free bottom-up growth of graphene nanofeatures along with molecules templates on dielectric substrates. Nanoscale. 2016;**8**:17022-17029. DOI: 10.1039/C6NR05657A

[83] Liu Z, Song L, Zhao S, Huang J, Ma L, Zhang J, Lou J, Ajayan PM. Direct growth of graphene/hexagonal boron nitride stacked layers. Nano Letters. 2011;**11**:2032-2037. DOI: 10.1021/nl200464j

[84] Trung PT, Delgado JC, Joucken F, Colomer JF, Hackens B, Raskin JP, Santos CN, Robert S. Direct growth of graphene on Si(111). Journal of Applied Physics. 2014;**115**:223704. DOI: 10.1063/1.4882181

[85] Xu SC, Man BY, Jiang SZ, Chen CS, Yang C, Liu M, Gao XG, Sun ZC, Zhang C. Direct synthesis of graphene on SiO_2 substrates by chemical vapor deposition. CrystEngComm. 2013;**15**:1840-1844. DOI: 10.1039/C3CE27029G

[86] Kwak J, Chu JH, Choi JK, Park SD, Go H, Kim SY, Park K, Kim SD, Kim YW, Yoon E. Near room-temperature synthesis of transfer-free graphene films. Nature Communications. 2012;**3**:645. DOI: 10.1038/ncomms1650

[87] Bi H, Sun S, Huang F, Xie X, Jiang M. Direct growth of few-layer graphene films on SiO_2 substrates and their photovoltaic applications. Journal of Materials Chemistry. 2012;**22**:411-416. DOI: 10.1039/C1JM14778A

[88] Kim H, Song I, Park C, Son M, Hong M, Kim Y, Kim JS, Shin HJ, Baik J, Choi HC. Copper-vapr-assisted chemical vapor deposition for high-quality and metal-free single-layer graphene on amorphous SiO_2 substrate. ACS Nano. 2013;**7**:6575-6582. DOI: 10.1021/nn402847w

[89] Li J, Shen C, Que Y, Tian Y, Jiang L, Bao D, Wang Y, Du S, Gao HJ. Copper vapor-assisted growth of hexagonal graphene domains on silica islands. Applied Physics Letters. 2016;**109**:023106. DOI: 10.1063/1.4958872

[90] Tang S, Wang H, Wang HS, Sun Q, Zhang X, Cong C, Xie H, Liu X, Zhou X, Huang F. Silane-catalysed fast growth of large single-crystalline graphene on hexagonal boron nitride. Nature Communications. 2015;**6**:6499. DOI: 10.1038/ncomms7499

[91] Yang G, Kim HY, Jang S, Kim J. Versatile polymer-free graphene transfer method and applications. ACS Applied Materials & Interfaces. 2016;**8**:27115-27121. DOI: 10.1021/acsami.6b00681

[92] Wang D, Tian H, Yang Y, Xie D, Ren TL, Zhang Y. Scalable and direct growth of graphene micro ribbons on dilectric substrates. Scientific Reports. 2013;**3**:1348. DOI: 10.1038/srep01348

[93] Mehta R, Chugh S, Chen Z. Transfer-free multi-layer graphene as a diffusion barrier. Nanoscale. 2017;**9**:1827-1833. DOI: 10.1039/C6NR07637H

[94] Muñoz R, Munuera C, Martínez J, Azpeitia J, Gómez-Aleixandre C, García-Hernández M. Low temperature metal free growth of graphene on insulating substrates by plasma assisted chemical vapor deposition. 2D Materials. 2016;**4**:015009. DOI: 10.1088/2053-1583/4/1/015009

[95] Pang J, Mendes RG, Wrobel PS, Wlodarski MD, Ta HQ, Zhao L, Giebeler L, Trzebicka B, Gemming T, Fu L. Self-terminating confinement approach for large-area uniform monolayer directly over Si/SiOx by chemical vapor depostion. ACS Nano. 2017;**11**:1946. DOI: 10.1021/acsnano.6b08069

[96] Sun J, Chen Y, Priydarshi MK, Chen Z, Bachmatiuk A, Zou Z, Chen Z, Song X, Gao Y, Rümmeli MH, Zhang Y, Liu Z. Nano Letters. 2015;**15**:5846-5854

[97] Lee JH, Kim MS, Lim JY, Jung SH, Kang SG, shin HJ, Choi JY, Hwang SW, Whang D. Direct chemical vapor deposition-derived graphene glasses taegeting wide ranged applications. Applied Physics Letters 2016;**109**:053102. DOI: 10.1021/acs.nanolett.5b01936

[98] Marchena M, Janner D, Chen TL, Finazzi V, Pruneri V. Low temperature direct growth of graphene patterns on flexible glass substrates catalysed by a sacrificial ultrathin Ni film. Opt. Mater. Express. 2016;**6**:2487-2057. DOI: 10.1364/OME.6.002487

[99] Kalita G, Sugiura T, Wakamatsu Y, Hirano R, Tanemura M. Controlling the direct growth of graphene on an insulating substrate by the solid phase reaction of a polymer layer. RSC Advances. 2014;**4**:38450-38454. DOI: 10.1039/ C4RA05393A

[100] Sun J, Chen Y, Cai X, Ma B, Chen Z, Priydarshi MK, Chen K, Gao T, Song X, Ji Q, Guo X, Zou D, Zhang Y, Liu Z. Direct low-temperature synthesis of graphene on various glasses by plasma-enhanced chemical vapor deposition for versatile, cost-effective electrodes. Nano Research. 2015;**8**:3496-3504. DOI: 10.1007/s12274-015-0849-0

[101] Choi S, Lee H, Ghaffari R, Hyeon T, Kim DH. Recent advances in flexible and strectchable bio-electronic devices intergrated with nanomaterials. Advanced Materials. 2016;**28**:4203-4218. DOI: 10.1002/adma.201504150

[102] Hammock ML, Chortos A, Tee BCK, Tok JBH, Bao Z. 25th anniversary article: The evolution of electronic skin (e-skin): A brief history, design considerations, and recent progress. Adv. Mat. 2013;**25**:5997-6038. DOI: 10.1002/adma.201302240

[103] Kim H, Ahn JH. Graphene for flexible and wearable device applications. Carbon. 2017;**120**:244-257. DOI: 10.1016/j.carbon.2017.05.041

[104] Fan G, Zhu H, Wang K, Wei J, Li X, Shu Q, Guo N, Wu D. Graphene/silicon nanowire schottky junction for enhaced light harvesting. ACS Applied Materials & Interfaces. 2011;**3**:721-725. DOI: 10.1021/am1010354

[105] Wu T, Ding G, Shen H, Wang H, Sun L, Jiang D, Xie X, Jiang M. Triggering the continuous growth of graphene toward milimeter-sized grains. Advanced Functional Materials. 2013;**23**:198-203. DOI: 10.1002/adfm.201201577

[106] Yan Z, Lin J, Peng Z, Sun Z, Zhu Y, Li L, Xiang C, Samuel EL, Kittrell C, Tour JM. Toward the synthesis of wafer-scale single-crystal graphene on copper foils. ACS Nano. 2012;**6**:9110-9117. DOI: 10.1021/nn303352k

[107] Ma T, Ren W, Liu Z, Huang L, Ma LP, Ma X, Zhang Z, Peng LM, Cheng HM. Repeated growth-etching-regrowth for large-area defect-free single-crystal graphene by chemical vapor deposition. ACS Nano. 2014;**8**:12806-12813. DOI: 10.1021/nn506041t

[108] Zhang Z, Xu X, Qiu L, Wang S, Wu T, Ding F, Peng H, Liu K. The way towards ultrafast growth of single-crystal graphene on copper. Advancement of Science. 2017;**4**:1700087. DOI: 10.1002/advs.201700087

[109] Nguyen VL, Shin BG, Duong DL, Kim ST, Perello D, Lim YJ, Yuan QH, Ding F, Jeong HY, Shin HS, Lee SM, Chae SH, Vu QA, Lee SH, Lee YH. Seamless stitching of graphene domains on polished copper (111) foil. Advanced Materials. 2015;**27**:1376. DOI: 10.1002/adma.201404541

[110] Brown L, Lochocki EB, Avila J, Kim CJ, Ogawa Y, Havener RW, Kim DK, Monkman EJ, Shai DE, Wei HI, Levendorf MP, Asensio M, Shen KM, Park J. Polycrystalline graphene with single crystalline electronic structure. Nano Letters. 2014;**14**:5706. DOI: 10.1021/nl502445j

[111] Xue J, Sanchez-Yamagishi J, Bulmash D, Jacquod P, Deshpande A, Watanabe K, Taniguchi T, Jarillo-Herrero P, LeRoy BJ. Scanning tunnelling microscopy and spectroscopy of ultra-flat graphene on hexagonal boron nitride. Nature Materials. 2011;**10**:282-285. DOI: 10.1038/nmat2968

Chapter 5

Technological Integration in Printed Electronics

Almudena RivadeneyraFlorin C. LoghinAniello Falco

Additional information is available at the end of the chapter

http://dx.doi.org/10.5772/intechopen.76520

Abstract

Conventional electronics requires the use of numerous deposition techniques (e.g. chemical vapor deposition, physical vapor deposition, and photolithography) with demanding conditions like ultra-high vacuum, elevated temperature and clean room facilities. In the last decades, printed electronics (PE) has proved the use of standard printing techniques to develop electronic devices with new features such as, large area fabrication, mechanical flexibility, environmental friendliness and—potentially—cost effectiveness. This kind of devices is especially interesting for the popular concept of the Internet of Things (IoT), in which the number of employed electronic devices increases massively. Because of this trend, the cost and environmental impact are gradually becoming a substantial issue. One of the main technological barriers to overcome for PE to be a real competitor in this context, however, is the integration of these non-conventional techniques between each other and the embedding of these devices in standard electronics. This chapter summarizes the advances made in this direction, focusing on the use of different techniques in one process flow and the integration of printed electronics with conventional systems.

Keywords: printing techniques, process flow, compatibility, final systems, interconnects

1. Overview of printing techniques

1.1. Introduction to printing

The beginning of printing techniques can be followed back to ancient history [1]. Here the use of stencils was used to define patterns as part of cave paintings. As time progressed, techniques that are more complex were developed, with the most common being seals used to pattern clay and wax [2]. The idea behind was to replicate patterns that were commonly

used. The seal is an inverted image that is pressed into a soft material to create the desired pattern. Such a technique requires the material to be malleable as such with a similar idea, block printing was developed where a pre-defined carved block is inked and then brought into contact with the samples, in early times this being cloth and later following, paper. While this method allowed for the fast multiplication of the single block, it required a long time to alter the master block. Following this, it gave rise to the movable type where a big block would be composed of smaller blocks that could be permutated to create various designs. This along with the invention of the printing press gave rise to the printing revolution in Europe. With the tremendous technological advances of the twentieth century, fully automated printing technologies were developed leading to the digital household printers becoming the norm. Making use of these advances, throughput for printed media surged.

From an electronic point of view, inorganic electronics are predominantly used due to the inherent material properties of naturally found elements. Transition metals such as copper, gold or silver, display very good electrical conductance while silicon, germanium and III–V elements (among others) are employed as semiconductors in elements such as transistors and diodes. Although these materials offer ideal electrical characteristics, they have certain drawbacks when it comes to mechanical and or optical features. In terms of processing, these materials also tend to have limiting factors such as high processing temperatures, require high vacuum and/or involve chemical processes that are environmentally unfriendly. To overcome these shortcomings organic and nanomaterials have been developed, in the past decades, with the promise to enhance and cover the gaps in terms of possible devices. While extending the portfolio of material properties, the aforementioned materials can in most cases be brought into solution usually in form of a dispersion lending themselves to processing techniques widely used in printed technology. Such techniques have inherent advantages in comparison to commonly used CMOS technologies, both in terms of processing condition as well as throughput potential. In the following sub sections commonly used printed techniques used in the printed electronics community will be explored accompanied by state of the art devices fabricated herewith.

1.2. Gravure and flexographic printing

Gravure printing is one of the most common printing techniques and shares similarities to flexographic printing. The main difference is in the application of the ink to the substrate. Flexographic printing is a relief printing technique that employs a soft plate similar to stamping. In gravure printing the image is etched or laser written into a metal plate essentially creating pockets into which the ink can be filled. **Figure 1** displays the two processing techniques with their core components as well as the inking of the printing roll and transfer onto the substrate. Both these processes excel when it comes to throughput in comparison to other printing techniques. In terms of printed electronics gravure and flexographic printed have been employed to fabricate a plethora of devices spanning from organic photovoltaic (OPV) [3], transparent conductive films (TCFs) [4], thin-film transistors (TFTs) [5] and organic light emitting diodes (OLEDs) [6]. In addition Kraus et al. [7] have used gravure printing to deposit nanoparticles in the sub 100 nm range. As such proving that gravure printing not only profits from high throughput but can also provide very good resolution. A general drawback of this printing technique are the required costs in setting up the production in comparison to, for example, ink jetting where the pattern can be altered digitally.

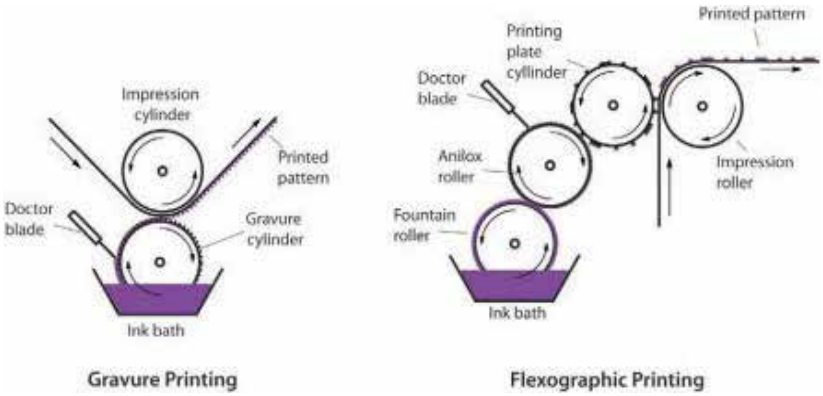

Figure 1. Schematic displaying the core principle of (left) gravure printing and (right) flexographic printing as well as the inking of the printing cylinders and transfer to the substrate (adapted from [3] with authorization).

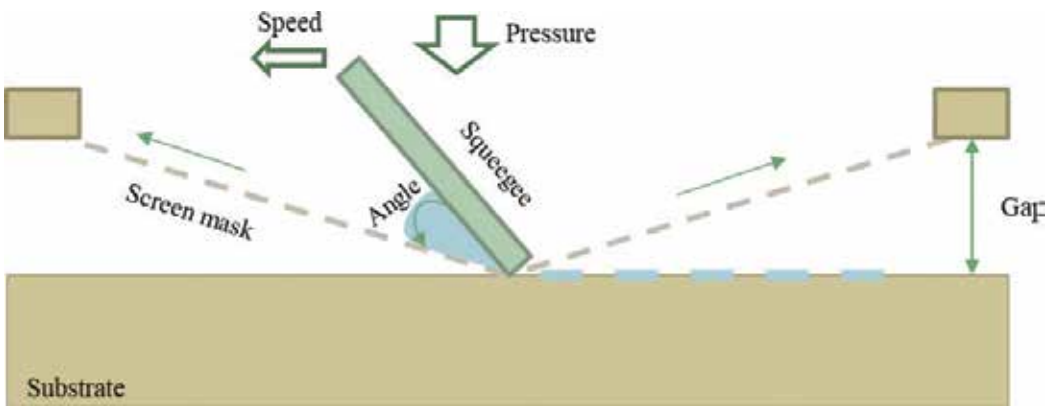

Figure 2. Schematic drawing of screen printer during a printing process. Key components as well resulting pattern are depicted.

1.3. Screen printing

Screen printing is a contact printing method that makes use of a patterned mesh to define structures on a variety of substrates. Highly viscous ink is pushed through the mesh that supports an ink-blocking stencil, with the aid of a squeegee. A typical printing process consists of inking the screen followed by a pass over with the squeegee. Due to the force exerted on the screen, by the squeegee, the screen is brought into contact with the substrate and the ink passes through creating a pattern. **Figure 2** displays the main components of the screen printer while in operation. Resolution is limited by ink formulation, thread thickness and density. Although commonly used in the printing of labels, signs as well clothing, screen printing has been widely used in flexible and printed electronics for a variety of devices including conductors [8], TFTs [9], RFID antennas [10]. An impressive work was done by Krebs et al. [11], who presented a fully screen printed, flexible solar cell based on a blend of organic acceptor and donor materials. The cells were integrated into household items to show the feasibility of such devices. Due to the possibility of integration into R2R framework, screen printing can be easily scaled to an industrial scale.

1.4. Inkjet

Inkjet is a widespread technology in the printing world, commonly employed in personal small printers. Although limited in terms of throughput, in comparison to technologies such as gravure printing, inkjet printing provides an affordable technology that offers itself especially to quick prototyping and alterations in print design. The functioning principle of this technology is the 'jetting' of individual droplets from a print head. Although there are a multitude of techniques to generate the individual droplets, the core principle is shared. Ink is brought into a chamber and through the addition of either thermal or mechanical energy, the fluid is perturbed. This creates a droplet that is released from the printing head. **Figure 3** displays the core components of an inkjet printer and its operation mode. In order to create closed layers droplets are overlapped and tessellated in order to form desired shapes. The processing speed can be dramatically increased with the use of a multitude of print heads simultaneously working. A difficulty arising from this is the sensitivity to clogging of individual nozzles leading to missing droplets and openings in the film. A further differentiation can be made in processing between drop on demand and continuous-mode. The name is indicative of the processing where drop are released as is required by the source image while the other mode jets continuously.

Due to the flexibility in terms of processable ink, inkjet printing has been successfully employed in the printed electronics world with great success. Devices presented include interconnects [12], chemical sensors [13], capacitors [14], OPV [15] and TFTs [16].

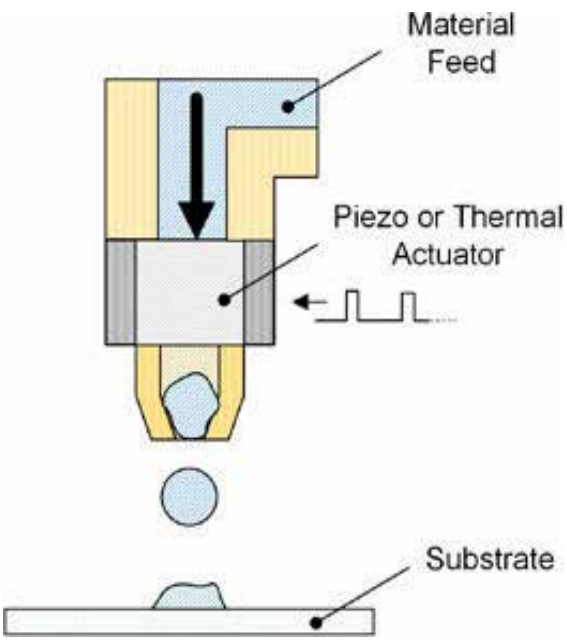

Figure 3. Schematic of an inkjet printer displaying key components and displaying operational mode.

1.5. Spray deposition

Although spray technology has a variety of applications ranging from humidification to combustion, the more relevant for printed electronics is its use as surface coating. Although spray deposition inherently is a coating technique, it can easily be enhanced to fit the criteria of printing with the aid of a shadow mask. Spray deposition is the deposition of, usually a material in liquid state, with the aid of a gas stream. The bulk liquid is separated into droplets; this process is known as atomization and subsequently carried to the substrate in a mix of gas and a stream of droplets. The atomization can be achieved by either mixing with an air stream (air-assisted atomization) or with kinetic energy (ultrasonic atomization). The two aforementioned will be briefly discussed below.

Air-assisted nozzles make use of a high velocity gas stream to produce atomization. The liquid is fed into the nozzle either under pressure or as a gravity fed alternative. At the orifice, the liquid is mixed with the gas stream, which disrupts the liquid causing atomization. **Figure 4** displays a standard air assisted nozzle with the inset displaying the point of atomization. The droplet size is dependent on many factors such as the velocity of the gas stream, the ratio of gas to fluid, fluid properties as well as nozzle dimensions.

Ultrasonic-assisted nozzles utilize a vibrating body based on a piezoelectric transducer that vibrates at ultrasonic frequencies. When this body is brought into contact with the body of fluid the liquid becomes unstable generating a mist of droplets. In most cases, this mist is mixed with a carrier gas that transports the droplets to the surface. Based on the applied frequency the droplet size can be varied. As with air-assisted nozzles the droplet formation also depends on a multitude of factors, both nozzle as well as fluid related. For further detail on spray technology the reader is referred to the work of Lefebrve [17].

In terms of printed electronics, spray deposition has been used for a multitude of device. Both conducting as well as semiconducting devices being produced. Some of these devices include TFTs [18], TCFs [19], chemical/bio sensors [20, 21], OPVs [22] as well as OPDs [23] to name a few. Falco et al. [24] presented a fully spray deposited, TCO free, flexible OPD based

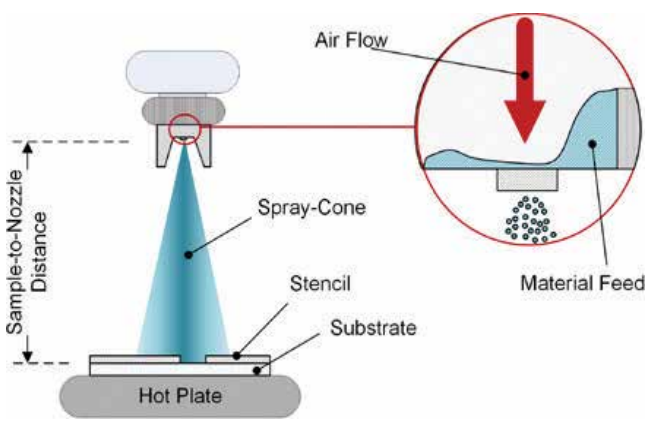

Figure 4. Schematic displaying a typical air-assisted atomization nozzle including key elements in a spray deposition setup. The insert displays the point of atomization.

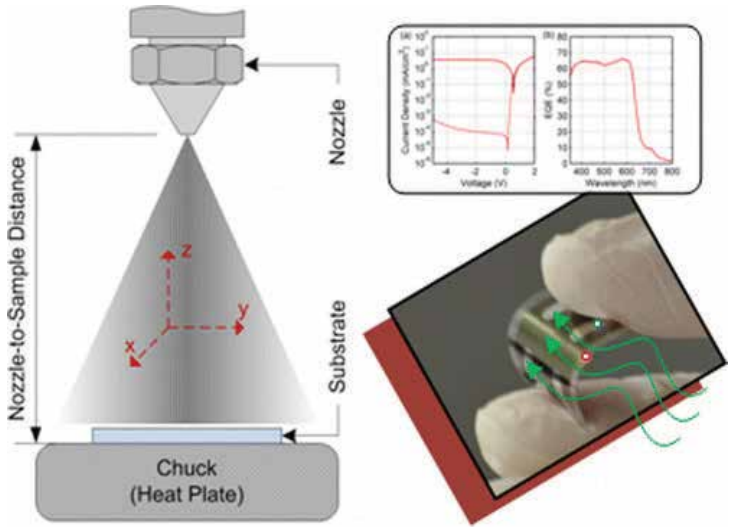

Figure 5. Summarizing figure displaying spray deposition setup used for the fabrication of fully-sprayed, flexible OPDs, the final device as well as key electrical characteristics (adapted from [24] with authorization).

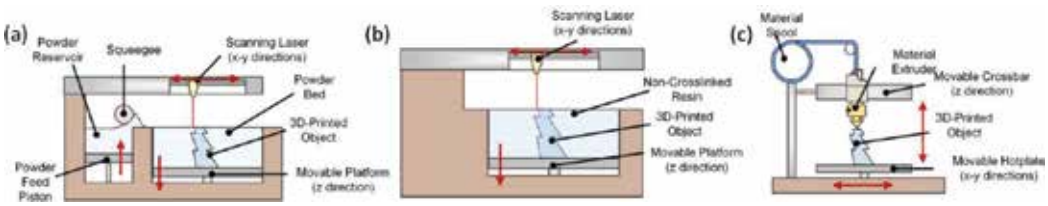

Figure 6. Schematic depictions of common 3D processing techniques of (a) Selective Laser Sintering and (b) Stereolithography and Fused Deposition Modeling.

on a blend of regioregular poly (3-hexylthiophene-2,5-diyl) and [6,6]-phenyl C61 butyric acid methyl ester (PCBM). It demonstrated the feasibility of spray deposition as a method for printed organic electronics especially since all layers were successively deposited by the same technology. **Figure 5** summarizes the work displaying the setup used, the final device as well as key electrical performance.

1.6. 3D printing

3D printing is a term used to encompass additive manufacturing techniques that aim at fabricating solid objects through the deposition of material. Although only recently having gained broad awareness, due to the surge in available privately affordable devices, 3D printing patents date back to 1986 [25]. Used mostly for rapid prototyping and in research the main fabrication was limited to static objects with limited mechanical features. With the increase research of nano-based materials, 3D printing has moved beyond creating scaffolds for electrical devices with the integration of electrical characteristic being embedded into the 3D structure [26–28].

Leigh et al. employed a carbon black filler embedded in a biodegradable polyester to produce an electrically conductive filament [26]. This led to the fabrication of flex sensors as well as embedding it into a 3D printed glove to monitor finger movement. Most commonly, there are three types of processing techniques. Stereolithography (SLA) and Selective Laser Sintering (SLS) use the principle of solidification of a base material while Fused Deposition Modeling (FDM) melts a solid material, which is extruded through a nozzle. **Figure 6** depicts the aforementioned 3D processes marking critical components.

In SLS, a pulsed laser source is employed to solidify a base powder that can originate from plastics, resins and metals. Material is fed from a powder reservoir while the sample stage is moved downwards to expose more material to the laser spot. This process is continued until the desired object is finalized. The remaining material is removed and can be reused as such there is very limited waste material. Due to the sensitive interaction at the powder laser interface, precise calibration is required as to not cause unwanted sintering. Conceptually SLA is similar to SLS, employing a laser to crosslink photosensitive resins. Energetically such an approach is significantly advantageous in comparison to SLS. The limiting factor being the base material for SLA while both techniques suffer from a difficulty in further integration in in-line processes. FDM can cover these shortcomings, albeit at a cost in resolution as well as stability. In the FDM the melted filament is extruded through a nozzle and lines are overlapped and tessellated to create desired structures.

2. Synergy of printed electronics

After reviewing the main fabrication techniques for printed electronics, it is clear that each of them have potential to define different electronic components. For example, antennas require thicker metallic layers in order to enhance their performance. Although the desired thickness could be achieved with any of the described technologies, the most efficient one is screen printing because we can achieve tens of μm selecting a coarse mesh with only one turn. The same thickness would need 20 layers in case of using inkjet printing, resulting in a very time consuming process because it is needed to wait until the layer is dried and the area to cover is quite large. In the case of spray deposition, also the stack of several layers would be mandatory. This technique is much faster than inkjet printing but the pattern definition is poorer in comparison to screen printing.

Another example is the definition of interdigitated electrodes (IDE) for capacitive structures. If the IDE is going to be used to build a capacitive sensor, the distance among consecutive fingers determines the sensitivity of the sensors: the closer they are placed, the higher its sensitivity can be. In this sense, the resolution of the printing technique limits the performance of the device.

Therefore, each technique can be more suitable for different electronic components, as highlighted in the previous examples. As the ultimate goal is to fabricate a fully working and efficient electronic system, it is mandatory to properly combine manufacturing techniques to fulfill it. In the last years, some authors have worked in this director, using different printed techniques to design electronic circuits on flexible substrates.

Some authors have already illustrated how the fabrication of each component of a final device or system should be carefully selected in order to optimize its performance. In particular, Salmerón et al. described two ultrahigh frequency (UHF) radio frequency identification (RFID) tags with sensing capabilities [29]. As demonstrated before [30], they used screen printing to define the antenna in order to achieve a better performance in the RF link. The sensing capabilities comes from the substrate (a polyimide), whose electrical permittivity changes with the moisture content. To exploit this feature, they printed an array of planar capacitive structures. In one of the tags, the electrodes were fabricated with inkjet printing, whereas screen printing was employed in the other design. These tags include an UHF RFID chip with an in-built temperature chip and a sensor frontend capable of measuring capacitive sensors. Although both tags covered a 30% of relative humidity (RH) and showed very low thermal drifts (below 0.05%RH/°C), their features were different. In the case of the inkjetted capacitive array, the sensitivity achieved was 100 fF/RH%. Whereas in the case of the screen printed ones, the sensitivity was about the half (54 fF/RH%). The tag with the inkjetted sensor exhibited a higher performance than the screen printed one in terms of area saving and higher humidity sensitivity. The screen printed sensors approach can be fabricated with just one step but a much bigger area was needed (see **Figure 7a**).

Another device manufactured with two printing techniques was a hybrid sensor for simultaneous vapor determination of RH and toluene concentration [31]. They exploited two strategies to provide with sensing capabilities their device. The RH was measured again by changed in the selected substrate, whereas the toluene concentration was measured by a sensing layer deposited on top of the electrodes. The chosen electrode layout is shown in **Figure 8**, assuring that there was no electrical path between the capacitive electrode and the resistive electrode. Although other electrode configurations present higher, they do not allow the integration of more functionalities in the same side of the device with virtually no interference between them [32]. Inkjet printing was selected to define the electrodes, whereas screen printing was used to deposit the sensitive resistive composite. Inkjet printing allows better resolution, and

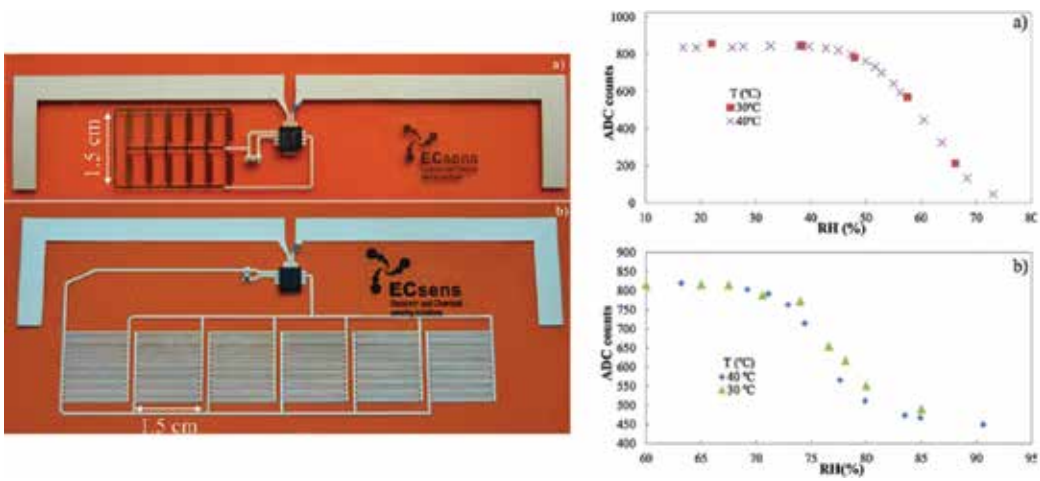

Figure 7. Left: (a) RFID tag with inkjetted serpentine sensors and (b) RFID tag with interdigitated sensors by screen printing. Right: (a) ADC counts of tag with inkjetted serpentine sensor and (b) ADC counts of screen printed tag with IDE sensors. Images adapted from [29] with authorization.

http://dx.doi.org/10.5772/intechopen.76520

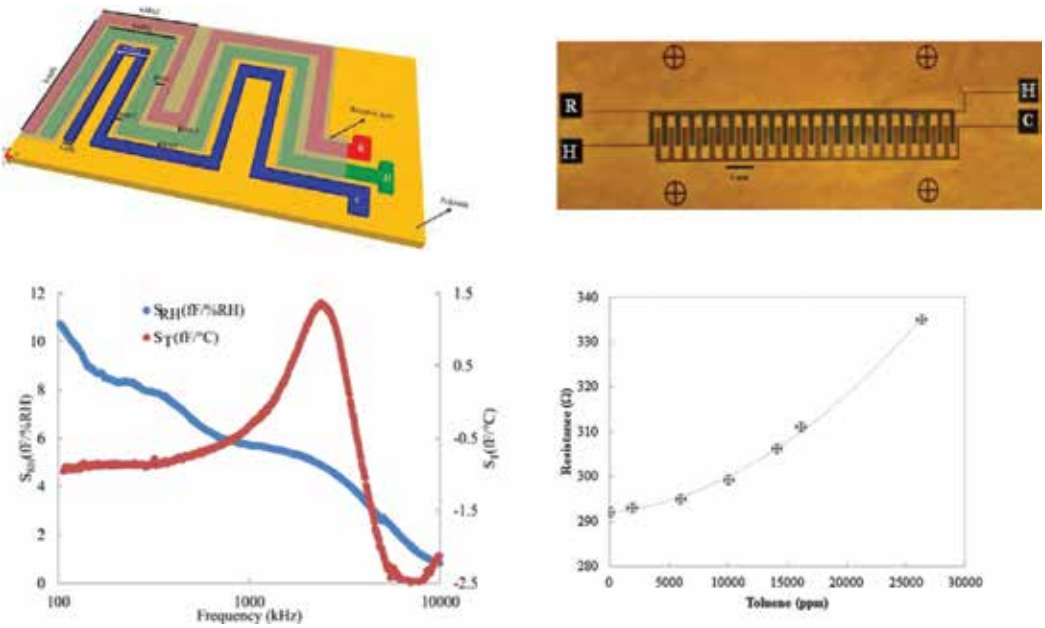

Figure 8. (a) Layout of the novel designed hybrid capacitive-resistive sensor indicating the notation of the dimensions. R corresponds to resistive terminal, C for capacitive sensor, and H corresponds to the common terminal. (b) Image of the hybrid sensor. The resistive element is shown in the upper part of the device, defined between the terminals R and H. The capacitive element is measured between the terminals H and C. (c) Experimental relative humidity and temperature sensitivities as a function of frequency, measuring between H and C. (d) Resistance vs. toluene concentration, measuring between H and R. Images adapted from [31] and [32] with authorization.

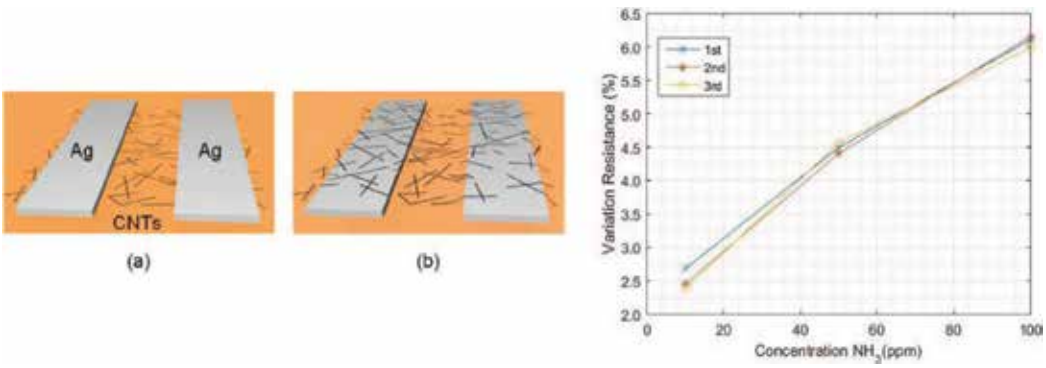

Figure 9. Left: schematics of the two fabricated sensors: (a) electrodes on top of CNT film; (b) CNT film on top of the electrodes. Right: normalized response under different values of NH_3 concentrations. Images adapted from [33] with authorization.

therefore, electrodes can be placed closer, increasing the sensitivity, especially of the capacitive part. But the viscosity of the resistive composite sensitive to toluene was too high to be deposited by inkjet printing, and therefore they employed screen printing to define this layer on top of the electrodes.

Another example of mixing PE techniques was illustrated by Abdelhalim et al. [33]. They showed a fully printed ammonia sensor on a flexible substrate. The electrodes were fabricated

by inkjet printing of silver nanoparticles whereas the sensitive film was made of carbon nanotubes (CNT) deposited by spray by an air atomizing nozzle. Two different approaches were followed to manufacture the sensors: first, spraying the CNT solution on top of the electrodes (**Figure 9a**) (conventional approach) and second, printing the electrodes on top of the sprayed CNT film (**Figure 9b**). In the case of conventional approach, the resistance values were one order of magnitude higher than in the case inverted method (printing the electrodes on top of the sensing layer). This can be explained by the fact that the thickness of the silver layer and the mean value of the CNT are about the same value (~450 nm), therefore, the establishment of an electrical path between the CNT is more difficult in the classical approach than in the inverted one.

The results obtained for NH_3 sensing showed a good performance in terms of sensitivity and time response to the test gas, with performance comparable with that obtained with evaporated metal electrodes and conventional approach [34].

As apparent from what we have described so far, the integration of different printing techniques can bring to innumerable benefits, and lets the designer exploit the advantages of each method. Conventional printing, however, constrains the degrees of geometrical freedom two, limiting the possibilities of integration to an *in plane* approach. It is, nevertheless, possible to push the boundaries of technological integration, embedding 2D thin film devices into 3D structures, in order to create *electronic objects,* more than just electronic devices. One of the possible approaches for the obtainment of such structures is 3D printing of scaffolds, in which discrete electronics are cast and embedded. The 3D printed object and the electronics can be designed separately and the only major concern would be the attachment and interconnection of the devices in the 3D housing. Opposed to this approach, Falco et al. demonstrated the facile integration of conformal organic electronics devices in 3D printed structures, where the device is directly fabricated on or in the printed object [35]. The 3D printing technique of choice was FDM, because of its low cost, ease of use and high customizability. The major caveat, though, is the elevated RMS roughness (tens of microns) of the objects produced with means of this method. As the typical active layers employed in organic and printed electronics have thickness of few hundreds of nanometers, it was necessary to also develop a high throughput, sustainable and easy-to-integrate planarization process.

In this work the authors exploit spray deposition not only for the definition of the active materials (i.e. conductive polymers, silver nanowires, carbon nanotubes), but also to achieve the required planarization **Figure 10**.

The spray-planarization is obtained dissolving the 3D printable material itself in an organic solvent, and spraying it on the rough as-printed structure in a wet deposition regime. In this manner, it is possible to re-utilize some wastes of the 3D printing process (material employed to prime the nozzle or to print the outskirts of the pieces), while preparing the structure for successive thin film deposition. Their results outperform alternative methods presented in previous works, and yield RMS roughness of the substrate lower by one order of magnitude with respect to literature [36, 37]. In order to test the viability of this method as preparation tool for printed electronics, the authors deposited and characterized thin films of a conducting polymer (PEDOT:PSS), silver nanowires and carbon nanotubes. Remarkably, the sheet resistance of the layers deposited on planarized samples were up to ten times lower than what

http://dx.doi.org/10.5772/intechopen.76520

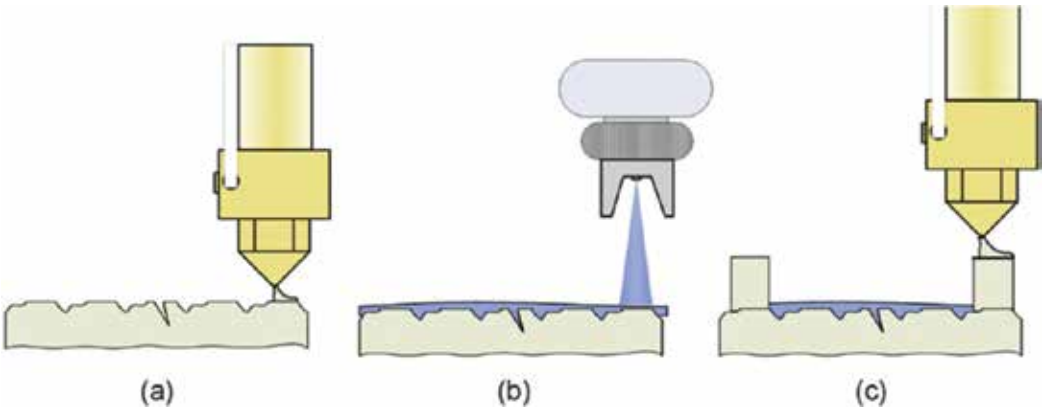

Figure 10. Proposed schematic for multi-technology integration. The substrate is printed with FDM printing technology (a). Spray deposition—or other printing techniques—is employed to deposit a functional layer (b), and (c) the upper stacks of the 3D printed object are realized on top of the spray deposited thin film. Image adapted from [35] with authorization.

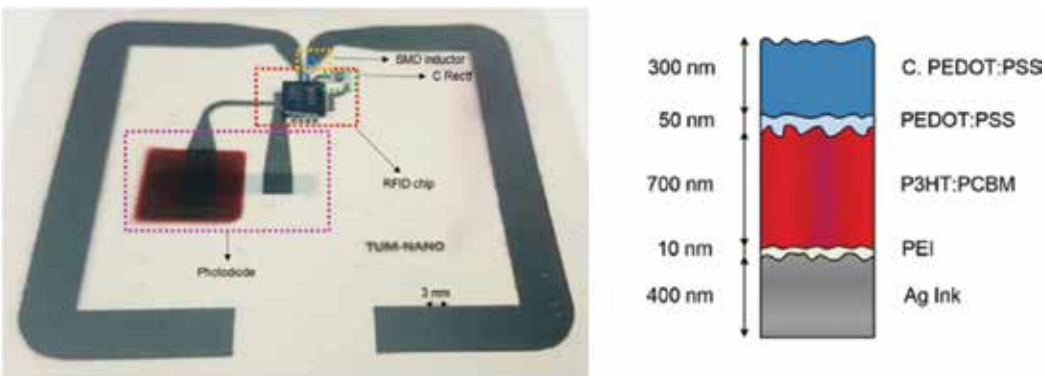

Figure 11. Left: image of the tag with all its elements labeled; right: cross-sectional view of the OPD. An inkjet-printed Ag line modified with spray-coated PEI. Both images adapted from [38] with authorization.

could be measured on the as-printed ones, and comparable to the reference material on glass. Finally, they show an application of 3D print and spray concept, by designing a semitransparent 3D printed heating chamber, which represents the first example of a fully-printed and cost effective functional object.

One last example of combination of PE techniques is a printed passive radiofrequency identification (RFID) tag in the UHF band for light and temperature monitoring [38]. In this case, the antenna and interconnects were realized with silver nanoparticles via inkjet printing. Temperature measurements came from an in-built sensor in the silicon RFID chip whereas the light monitoring was performed by a sprayed photodetector. This work showed for the first time the feasibility of the embedment of large-scale organic photodetectors onto inkjet-printed RFID tags. To succeed in the fabrication process, it was necessary to spray polyethylenimine (PEI) thin layer on top of the inkjetted silver electrode to obtain a working photodiode. In this case, they claimed that the antenna was done by inkjet printing instead of screen printing

for simplicity of the process but in order to obtain an antenna with larger read range, screen printing would be the optimal process **Figure 11**.

Therefore, the manufacturing choice will depend on the restrictions of each application, in terms of printing technology availability, performance, area and materials and processes compatibility.

3. Towards on-chip integration

Integrating the different deposition techniques on one single substrate constituted the final step towards the obtainment of fully printed and hybrid circuits, with tuned capabilities and functionalities. Flexible tags, as the one presented earlier, however, are characterized by an inherently weaker link: the connection between the integrated circuits and the printed devices. Research in solving the interconnection issues, or eliminating them by realizing inherently flexible circuits, has seen a tremendous surge in the last decade.

In every application, in which it is not possible to construct an entirely flexible circuit, the necessity to solder (or, more correctly, to "attach") monolithic integrated circuits to the printed tag arises. The immediate problematics to be faced are mainly three: attaching the component with no harm to the flexible substrate, achieving a low contact resistance and retaining the flexibility of the overall circuit, at no performance loss. The most straightforward approach for the integration of ICs onto flexible circuits, is the adaptation of industrial soldering processes, with the employment of low-temperature soldering alloys. In a systematic and well-presented work by Andersson et al. [39], a series of SMD components with different packaging was soldered keeping the reflowing temperature below 150°C. The study showed mixed results: on the one hand, it proved the feasibility of soldering on paper with standard industrial devices, obtaining contact resistances in the order of few ohms; on the other hand, it was partially inconclusive, as it showed the inevitable presence of cracks after soldering and bending (shown in **Figure 12a**). Furthermore, the soldering yield was rather low (ca. 80% for the smallest packaging, much lower for bigger components), which might be a serious issue in commercial applications. An apparently more complicated—although much more appealing and promising—solution, stems out from treating flexible electronic chips for what they are: non-classical electronic systems, with the need of dedicated solutions. In this avenue, a very interesting work from Quintero et al. compares two technologies with a similar common denominator: the employment of conducting adhesive layers [40]. In particular, the present a selective etching of an isotropic conductive adhesive and the stencil-printing of Anisotropic Conductive Adhesives (ACAs), applied to the bonding of two separate flexible chips. The latter approach, extensively studied and applied in many material combinations, is the one that, so far, has been attracting the highest interest. ACA-based interconnects are obtained in a simple three-step procedure: first, the adhesive conducting film is deposited through a stencil, then the target component is placed on top of it, finally, the temperature of the substrate is raised to the bonding temperature (usually lower than 150°C). When the resin is heated up, it creates an electrical bond between carrier substrate and component, and creates a mechanically stable link. Nilsson et al. [41], present a remarkable application of printed circuits with ACA

connected chips: a semipassive RFID chip, used to log eventual intrusions in carton packages. The system includes a resistive sensing network, an active microcontroller used to record and log the sensor data, powered up by a flexible battery, and a passive communication system. The connecting lines were ink-jet printed and screen-printed, while the hybrid interconnections were obtained with means of a commercial ACA, as shown in **Figure 13**. An extensive study on the stability and reliability of similar solutions has been presented, already in 2014, by Happonen et al. [42], who thoroughly investigated the resiliency of conducting adhesives employed for the connection of separate flexible foils. They explored different bonding solutions and performed a live measurement of the DC 4-wires resistance during several thermal and bending cycles. Interestingly, they show that the stability of hybrid interconnections is enhanced by the presence of supportive, non-conductive adhesives. These hybrid structures can undergo more than 1000 thermal cycles (0–100°C and back to 0°C in 1 h) and bending cycles (with bending radius down to 20 mm). The number of samples and the statistical analyses behind this analysis are solid and prove how flexible to flexible interconnects can be sufficiently reliable for consumer electronics applications. In spite of such promising results, however, the interconnections remain a significant point of failure.

An altogether different approach, however, could reduce the problematics of interconnection technology to their minimum terms. The newest research in flexible electronics, in fact, shows how it is possible to develop complex and fully functional circuits, with the employment of metal-oxide n-type and carbon based p-type semiconductors. Complete circuital systems, which are inherently flexible, would restrict the need for interconnects to very few and controllable points. These points can be designed to be in positions subject to minimal mechanical stress, hence reducing the probability of failure. Most of the effort in this direction has been put in the realization of only n-type semiconducting circuits, given the superior stability of metal oxides with respect to carbon based materials [8]. Although limited by the high power consumption of unipolar circuits, these studies show the avenue to follow to reach flexible and integrated electronics with the minimal interconnection technology. A remarkable work in this context is the one presented by Hung et al. [43], where an ultra-low power RFID tag is developed on plastic foil. All the components of the tag, including logic gates, decoders,

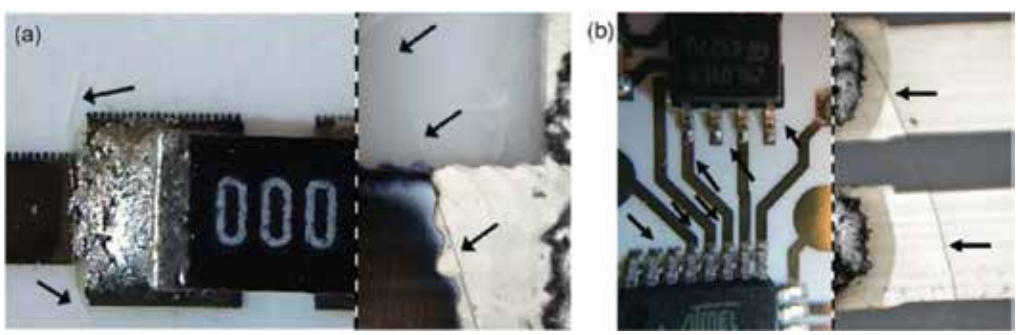

Figure 12. (a) Cracks left on the paper coating, on the printed lines and at the soldering, indicated by arrows, for a 0805 packaging component (b) similar issues for QFP and SOP packages, showing that the problematic is insensitive of packaging type and, up to a certain extent, size insensitive. Image adapted from [39] with authorization.

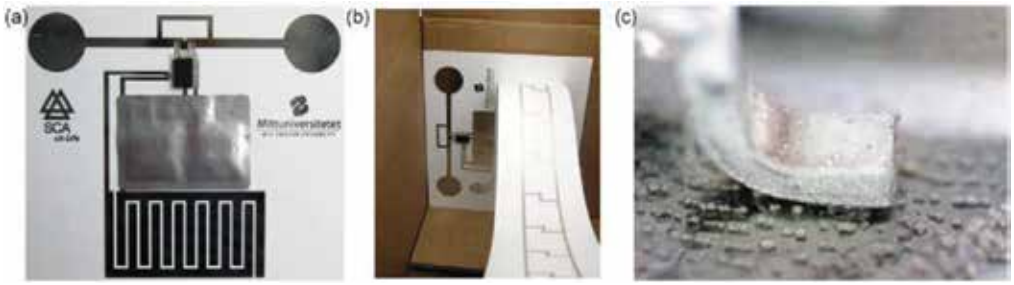

Figure 13. (a) A complete tag with RFID chip, antenna and flexible battery for a complete sensing kit (b) realization of an anti-intrusion system with sensing elements integrated in the sealing tape (c) photo of chip connected to printed line with an ACA. Figure adapted from [41] with authorization.

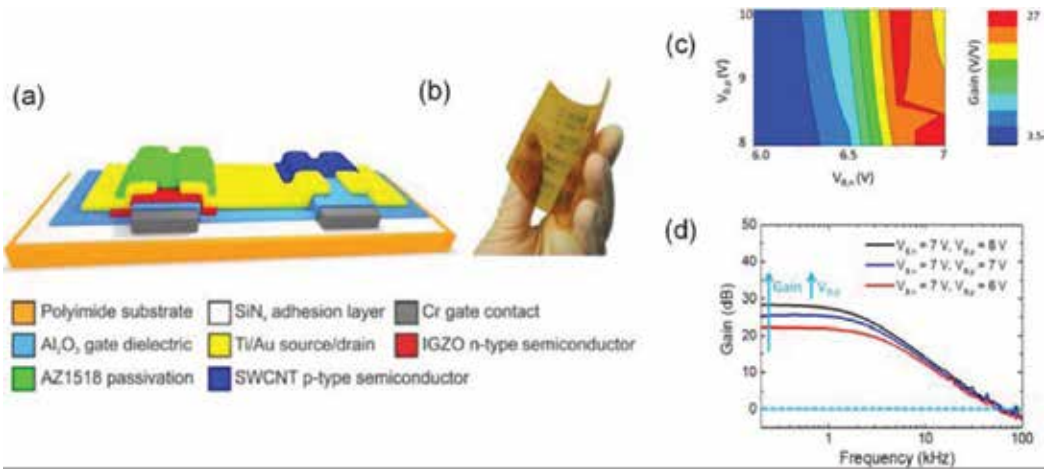

Figure 14. (a) Cross-section of the CMOS amplifier, with the different layers emphasized in different colors (b) photograph of a flexible substrate with many devices (c) voltage gain as a function of bias voltages, measured in ambient air (d) bode plot for different bias voltages, showing how the gain can be gate tuned. Figure adapted from [47] with authorization.

memory and clock generator were fabricated employing amorphous-IGZO FETs and were functioning at 1 V. Such systems, does not need any external driving element, and, thus, no further interconnection is necessary. In a similar direction, Myny et al. presented a flexible NFC barcode tag, with direct clock division circuit, which is compliant with ISO14443-A [44].

To further extend the spectrum of possibilities of printed, interconnectionless electronics, the group led by Prof. Jan Genoe, for instance, has demonstrated the feasibility of flexible control, driver and conversion electronics for photovoltaics-powered micro LCD screens, suggestively integrated onto a contact lens [45]. In this article they demonstrate the great potential of oxide-based electronics, fabricating a system which would have needed a high number of interconnects, and it would have not been realizable without this enabling technology. Finally, although flexible sensors have been often presented in many works, their biggest limitation was the necessity to connect them to external amplifiers and read-out electronics. Recent efforts in literature have shown how stable and reliable amplifier can be obtained employing a-IGZO FETs [46], although they still present the classic limitation of unimodal pseudo-CMOS

logics. Significant breakthroughs are, nevertheless, achieved with a steady pace. Petti and co-workers recently reported a flexible full-CMOS amplifier, with a gain bandwidth product of 60 kHz, realized with sputtered IGZO and spray-deposited CNTs as n-type and p-type semiconductors, respectively [47]. The structure and characteristics of these devices are presented in **Figure 14**. The resulting amplifier is stable in ambient conditions, completely flexible and easy to integrate in other circuits, and it also shows the remarkable adaptability of solution processing (in this particular case, spray-deposition) to different substrates and pre-existent circuits. Albeit in this work the n-type material is sputtered, the specialized literature is abundant with reports of solution-processed IGZO transistors [48, 49], which could be readily employed for the realization of fully printed circuits.

The achievement of a complete set of electronic blocks—such as flexible oscillators, controllers, diving circuits, and amplifiers—is certainly a significant milestone towards a future of flexible electronics. However, considering their performances, it is also evident how printed and oxide-based circuits do not aim at substituting traditional silicon-based electronics for computationally intense tasks. What appears certain, though, is that with a careful and considerate interconnection of classical ICs and energy harvesters, with the exploitation of the advantages of each solution-processing technique, and with a systematic understanding of the underlying processes, flexible circuits will soon be able to permeate our lives.

Acknowledgements

This work was partially funded by TUM Graduate School.

Conflict of interest

Authors declare no conflict of interest.

Author details

Almudena Rivadeneyra[1]*, Florin C. Loghin[1] and Aniello Falco[2]

*Address all correspondence to: almudena.rivadeneyra@tum.de

1 Institute for Nanoelectronics, Technical University of Munich, Munich Germany

2 Faculty of Science and Technology, Free University of Bolzen-Bolzano, Bolzen Italy

References

[1] Pike AW, Hoffmann DL, García-Diez M, Pettitt PB, Alcolea J, De Balbin R, et al. U-series dating of Paleolithic art in 11 caves in Spain. Science. 2012;**336**:1409-1413

[2] Bruère RT. Pliny: Natural History. In: JSTOR. 1953

[3] Søndergaard R, Hösel M, Angmo D, Larsen-Olsen TT, Krebs FC. Roll-to-roll fabrication of polymer solar cells. Materials Today. 2012;**15**:36-49

[4] Lee W, Koo H, Sun J, Noh J, Kwon K-S, Yeom C, et al. A fully roll-to-roll gravure-printed carbon nanotube-based active matrix for multi-touch sensors. Scientific Reports. 2015;**5**:17707

[5] Vaklev NL, Müller R, Muir BV, James DT, Pretot R, van der Schaaf P, et al. High-performance flexible bottom-gate organic field-effect transistors with gravure printed thin organic dielectric. Advanced Materials Interfaces. 2014;**1**:1300123 (1)-1300123 (6)

[6] Nakajima H, Morito S, Nakajima H, Takeda T, Kadowaki M, Kuba K, et al. 30.2: Flexible oleds poster with gravure printing method. In: SID Symposium Digest of Technical Papers. 2005. pp. 1196-1199

[7] Kraus T, Malaquin L, Schmid H, Riess W, Spencer ND, Wolf H. Nanoparticle printing with single-particle resolution. Nature Nanotechnology. 2007;**2**:570

[8] Kim SJ, Yoon S, Kim HJ. Review of solution-processed oxide thin-film transistors. Japanese Journal of Applied Physics. 2014;**53**:02BA02

[9] Gray C, Wang J, Duthaler G, Ritenour A, Drzaic PS. Screen printed organic thin film transistors (OTFTs) on a flexible substrate. Organic Field Effect Transistors. 2001;**4466**:89-95

[10] Colella R, Rivadeneyra A, Palma AJ, Tarricone L, Capitan-Vallvey LF, Catarinucci L, et al. Comparison of fabrication techniques for flexible UHF RFID tag antennas [wireless corner]. IEEE Antennas and Propagation Magazine. 2017;**59**:159-168

[11] Krebs FC, Jørgensen M, Norrman K, Hagemann O, Alstrup J, Nielsen TD, et al. A complete process for production of flexible large area polymer solar cells entirely using screen printing—First public demonstration. Solar Energy Materials and Solar Cells. 2009;**93**:422-441

[12] Albrecht A, Rivadeneyra A, Abdellah A, Lugli P, Salmerón JF. Inkjet printing and photonic sintering of silver and copper oxide nanoparticles for ultra-low-cost conductive patterns. Journal of Materials Chemistry C. 2016;**4**:3546-3554

[13] Jang J, Ha J, Cho J. Fabrication of water-dispersible polyaniline-poly (4-styrenesulfonate) nanoparticles for inkjet-printed chemical-sensor applications. Advanced Materials. 2007;**19**:1772-1775

[14] Liu Y, Cui T, Varahramyan K. All-polymer capacitor fabricated with inkjet printing technique. Solid-State Electronics. 2003;**47**:1543-1548

[15] Hoth CN, Choulis SA, Schilinsky P, Brabec CJ. High photovoltaic performance of inkjet printed polymer: Fullerene blends. Advanced Materials. 2007;**19**:3973-3978

[16] Sirringhaus H, Kawase T, Friend R, Shimoda T, Inbasekaran M, Wu W, et al. High-resolution inkjet printing of all-polymer transistor circuits. Science. 2000;**290**:2123-2126

[17] Lefebvre AH. Atomization and Sprays, Hemisphere Pub. vol. 1989. New York: Corp.; 1989

[18] Loghin F, Colasanti S, Weise A, Falco A, Abdelhalim A, Lugli P, et al. Scalable spray deposition process for highly uniform and reproducible CNT-TFTs. Flexible and Printed Electronics. 2016;**1**:045002

[19] Bobinger M, Angeli D, Colasanti S, La Torraca P, Larcher L, Lugli P. Infrared, transient thermal, and electrical properties of silver nanowire thin films for transparent heaters and energy-efficient coatings. Physica Status Solidi (a). 2017;**214**

[20] Abdelhalim A, Winkler M, Loghin F, Zeiser C, Lugli P, Abdellah A. Highly sensitive and selective carbon nanotube-based gas sensor arrays functionalized with different metallic nanoparticles. Sensors and Actuators B: Chemical. 2015;**220**:1288-1296

[21] Münzer A, Heimgreiter M, Melzer K, Weise A, Fabel B, Abdellah A, et al. Back-gated spray-deposited carbon nanotube thin film transistors operated in electrolytic solutions: An assessment towards future biosensing applications. Journal of Materials Chemistry B. 2013;**1**:3797-3802

[22] Steirer KX, Reese MO, Rupert BL, Kopidakis N, Olson DC, Collins RT, et al. Ultrasonic spray deposition for production of organic solar cells. Solar Energy Materials and Solar Cells. 2009;**93**:447-453

[23] Abdellah A, Fabel B, Lugli P, Scarpa G. Spray deposition of organic semiconducting thin-films: Towards the fabrication of arbitrary shaped organic electronic devices. Organic Electronics. 2010;**11**:1031-1038

[24] Falco A, Cinà L, Scarpa G, Lugli P, Abdellah A. Fully-sprayed and flexible organic photodiodes with transparent carbon nanotube electrodes. ACS Applied Materials & Interfaces. 2014;**6**:10593-10601

[25] Hull CW. Apparatus for production of three-dimensional objects by stereolithography. Google Patents; 1986

[26] Leigh SJ, Bradley RJ, Purssell CP, Billson DR, Hutchins DA. A simple, low-cost conductive composite material for 3D printing of electronic sensors. PLoS One. 2012;**7**:e49365

[27] Espalin D, Muse DW, MacDonald E, Wicker RB. 3D printing multifunctionality: Structures with electronics. The International Journal of Advanced Manufacturing Technology. 2014;**72**:963-978

[28] Macdonald E, Salas R, Espalin D, Perez M, Aguilera E, Muse D, et al. 3D printing for the rapid prototyping of structural electronics. IEEE Access. 2014;**2**:234-242

[29] Salmerón JF, Rivadeneyra A, Agudo M, Capitan-Vallvey LF, Banqueri J, Carvajal MA, et al. Printed single-chip UHF passive radiofrequency identification tags with sensing capability. Sensors and Actuators A: Physical. 2014;**220**:281-289

[30] Salmerón JF, Molina-Lopez F, Briand D, Ruan JJ, Rivadeneyra A, Carvajal MA, et al. Properties and printability of inkjet and screen-printed silver patterns for RFID antennas. Journal of Electronic Materials. 2014;**43**:604-617

[31] Rivadeneyra A, Fernández-Salmerón J, Agudo-Acemel M, López-Villanueva JA, Capitán-Vallvey LF, Palma AJ. Hybrid printed device for simultaneous vapors sensing. IEEE Sensors Journal. 2016;**16**:8501-8508

[32] Rivadeneyra A, Fernández-Salmerón J, Agudo-Acemel M, López-Villanueva JA, Palma AJ, Capitan-Vallvey LF. A printed capacitive-resistive double sensor for toluene and moisture sensing. Sensors and Actuators B: Chemical. 2015;**210**:542-549

[33] Abdelhalim A, Falco A, Loghin F, Lugli P, Salmerón JF, Rivadeneyra A. "Flexible NH_3 sensor based on spray deposition and inkjet printing. In: SENSORS, 2016 IEEE. 2016. pp. 1-3

[34] Abdellah A, Abdelhalim A, Horn M, Scarpa G, Lugli P. Scalable spray deposition process for high-performance carbon nanotube gas sensors. IEEE Transactions on Nanotechnology. 2013;**12**:174-181

[35] Falco A, Petrelli M, Bezzeccheri E, Abdelhalim A, Lugli P. Towards 3D-printed organic electronics: Planarization and spray-deposition of functional layers onto 3D-printed objects. Organic Electronics. 2016;**39**:340-347

[36] Galantucci LM, Lavecchia F, Percoco G. Experimental study aiming to enhance the surface finish of fused deposition modeled parts. CIRP Annals. 2009;**58**:189-192

[37] Boschetto A, Bottini L. Roughness prediction in coupled operations of fused deposition modeling and barrel finishing. Journal of Materials Processing Technology. 2015;**219**:181-192

[38] Falco A, Salmerón JF, Loghin FC, Lugli P, Rivadeneyra A. Fully printed flexible single-chip RFID tag with light detection capabilities. Sensors. 2017;**17**:534

[39] Andersson H, Sidén J, Skerved V, Li X, Gyllner L. Soldering surface mount components onto inkjet printed conductors on paper substrate using industrial processes. IEEE Transactions on Components Packaging and Manufacturing Technology. 2016;**6**:478-485

[40] Quintero AV, Van Remoortere B, Smits EC, Van Den Brand J, Briand D, Schoo HF, et al. Foil-to-foil lamination and electrical interconnection of printed components on flexible substrates. Microelectronic Engineering. 2013;**110**:52-58

[41] Nilsson H-E, Unander T, Siden J, Andersson H, Manuilskiy A, Hummelgard M, et al. System integration of electronic functions in smart packaging applications. Components, Packaging and Manufacturing Technology, IEEE Transactions on. 2012;**2**:1723-1734

[42] Happonen T, Voutilainen J-V, Fabritius T. Reliability study on adhesive interconnections in flex-to-flex printed electronics applications under environmental stresses. IEEE Transactions on Device and Materials Reliability. 2014;**14**:1005-1012

[43] Hung M-H, Chen C-H, Lai Y-C, Tung K-W, Lin W-T, Wang H-H, et al. Ultra low voltage 1-V RFID tag implement in a-IGZO TFT technology on plastic. In: RFID (RFID), 2017 IEEE International Conference on. 2017. pp. 193-197

[44] Myny K, Lai Y-C, Papadopoulos N, De Roose F, Ameys M, Willegems M, et al. 15.2 A flexible ISO14443-A compliant 7.5 mW 128b metal-oxide NFC barcode tag with direct clock division circuit from 13.56 MHz carrier. In: Solid-State Circuits Conference (ISSCC), 2017 IEEE International. 2017. pp. 258-259

[45] De Roose F, Steudel S, Myny K, Willegems M, Smout S, Ameys M, et al. An active artificial iris controlled by a 25-μW flexible thin-film driver. In: Electron Devices Meeting (IEDM), 2016 IEEE International. 2016. pp. 32.1.1-32.1.4

[46] Garripoli C, van der Steen J-LP, Torricelli F, Ghittorelli M, Gelinck GH, Van Roermund AH, et al. Analogue frontend amplifiers for bio-potential measurements manufactured with a-IGZO TFTs on flexible substrate. IEEE Journal on Emerging and Selected Topics in Circuits and Systems. 2017;**7**:60-70

[47] Petti L, Loghin F, Cantarella G, Vogt C, Münzenrieder N, Abdellah A, et al. Gain-tunable complementary common-source amplifier based on a flexible hybrid thin-film transistor technology. IEEE Electron Device Letters. 2017;**38**:1536-1539

[48] Jariwala D, Sangwan VK, Seo J-WT, Xu W, Smith J, Kim CH, et al. Large-area, low-voltage, antiambipolar heterojunctions from solution-processed semiconductors. Nano Letters. 2014;**15**:416-421

[49] Everaerts K, Zeng L, Hennek JW, Camacho DI, Jariwala D, Bedzyk MJ, et al. Printed indium gallium zinc oxide transistors. Self-assembled nanodielectric effects on low-temperature combustion growth and carrier mobility. ACS Applied Materials & Interfaces. 2013;**5**:11884-11893

Edited by Simas Rackauskas

The interest in flexible electronics is on the rise as it brings an added functionality and esthetic value in the unconventional interfaces, such as biomonitoring systems, wearables, flexible textiles, paper-based technologies, and many other curves of soft schemes, for which traditional electronics are not suitable. The demand in new flexible platforms turns to a pursuit for functional materials and technologies commonly compatible with a low temperature, high-throughput processing, and novel methods for device integration. A wide range of functional materials involving nanoparticles, composites, semiconductor and metallic nanowires, carbon nanomaterials, polymers, conductive inks, and different hybrid structures are particularly interesting. This book brings a comprehensive overview on the most important technology development in the field of flexible electronics.

Published in London, UK

IntechOpen

ISBN 978-1-83881-697-1